UNIVERSITY OF CALIFORNIA

Los Angeles

The significance of the leaf surface during drought: insight into function of stomata and leaf hair

A dissertation submitted in partial satisfaction of the

requirements for the degree Doctor of Philosophy

in Biology

by

Christian Henry

2022

ABSTRACT OF THE DISSERTATION

The significance of the leaf surface during drought: insight into function of stomata and leaf hair

by

Christian Henry

Doctor of Philosophy in Biology

University of California, Los Angeles, 2022

Professor Lawren Sack

The leaf surface is the locus of a multitude of physiological processes important in determining plant performance including responses to the environment. In my dissertation research, I identified specific adaptive and functional roles and constraints on stomata and trichomes. My approach utilized physiological experiments on diverse species native to California with potential applications toward understanding and improving plant drought tolerance. First, I clarified the mechanistic basis for leaf level drought response and the regulatory factors by which a stomatal safety-efficiency trade-off arises across diverse woody angiosperms. Second, I quantified foliar water uptake across diverse pairs of native California tree, shrub, and vine species with contrasting trichome densities adapted to a wide range of aridity. Lastly, I tested whether trichome presence was associated with differences in light-saturated gas exchange, water use efficiency, and climatic variables across diverse California species. This work highlighted underlying factors influencing water relations and gas exchange, including constraints on stomatal function and the key role of leaf trichomes, providing a clearer picture of the importance of these structures in species evolution and ecology.

The dissertation of Christian Henry is approved.

Tom Buckley

Van Savage

Felipe Zapata

Lawren Sack, Committee Chair

University of California, Los Angeles

2022

1. Table of Contents

2. List of figures

3. List of Tables

ACKNOWLEDGEMENTS

I would like to acknowledge my advisor Lawren Sack, who has pushed me forward every year, thank you. I would also like to thank the other members of my committee Tom Buckley, Van Savage, and Felipe Zapata insightful feedback and words of support. I have enjoyed working with you all and look forward to continuing our relationship.

I would like to acknowledge Grace John, Ruihua Pan, Megan Bartlett, Christine Scoffoni, and Leila Fletcher for their work on chapter 2 of my thesis regarding collecting and sharing data, developing R scripts, and edits to the submitted manuscript.

I would like to acknowledge Tom Buckley for the development of equations in chapter 3 and 4 of my dissertation. Thank you to Marvin Browne and Marissa Ochoa for help with data collection. Also, thank you to Craig Brodersen for micrographs of all my species for these chapters.

4. VITA

EDUCATION

2022	PhD Candidate, Ecology and Evolutionary University of California, Los Angeles | Los Angeles, CA
2014	Bachelor of Science, Biology Hampton University | Hampton, VA

PEER-REVIEWED PUBLICATIONS

Henry, C. *et al.* A stomatal safety-efficiency trade-off constrains responses to leaf dehydration. *Nature Communications* **10**, 3398, doi:10.1038/s41467-019-11006-1 (2019).

John, G. P., **Henry, C.** & Sack, L. Leaf rehydration capacity: associations with other indices of drought tolerance and environment. *Plant, Cell & Environment* **41**, 2638-2653 (2018).

1. Chapter 1: Introduction

Stomata are pores in the leaf epidermis, each consisting of two guard cells, which enable CO_2 uptake and resulting in loss of water vapor. Species differ strongly in their stomatal responses to leaf dehydration. Leaf hairs (trichomes) also play important roles in plant function, including reflecting light, taking up water and/or slowing transpiration via a thicker boundary layer. The multiple functions of leaf trichomes can explain several contradictory trends observed across floras. For example, leaf trichome density tends to be higher for species adapted to drought stress, and yet many species of wet places also bear trichomes[1]. To date, there are no physiological studies highlighting comparative differences between species with and without trichomes across genera.

In **chapter 2** of my thesis, "The control of stomata by leaf water status: trade-off between safety and efficiency" was published in *Nature Communications*[2]. I found a novel relationship between maximum stomatal conductance (g_{max}), which is a major determinant of maximum rates of plant gas exchange, and the leaf water potential at stomatal closure (Ψ_{gs50}), which contributes to sensitivity to drought. I identified this relationship among 15 native California species, and by re-analyzing global data for species worldwide. Further, I found evidence that this trade-off could be driven by multiple underlying mechanisms, including variation in stomatal size and density, and/or solute concentrations within the leaf cells and/or a trade-off between photosynthetic productivity and protection from dehydration stress during drought, and might arise as part of a broader life history trade-off.

Chapter 3 focuses on how leaf surface properties and structure affect water loss and thus leaf dehydration stress. Several species of plants bearing trichomes have been previously shown

to take up water through their trichomes. However, the quantitative benefit of leaf trichomes in water uptake has not been tested for any species, or whether they influence the uptake of water through stomata. To test the functional role of pubescence in leaf level rehydration mechanics, I measured the leaf surface water uptake conductance (K_{surf}) in pairs of species in six native California genera, including species with and without leaf trichomes, all growing in a greenhouse common garden in a fog chamber. Using high resolution (micron-scale) images of the trichomes taken by micro-computed tomography, I analyzed leaf trichome traits (trichome density, height, diameter, branching, and tapering).

Chapter 4 explores the role of leaf trichomes in light saturated gas exchange and climate association. Leaves bearing pubescence can absorb less light, and develop a thicker boundary layer, allowing them to maintain optimal temperature and water relations, including a higher water use efficiency. I tested this hypothesis in species in six native California genera, including species with and without leaf trichomes, measuring gas exchange and integrated water use efficiency with stable isotopes. I found evidence for an adaptive coordination of leaf hairs and high gas exchange rates in species adapted to greater aridity, enabling these species to achieve higher rates of gas exchange to mitigate shorter growing periods with available moisture. This work contributes to a clearer understanding of the importance of small-scale structures in defining species' ecology and environmental adaptation.

1.1 References

Berry, Z. C., Emery, N. C., Gotsch, S. G. & Goldsmith, G. R. Foliar water uptake: Processes, pathways, and integration into plant water budgets. *Plant, Cell & Environment* **42**, 410-423, doi:https://doi.org/10.1111/pce.13439 (2019).

2. Chapter 2 : A stomatal safety-efficiency trade-off constrains responses to leaf dehydration

2.1 Introduction

Stomata exert major influences on plant and ecosystem productivity and drought tolerance [1-3]. Across the diversity of plant species, leaves with a greater area of open stomatal pores have higher stomatal conductance (g_s), and typically, greater rates of photosynthetic CO_2 assimilation and of transpiratory water loss[4-6]. However, plants must maintain their hydration within narrow limits, and a high g_s and transpiration rate drive declines in water potential throughout the plant[7] which would cause mesophyll damage and xylem embolism during drought[8]. Plants thus close stomata in response to decreasing leaf water potential (Ψ_{leaf}). The decline of g_s (i.e., stomatal closure) with decreasing Ψ_{leaf} is important among the complex of internal and external factors that determine overall stomatal responses, including root-derived signals, ambient irradiance and CO_2 [9-11] and influences the dynamics of gas exchange and productivity and drought tolerance across plant species[1,12-15].

One potentially general constraint on the response of g_s to Ψ_{leaf} would be a trade-off between high maximum stomatal conductance (g_{max}) in hydrated leaves and greater sensitivity to closure during dehydration, i.e., a higher Ψ_{leaf} at 50% loss of stomatal conductance (Ψ_{gs50}). Such trade-offs between “safety” and “efficiency”, or, similar in logic, between “stress tolerance” and “potential growth” are common in plant and animal biology [16,17] and industrial systems[18]. A well-known hypothesis in whole plant physiology is a constraint on internal water transport known as the hydraulic safety-efficiency trade-off: an association across species between high values for the maximum stem or leaf hydraulic conductivity and a greater sensitivity to decline during dehydration[19-21]. Hydraulic safety-efficiency trade-offs are often strong within lineages of closely-related species, significant though weak across the sampled diversity of species globally[19,20], and

may contribute to adaptation to habitat and climate[22,23]. The evolution of an analogous g_{max}- Ψ_{gs50} trade-off would be expected based on multiple, nonexclusive rationales from stomatal biomechanics, hydraulic design, and life history theory (Fig. 1A-1D).

First, a g_{max}- Ψ_{gs50} trade-off might arise mechanistically according to variation in stomatal size and density (Fig. 1A). Smaller, denser stomata are associated with higher g_{max}, both by contributing to a greater anatomical maximum stomatal conductance ($g_{max,anatomy}$) and to a greater stomatal opening ratio during gas exchange ($g_{max\ ratio} = g_{max} / g_{max,anatomy}$)[5,24,25]. Further, smaller stomata have a greater surface area to volume ratio, facilitating ion exchange and thus stronger and faster movements in response to changing irradiance and leaf hydration status[26-28].

Additionally, a g_{max}- Ψ_{gs50} trade-off might arise due to variation in solute concentrations within leaf cells (Fig. 1B). For stomata to open, guard cells must accumulate solutes from the apoplast, driving water uptake to build sufficient hydrostatic pressure to inflate against the surrounding pressure of the epidermal pavement cells[27,29]. Opening to a higher g_{max} may thus be mechanically facilitated, requiring less guard cell ion uptake, when epidermal pavement cells have lower osmotic concentration and lower turgor pressure at full hydration[27,29], which tissue-scale studies have shown would be associated with a higher bulk leaf osmotic potential at full turgor (π_o)[30]. A higher π_o would also cause greater stomatal sensitivity to closure under drought, as it corresponds to a higher turgor loss point (π_{tlp}), i.e., greater sensitivity to wilting, and stomatal closure is a typical wilting response[12,31-34].

A g_{max} - Ψ_{gs50} trade-off may also arise as a leaf economic or life history trade-off (Fig. 1C). Theoretical and empirical analyses support trade-offs across species among traits that confer benefits for resource acquisition and those that confer stress tolerance[35,36]. Species adapted to high resource supplies tend to allocate less to leaf structural protection, resulting in lower leaf mass per area (LMA) and higher rates of photosynthesis per unit leaf mass, at the cost of stronger

photosynthetic declines under resource scarcity, and shorter leaf lifetimes. By contrast, species adapted to low resource supplies tend to invest in structural protection and higher LMA at the expense of photosynthetic machinery, and to maintain leaves longer into periods of scarcity and to achieve longer leaf lifetimes[36,37]. A g_{max} - Ψ_{gs50} trade-off would be consistent with leaf economic and life history trade-offs, such as between maximum photosynthetic rate under well-watered conditions, and sensitivity to photosynthetic decline during drought[36], given that g_{max} is a key determinant of maximum photosynthetic rate[6], and Ψ_{gs50} of the ability to maintain photosynthesis during drought[1].

Our fourth and final hypothesis was that a g_{max}- Ψ_{gs50} trade-off may balance photosynthetic productivity against protection from dehydration stress under atmospheric or soil drought (Fig. 1D). A higher g_{max} would facilitate rapid photosynthetic rates in moist soil, but would also result in greater transpiration rates and steeper declines in water potential throughout the plant, which under drought would increase the danger of xylem embolism[1]. Species with higher g_{max} thus would require greater sensitivity to closure to avoid dehydration stress during soil and/or atmospheric drought. The g_{max}- Ψ_{gs50} trade-off would enable plants to maintain high photosynthetic rates under high water availability, yet minimize dehydration stress during drought.

We report on the demonstration of g_{max}- Ψ_{gs50} trade-off and its mechanistic basis in a controlled experiment on 15 California tree and shrub species, and in analyses of a unique compiled database of previous studies of stomatal responses for diverse species (Fig. 2; Supplementary Data 1-8).

2.2 Methods and Material

Plant species and growth conditions

We selected 15 morphologically and ecologically diverse tree and shrub species native to California semi-desert, chaparral, coastal scrub and woodlands (Supplementary Data 2). Plants were cultivated in a greenhouse common garden at the UCLA Plant Growth Center from August 2012 to April 2016[55]. Nine individual seedlings of each species were acquired in 3.8 L pots (Tree of Life Nursery; San Juan Capistrano, CA), and randomized within each of nine blocks containing one individual of each species spread across four greenhouse benches in two greenhouse rooms. Plants were acclimated 12–18 months prior to initial measurements to establish similar external conditions across individuals and species, and to ensure canopies of mature leaves. Plants were carefully monitored for root expansion and repotted when roots filled the pots. Given the species variation in natural history, phenology and growth rate, 19- to 38-L pots were used, as appropriate for each species to minimize stress and accommodate species of different sizes and intrinsic growth rates[56]. Potting soil (18.75% washed plaster sand, 18.75% sandy loam, 37.5% grower grade peat moss, 12.5% horticultural grade perlite, 12.5% coarse vermiculite; Therm-O-Rock West, Inc., Chandler, AZ) was autoclaved prior to use. Plants were irrigated every second day with 200-250 ppm 20:20:20 NPK fertilizer. Daily irradiance ranged up to 1400 μmol m^{-2} s^{-1} (LI-250 light meter; LI-COR Biosciences, Lincoln, NE, USA), while mean minimum, mean and maximum values for temperature were 22.1°C, 23.9°C, and 25.2°C and relative humidity were 47.3%, 60.1%, and 72.8% over the course of our experiments (HOBO Micro Station with Smart Sensors; Onset, Bourne, MA, USA).

Prior to experiments, plants were drought-hardened by watering to field capacity then suspending watering until visible wilting was observed in the morning. A single drought-hardening cycle was used to enable the standardized comparison of plants that had acclimated to strong leaf dehydration, with the recognition that multiple drought cycles may further modify stomatal responses[50]. The initial hardening drought was 1-3 weeks depending on species, and Ψ_{leaf} was

measured at mid-day for leaves of three to six individuals per species; species means ranged from -1.1 to -4.3 MPa (Plant Moisture Stress pressure chamber model 1000; PMS Instrument Co., Albany, OR, USA).

Response of stomatal conductance to leaf dehydration

The response of g_s to dehydration was determined using a refinement of previously used methods applied to excised shoots[15,45]. Three individual plants of each species were selected that had the largest numbers of healthy leaves. Plant shoots with 3-15 leaves (range in length 30-60 cm) were excised from three individual plants per species and rehydrated overnight with cut ends in deionized water and covered with plastic. Mature leaves were sampled from the most recent flushes. At the beginning of the experiment, a water-filled bag was sealed to the cut end of each shoot to maintain full hydration and shoots were acclimated for at least 30 min under high irradiance (>1000 μmol m^{-2} s^{-1}; LI-250 light meter; LI-COR Biosciences, Lincoln, NE, USA) and held in frames adaxial side up with fishing line and small pieces of tape at leaf margins on top of a fan. Stomatal conductance was measured on the abaxial surface of given leaves using a porometer (AP-4, Delta-T Devices Ltd, Cambridge, United Kingdom) after which leaves were excised with a razor blade, placed in bags and allowed to equilibrate for at least 30 min before leaf water potential (Ψ_{leaf}) was determined (Plant Moisture Stress pressure chamber model 1000; PMS Instrument Co., Albany, OR, USA). A single porometer measurement was taken once stable repeated values were achieved for each leaf before harvesting that leaf for Ψ_{leaf} measurement. Porometry measurements were taken on leaves at intervals ranging from 2 to 60 min as shoots dried, aiming for a range of leaf dehydration. Measurements were made with the bags still attached to the cut ends of shoots, to assess relatively well-hydrated transpiring leaves. Then, the shoot ending with its attached bag was excised using a razor

blade, and subsequent measurements were made on remaining leaves as they dehydrated to stomatal closure. We aimed to collect points between maximum opening and full closure across the range of leaf water potentials. All measurements were taken from 0800 to 1400h. Lab temperature and relative humidity ranged 22.8 ± 0.08°C and 38.5 ± 0.50%. Notably, our study focused on standardized and controlled measurements in stomatal responses in excised shoots, and their mechanisms. Indeed, most previous studies of stomatal responses to leaf dehydration have focused on excised shoots as tests on a number of species have suggested good agreement with responses measured during the photosynthetic period for whole plants experiencing drought, e.g., refs[15,31,45,57,58]. Yet, some uncertainties remain about scaling shoot scale responses to whole-plants during drought, due to additional influences (e.g., root signals in drying soil)[59]. To further test the potential generality of the trade-off at whole plant scale we also compiled data from previous studies of stomatal responses of leaves on whole plants subjected to drought (see "*Literature compilation for testing of generality of trade-off across species"*).

Fitting stomatal responses to leaf water potential

Curves were fitted for the response of stomatal conductance (g_s) to declining leaf water potential (Ψ_{leaf}), such that the range of stomatal response characterized was relative to the minimum stomatal conductance. Thus, before curve fitting, the mean minimum epidermal conductance (g_{min}) for each species, determined for the same experimental plants, was subtracted from each g_s measurement. For curve-fitting, the datasets for each species were analyzed in two ways. First, all data points were considered for each species' response of g_s to Ψ_{leaf} ("all data"). In these responses a number of well-hydrated leaves had closed stomata ("squeeze points"; Supplementary Figure 4); this closure may represent the effect of the mechanical advantage of

epidermal pavement cells or subsidiary cells against guard cells in turgid leaves[29,45]. Further, some leaves showed stomata open when strongly dehydrated beyond the point at which stomata had typically shut, potentially representing re-opening in leaves that lost stomatal control after the epidermis became flaccid[60] ("re-opening points"; Supplementary Figure 4). Thus using all data, the responses were not statistically significant for four species. To address these issues, a second dataset ("refined dataset") was generated excluding the squeeze points, i.e., leaves with g_s (after subtracting g_{min}) <50 mol m^{-2} s^{-1} at Ψ_{leaf} > -0.5 MPa, and the re-opening points, i.e., g_s > 50 mol m^{-2} s^{-1} at Ψ_{leaf} > -2.0 MPa; or after the bulk of leaves showed complete stomatal closure. These points constituted 1-14 of 14-77 points per species (3-17%; 8% on average) The responses fitted to this second dataset showed higher goodness of fit (R^2 values), and $P < 0.05$ for all species but *Cercocarpus betuloides* ($P = 0.07$; Supplementary Data 4). The parameters calculated from the "all data" and "refined" datasets were highly correlated, and consistent in their ahistorical and evolutionary correlations with other variables (see "*Statistics*" below; Supplementary Data 5 and 6). Thus, the parameters of responses using all data are described in the main text and Figures, with the results from both analyses provided in the supplement (Supplementary Data 2).

For each species, we determined the functional response of g_s to Ψ_{leaf} using maximum likelihood to select among four functions[61]: linear ($g_s = a\,\Psi_{leaf} + g_{max}$); sigmoidal $\left[g_s = \frac{a}{1+e^{-(\frac{\Psi_{leaf}-x_0}{b})}}\right]$; logistic $\left\{g_s = a/\left[1+(\frac{\Psi_{leaf}}{x_0})^b\right]\right\}$; and exponential $\left(g_s = g_{max} + ae^{-b\Psi_{leaf}}\right)$. Curves were fitted using the *optim* function in R.2.9.2 (http://www.r-project.org [62]; our scripts are available on request). The function with the lowest Akaike Information Criterion, corrected for low *n* (AICc) was selected for each data set, with differences >2 considered as meaningful [62]. From the equations for the selected model, we determined the maximum g_s for hydrated leaves (g_{max}), i.e., the g_s extrapolated to Ψ_{leaf} = 0 MPa, and the Ψ_{leaf} corresponding to decline of g_s by 20, 50, and

80% (Ψ_{gs20}, Ψ_{gs50}, and Ψ_{gs80}). We considered various forms of presenting g_{max}, and used the extrapolated theoretical parameter following previous studies[32,45]. This extrapolated g_{max}, like other theoretical physiological variables, such as maximum leaf hydraulic conductance, or photosynthetic parameters including the maximum rate of carboxylation (V_{cmax}), cannot be reached in practice but is useful for generating and testing hypotheses concerning mechanisms or association with other traits[63]. Practically, an extrapolated g_{max} was preferred over averaging g_s values above a threshold Ψ_{leaf}, as species differed in the exact Ψ_{leaf} at which g_s was measured at initial states of dehydration, when g_s declines steeply in many species. To check that the trade-off did not arise only when using g_{max} determined by extrapolation to Ψ_{leaf} = 0 MPa, for the 15 California species we re-analyzed the trend, using g_s estimated from the selected g_s versus Ψ_{leaf} functions at Ψ_{leaf} = -0.1 MPa, and calculated Ψ_{gs50} as the Ψ_{leaf} at which g_s declined by 50%; we found a similar g_{max} - Ψ_{gs50} trade-off (phylogenetic least squares regression r = 0.61; P = 0.015; Supplementary Figure 5). In several species, g_s begins to decline strongly by Ψ_{leaf} = -0.1 MPa, precluding testing for a safety-efficiency trade-off using lower values of Ψ_{leaf} to estimate "g_{max}".

Compilation and analysis of previous literature

Data were collected from previous studies that reported the responses of g_s to leaf water potential (Ψ_{leaf}), based on searches of Web of Science and Google using search terms "leaf water potential" and "dehydration" or "desiccation". We compiled all studies that included the response of stomatal conductance to Ψ_{leaf} for two or more species or varieties of a given species, including studies of excised branches, or of potted plants or trees in the field measured for g_s and Ψ_{leaf} during progressive drought. We included data for responses that included measurements at Ψ_{leaf} >-0.5 MPa and decline of g_s to 20% of g_{max}. We found 9 studies of diverse sets of species or varieties, measured with different techniques, and growing conditions (n = 2-16; Supplementary Data 2),

virtually all of angiosperms, though including one study of two varieties of a fern species[64]. We extracted data points from published figures using ImageJ software version 1.42q. We fitted curves using the same methods as for our experimental plants, though without subtracting g_{min} as data were not generally available for the species in the compiled studies.

Stomatal anatomy

We measured stomatal traits on one leaf from each of three individuals per species. After rehydration, we fixed the leaves in formalin acetic acid (FAA; 48% ethanol: 10% formalin: 5% glacial acetic acid: 37% water). We visualized stomata using nail varnish impressions at the center of the top, middle, and bottom third of the leaf, halfway between the margin and midrib, for the abaxial and adaxial leaf surfaces, using light microscopy. For each image we calculated total stomatal density (*d*) by dividing the number of stomata in the image by the area of the image after subtracting those areas including any blurriness. We calculated mean stomatal areal size (*s*) and width (*W*), and guard cell and stomatal pore lengths (*L* and *p*) for the abaxial surface based on measurements of four stomata selected as nearest to the center of each quadrant of each image. For three species, *Ceanothus spinosus*, *Encelia farinosa* and *Platanus racemosa*, dense trichomes prevented measurement of stomatal traits. We estimated the theoretical anatomical maximum stomatal conductance ($g_{max,\ anatomy}$;[4,63]):

$$g_{\mathrm{max,anatomy}} = \frac{bmds}{s^{0.5}} \quad (1)$$

In which *b* is a biophysical constant given as $b = \frac{D}{v}$, where *D* represents the diffusivity of water in air (2.82×10^{-5} m^2 s^{-1}) and *v* is the molar volume of air (2.24×10^{-2} m^3 mol^{-1}); *m* is a factor based on the proportionality of stomatal dimensions ($m = \frac{\pi c^2}{j^{0.5}(4hj+\pi)}$), with $c = p/L$ and $j = W/L$. As data were not available for stomatal pore depth, a constant value of 0.5 was assumed for the ratio of

stomatal pore depth to width, *h* for the estimation of $g_{max,anatomy}$[4,5]. We estimated the stomatal opening ratio as g_{max} / $g_{max,anatomy}$ ($g_{max\ ratio}$, equivalent to the " *a* ratio" in ref [5]).

Pressure-volume curves and leaf structure

Measurements were made of pressure volume curves and of leaf structure, i.e., leaf dry mass per unit area (LMA), for the study plants[55]. For 6-9 plants per species, 5-6 leaves were measured for leaf water potential and leaf mass during dehydration and from the plotted pressure-volume curves, we determined water potential at full turgor (π_o) and turgor loss point (π_{tlp})[59]. For two species with very small leaves and fragile petioles, *Ceanothus spinosus* and *Encelia californica,* pressure-volume curves were not constructed.

Modeling the g_{max}- Ψ_{gs50} trade-off at plant scale

To test the hypothesis that a g_{max}- Ψ_{gs50} trade-off would benefit plant hydraulic design, we used a modeling approach to simulate the consequences for gas exchange and tissue dehydration stresses of variation in g_{max} and Ψ_{gs50}, and of a trade-off among these variables[38,61]. We implemented a plant hydraulic-stomatal-photosynthetic model based on Darcy's law, assuming steady-state flow, which simultaneously resolves bulk water potentials (Ψ) and hydraulic conductance (*K*) for each plant organ, given inputs of soil water potential (Ψ_{soil}) and vapor pressure deficit (*VPD*) and parameters for the response of the hydraulic conductance of whole root, whole stem, and leaf, and of leaf stomatal conductance to water potential within the respective organ. In the model, the volumetric flux of water into each plant component (*F*) is calculated as:

$$F_{\mathrm{leaf}} = \int_{\Psi_{\mathrm{leaf}}}^{\Psi_{\mathrm{stem}}} K_{\mathrm{leaf}}(\Psi) d\Psi - g_{\mathrm{s}}(\Psi_{\mathrm{leaf}}) VPD \quad (2)$$

$$F_{\mathrm{stem}} = \int_{\Psi_{\mathrm{stem}}}^{\Psi_{\mathrm{root}}} K_{\mathrm{stem}}(\Psi) d\Psi - \int_{\Psi_{\mathrm{leaf}}}^{\Psi_{\mathrm{stem}}} K_{leaf}(\Psi) d\Psi \quad (3)$$

$$F_{\mathrm{root}} = \int_{\Psi_{\mathrm{root}}}^{\Psi_{\mathrm{soil}}} K_{\mathrm{root}}(\Psi) d\Psi - \int_{\Psi_{\mathrm{stem}}}^{\Psi_{\mathrm{root}}} K_{\mathrm{stem}}(\Psi) d\Psi \quad (4)$$

where stomatal conductance is assumed to decline exponentially with Ψ_{leaf}. We used an exponential decay function in the modeling, because that response was the most frequently selected by maximum likelihood across species when testing the four functions, i.e., for 7 of 15 species (Supplementary Data 4). In these model simulations, all was kept equal other than g_{max} and Ψ_{gs50}, including the shape of the response of g_s to Ψ_{leaf}, to assess the consequences of the trade-off; the findings of this modeling exercise would be qualitatively similar using another common stomatal response function. Water transport through the hydraulic system was represented with the Kirchoff transform (i.e., $\int_{\Psi_{\mathrm{leaf}}}^{\Psi_{\mathrm{stem}}} K_{\mathrm{leaf}}(\Psi) d\Psi$) to account for the non-linearity of the relationship between hydraulic conductance (*K)* and water potential (Ψ)[65]. *K* for each organ was assumed to decline with water potential following a sigmoidal response

$$K = \frac{K_{\max}}{1 + e^{\alpha(\Psi - \Psi_{50})}} \quad (5)$$

where K_{max} is the maximum conductance of the plant component, Ψ_{50} is the water potential inducing a 50% decline in conductance, and α is a shape parameter. Because water transport is assumed to be at steady-state, the flux into each component (*F*) is equal to 0. The water potentials of the leaf, stem, and root that satisfied this assumption for given environmental conditions (i.e., vapor pressure deficits and soil water potentials) were then solved using the *fsolve* function in MATLAB (R2016b). Stomatal conductance was then calculated from the g_s versus Ψ_{leaf} curves. Photosynthesis (A_{max}) was calculated from g_s using the equations from the Farquhar model and photosynthetic parameters collected from the literature for *Quercus ilex*, which was selected to represent a typical Mediterranean species[66,67]. Photosynthetic rate was assumed to be light-

saturated (i.e, photosynthetically active radiation = 1500 μmol m^{-2} s^{-1}), and thus limited only by carboxylation. To derive an expression for *A* as a function of g_s, Fick's law of diffusion

$$A = u(c_a - c_i) \quad (6)$$

where *u* is the stomatal conductance to CO_2 (g_s/1600, units: mol m^{-2} s^{-1}), c_a is the atmospheric CO_2 concentration (400 ppm), and c_i is the intercellular CO_2 concentration (units: ppm), was substituted into the Farquhar equation for carboxylation-limited photosynthesis

$$A = V_{cmax}\frac{c_i - \Gamma_*}{c_i + K_m} \quad (7)$$

where V_{cmax} is the maximum rate of carboxylation (29.1 μmol m^{-2} s^{-1}), K_m is the Rubisco affinity for CO_2 and O_2 (550 ppm), and Γ_* is the CO_2 compensation point in the absence of dark respiration (40 μmol m^{-2} s^{-1}). This equation was rearranged to produce the expression

$$A = a + bu - \sqrt{b^2u^2 + cu + a^2} \quad (8)$$

where these coefficients are equal to

$$a = 0.5(V_{cmax} - R) \quad (9)$$

$$b = 0.5(c_a + K_M) \quad (10)$$

$$c = 0.5\left(R(c_a + K_m) + V_{cmax}(K_m - c_a + 2\Gamma^*)\right) \quad (11)$$

and *R* is the leaf respiration rate (1 μmol m^{-2} s^{-1}). The photosynthetic parameters for *Q. ilex* were interpolated from *A*/*C*i curves measured at a constant leaf temperature (30°C), and leaf temperature was assumed to be constant in the simulations.

We parameterized the model using simulated g_s versus Ψ_{leaf} responses based on every combination of g_{max} values ranging from 100 to 400 mmol m^{-2} s^{-1} in increments of 10 mmol m^{-2} s^{-1} and Ψ_{gs50} values ranging from -0.2 MPa to -3 MPa in increments of 0.2 MPa (Supplementary Data 8). As we did not have data for the response of the stem, root, or stomata to dehydration for juveniles of these species, and because we wished to isolate the putative benefit of the g_{max}- Ψ_{gs50}

trade-off, all else being equal, we set all the other parameters of the model at typical values, with leaf, stem and root hydraulic conductance declining with water potential as a sigmoidal response, with leaf area-normalized maximum hydraulic conductances of leaf, stem and root systems of 10, 20 and 10 mmol m^{-2} s^{-1} MPa^{-1}, respectively, and water potentials at 50% loss of hydraulic conductance of -1, -2 and -1 MPa respectively. The simulations were performed given soil water potential (Ψ_{soil}) of 0 MPa, i.e., high water availability, and -1.2 MPa, i.e., soil drought, under vapor pressure deficit of 1 kPa (0.01 mol mol^{-1}). Then, we determined the g_s, *A,* and leaf and stem water potentials.

Statistics

We analyzed both ahistorical trait correlations and evolutionary correlations among variables to assess both putative physically based mechanisms as well as evolutionary shifts. We present results of evolutionary correlations in the text, except where specified, and all results in the Supplementary Materials. For ahistorical correlations we used R statistical software to determine Pearson coefficients for untransformed and log- transformed data, to model relationships as either linear or non-linear, i.e., approximately power law[68]. For plotting trait-trait correlations, we used standard major axes to emphasize the structural relationship between two potentially independent variables similar in measurement error (using SMATR[69,70]). A test was made for whether the trade-off, i.e., the g_{max} vs Ψ_{gs50} relationship, varied in slope and/or intercept across studies, for the four studies with ≥6 species (i.e., sufficient species for this test), using log-transformed data, i.e., approximating a power law relationship, given the nonlinearity of the relationships (using SMATR).

For evolutionary correlations, we applied a phylogenetic generalized least-squares (PGLS) approach to both untransformed and log- transformed data, using a previously published megatree[71] pruned using the software Phylomatic v3[72]. For analyses based on traits for which

values were missing for given species (i.e., for the two species missing π_o and π_{tlp} values, and the three missing stomatal measurements), trees were pruned for the remaining species. For π_{tlp} and π_o, which are negative numbers, the values were multiplied by -1. PGLS were calculated using the caper package in R (version 3.4.4)[68] using models of Brownian motion, Pagel's lambda, and Ornstein–Uhlenbeck (OU), and the best fit model was selected using the Akaike Information Criterion[73,74]. Reported *r*-values are for the Pagel's lambda model when the Pagel's and OU models were equally good fits (difference in AIC score < 2).

2.3 Results

Across the California species, g_{max} varied by 7-fold, and Ψ_{leaf} at 20%, 50% and 80% stomatal closure (Ψ_{gs20}, Ψ_{gs50} and Ψ_{gs80}) by 2.1, 2.6 and 3.1 MPa respectively (stomatal parameters determined from fitted curves; Fig. 2A; Supplementary Figure 1; Supplementary Data 1, 3 and 4). Across these 15 species, a higher g_{max} was correlated with higher values of Ψ_{gs20}, Ψ_{gs50} and Ψ_{gs80} (Fig. 2A; Supplementary Data 5 and 6). Likewise, our analyses of the data from nine previous studies of stomatal responses in datasets on diverse species of mainly woody angiosperms (Supplementary Data 2) showed in each case an empirical tendency for species with high g_{max} to have higher values of Ψ_{gs20}, Ψ_{gs50}, and Ψ_{gs80} (Fig. 2B-J; Supplementary Data 7). Five of the six studies that tested ≥ 5 species showed a significant g_{max}- Ψ_{gs50} trade-off (Fig. 2A-F), with the slope of the relationship varying significantly across studies (Supplementary Data 2).

We tested four putative mechanisms for the g_{max}- Ψ_{gs50} trade-off in the California species, and found support for each (Figs 3 and 4). First, we tested whether the g_{max}- Ψ_{gs50} trade-off might arise mechanistically according to variation in stomatal size and density (Fig. 1A). The California species varied strongly in stomatal density, size, $g_{max,anatomy}$, and $g_{max\ ratio}$ (Supplementary Data 1). As hypothesized, leaves with smaller stomata had greater g_{max} and higher values of Ψ_{gs50} and

Ψ_{gs80}, and these were associated with higher $g_{max\ ratio}$, rather than with higher $g_{max,anatomy}$ (Fig. 3A and 3B; Supplementary Figure 2; Supplementary Data 5 and 6).

Second, we tested whether the g_{max}- Ψ_{gs50} trade-off might arise due to variation in solute concentrations within leaf cells (Fig. 1B). The California woody species varied strongly in π_o and π_{tlp} (Supplementary Data 1), and all species began closing stomata with dehydration well before π_{tlp}, at which point many had reduced stomatal conductance by >80% (Supplementary Figure 1). Species with lower π_o had lower g_{max} and species with lower π_o and π_{tlp} had lower Ψ_{gs50} and Ψ_{gs80} values (Fig. 3C and D; Supplementary Data 5 and 6).

Third, we tested whether the g_{max} - Ψ_{gs50} trade-off might arise as a leaf economic or life history trade-off linked with leaf mass per unit area (LMA; Fig. 1C). Across the California species, g_{max} and Ψ_{gs50} were both negatively related to *LMA* (Fig. 3E and F; Supplementary Data 5 and 6).

Finally, we tested whether a g_{max}- Ψ_{gs50} trade-off may balance photosynthetic productivity against protection from dehydration stress under atmospheric or soil drought (Fig. 1D). Using a plant hydraulic-stomatal-photosynthetic model[21,38], we simulated species with typical physiological parameters and differing in only their g_s versus Ψ_{leaf} responses, i.e., in their g_{max} and Ψ_{gs50} values, and calculated their light-saturated photosynthetic rates (*A*), and leaf and stem water potentials under high water availability, i.e., soil water potential (Ψ_{soil}) of 0 MPa, and soil drought, i.e., Ψ_{soil} of -1.2 MPa. Species with high g_{max} had higher *A* irrespective of Ψ_{soil} (Fig. 4A; Supplementary Figure 3A and D), but showed steep declines in both leaf and stem water potentials under low Ψ_{soil} (Fig. 4B; Supplementary Figure 3B, C, E and F). Conversely, species with sensitive stomatal closure (i.e., high Ψ_{gs50}) showed lower *A* under high water availability due to partial stomatal closure during transpiration, but substantially less leaf and stem dehydration stress under drought (Fig. 4B; Supplementary Figure 3). The g_{max}-Ψ_{gs50} trade-off would thus

enable the California species to avoid low *A* under high water availability as well as hydraulic damage during drought (Figs 4 and Supplementary Figure 3).

2.4 Discussion

A strong generality was observed for the g_{max}- Ψ_{gs50} trade-off across woody angiosperm species. Further study is required to test for this trade-off across a yet broader phylogenetic sample of angiosperms, such as herbs, including grasses, and other major lineages, such as ferns and gymnosperms, which also close stomata in response to declining Ψ_{leaf}, but differ in aspects of stomatal control physiology[39,40]. In the single study amenable to re-analysis of the response of g_s to Ψ_{leaf} for a fern species, the comparison of two varieties was consistent with the trade-off (Fig. 2J).

We found support for multiple mechanisms as putative causes of the g_{max}- Ψ_{gs50} trade-off[20,38]. Thus, the trade-off could be explained by species with smaller, denser stomata also having more sensitive closure. Indeed, the more sensitive stomatal closure of species with small stomata is consistent with their tendency to respond more quickly and/or strongly to transitions in light, water status and vapor pressure deficit, conferring greater tolerance of a variety of stresses[25,26,28,40]. The trade-off could also be explained by species with lower bulk leaf osmotic potentials having lower g_{max} and also less sensitive closure. While the contribution of low π_o and π_{tlp} to the maintenance of gas exchange during drought has been well recognized[12], our findings indicate a major cost, explaining why these traits are not universal, as the association of low π_o with low g_{max} would restrict gas exchange under high water availability. The trade-off was also consistent with life history theory, given that low LMA species with higher g_{max} would be expected to show greater stress sensitivity. Finally, the trade-off is consistent with theory that stomatal conductance and its dynamics evolved to enable maximum water use and therefore

photosynthetic productivity while reducing risk of hydraulic failure[1,8,20]. The mechanisms proposed would be interactive and mutually reinforcing, though our results do not exclude further mechanisms for the trade-off, including a role for the hormone abscisic acid which is involved in stomatal behavior[41].

The g_{max}- Ψ_{gs50} trade-off provides an important constraint on stomatal behavior in response to water supply. Stomatal behavior in response to soil and atmospheric water supply has often been considered according to a dichotomy or continuum from “isohydric” to “anisohydric” behaviors. Isohydric plants maintain high organ water potentials by closing stomata early during a drought, whereas anisohydric plants tolerate low water potentials, and maintain open stomata for prolonged photosynthesis[11]. However, recent work has shown that these useful categories can be difficult to define in a uniform way, especially as stomatal regulation alone does not explain leaf water potential maintenance, which depends on other internal and external variables such as hydraulic conductances throughout the plant, and soil water potential[21,42,43]. Further, the role of these categories in predicting species’ drought tolerance or water use has been questioned[43]. Several have suggested the consideration of alternative approaches for considering species’ overall variation in water relations. One alternative recommendation is to consider species on the basis of the response of g_s to Ψ_{leaf}[14]. Indeed, focusing on this response provides insights into processes at a range of scales—the response is directly related to leaf-scale physiology, and easily applied as a component of models to predict plant and ecosystem scale water use[14,44]. A g_{max}- Ψ_{gs50} trade-off that constrained variation in the response of g_s to Ψ_{leaf} across species would greatly simplify the consideration of this relationship across species within and across communities and ecosystems. Thus, according to the g_{max} - Ψ_{gs50} trade-off, many species may be expected to fall along a continuum from high g_{max} - high Ψ_{gs50} to low g_{max} - low Ψ_{gs50}. Notably, as for other functional trait trade-offs, outliers may be expected, as an important minority of individual

species would be expected to depart from this trade-off by evolving independent variation in either trait[48].

The g_{max}- Ψ_{gs50} trade-off would likely constrain stomatal behavior in a wide range of natural environments, especially during drought. Among stomatal responses to environmental factors, a quantitatively important role of closure in response to low Ψ_{leaf} in the overall regulation of stomatal conductance is supported by studies of species' stomatal responses to multiple environmental factors individually and in combination[10,45], by studies partitioning the role of Ψ_{leaf} in determining g_s diurnally and during periods of growth[46,47] and in studies of the role of the response of g_s to Ψ_{leaf} in predicting ecosystem water use[44]. Notably, the multiple dimensions of stomatal sensitivity to leaf water status present exciting avenues for further research. Species vary not only in the Ψ_{leaf} threshold for a given % closure, as examined in this study, but also in the timing of changes in g_s in response to changes in water status and multiple other factors[9,25,40,48]. Further studies are needed, for example, to determine whether there is an analogous trade-off between g_{max} and the speed of closure during a given level of dehydration.

Future studies are also needed of variation in the response of g_s to Ψ_{leaf} within and across individuals of a given species, as this response can show strong plasticity. Thus, g_{max} and Ψ_{gs50} can change with growing conditions, leaf age, and the degree and duration of water stress regime[11,49,50]. Further research should examine the possibility that the trade-off would apply for given species during progressive or repeated droughts, as would happen if g_{max} and Ψ_{gs50} both decline after a drought event due to plasticity[51].

The g_{max}- Ψ_{gs50} trade-off has potential implications for ecosystem-level processes. The trade-off would potentially influence species' distributions along gradients of evapotranspirational demand, as previously shown for safety-efficiency trade-offs in hydraulic conductance[15]. Further, the trade-off may scale up to influencing the water use of whole plants and ecosystems**.** While

multiple factors can decouple water use at plant scale from the response of g_s to Ψ_{leaf}, e.g., water storage capacitance, allocation to leaf area relative to sapwood area, and allocation to below versus above-ground biomass[44], measured and modelled plant and ecosystem water use show strong dependency on the g_s of the component species[52,53]. Indeed, the response of g_s to Ψ_{leaf} is fundamental in models for predicting water fluxes of individual plants and ecoregions especially under drought[13,20,38,44,54]. Given its generality, the g_{max}- Ψ_{gs50} trade-off therefore would have potential applications for prediction of plant water use at a range of scales.

2.5 Figures

Figure 2.1: Hypothesized rationales for a stomatal safety-efficiency trade-off.

(A) *Stomatal size and density*: leaves with smaller, denser stomata (left) have higher maximum stomatal conductance (g_{max}) and stomata more sensitive to closure during drought (i.e., higher Ψ_{gs50}, indicated by thinner red lines) than leaves with larger, less dense stomata (right); (B) *Osmotic concentration*: leaves with weaker osmotic potentials at full turgor and turgor loss (left) are associated with higher g_{max} and higher Ψ_{gs50} than leaves with stronger osmotic potentials (right); (C) *Leaf economics and life history trade-off*: species selected for greater resource acquisitiveness, and with lower leaf mass per area (LMA; top row) would have higher g_{max} and photosynthetic rate under high water supply (left column), and more sensitive stomatal closure under low water supply (right column) than species with high LMA (bottom row), which have lower g_{max} and photosynthetic rate under high water supply, and can better maintain stomatal conductance and photosynthetic rate under low water supply; (D) *Plant hydraulic design*: under high water supply (left column), species with high g_{max} have higher photosynthetic rate than species with low g_{max} and both maintain leaf turgor and xylem water column continuity; under low water supply (right column), species with high g_{max} must show sensitive stomatal closure (i.e., higher Ψ_{gs50}) and therefore strong reduction of photosynthetic rate to avoid leaf damage and xylem embolism (right column, top two schematics), whereas species with low g_{max} can maintain stomatal conductance and photosynthetic rate under low water availability (right column, lowest schematic).

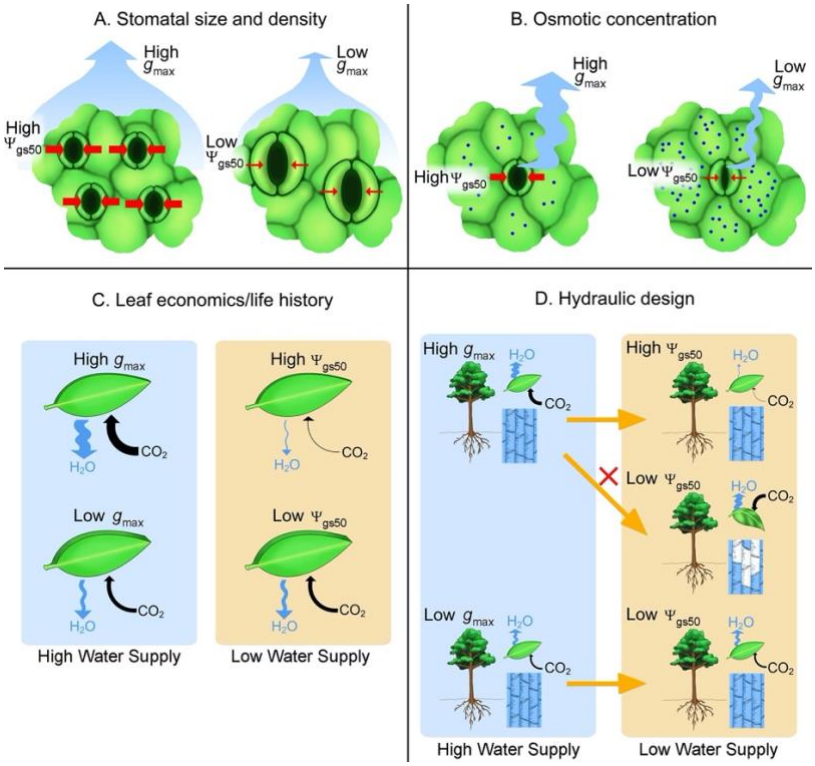

Figure 2.2: The generality of the stomatal safety-efficiency trade-off.

Relationship of maximum stomatal conductance (g_{max}) and sensitivity to stomatal closure (Ψ_{gs50}) for (A) 15 California species grown in a common garden design for this study (r = 0.69; P = 0.005; phylogenetic least squares regression), and in analyses of previous studies of stomatal responses in excised leaves or dehydrating plants of diverse species, measured with different techniques, and under different growing conditions (Pearson correlations): (B) 16 diverse angiosperm species (r = 0.50; P = 0.05)[75],(C) ten Chinese *Ficus* species[32] (r = 0.82; P = 0.003), (D) five European tree species[33] (r = 0.79; P = 0.03), (E) five tree species[76] (r= 0.95; P = 0.009), (F) eight tree species of Costa Rican dry forest[77] (r = 0.55; P > 0.05), (G) four woody species[45], (H) two *Vitis vinifera* cultivars[78], (I) two *Vaccinium* species of subalpine Austria[79] and (J) two varieties of a fern species[64]. The g_{max} and Ψ_{gs50} values were derived from fitted curves (Supplementary Figure 1). Lines are standard major axes for log-transformed data, i.e., for power law fits. Different scales were used in the panels to highlight the generality of the trend across studies of species diverse in stomatal responses to leaf water status. Source data are provided as a Source Data file.

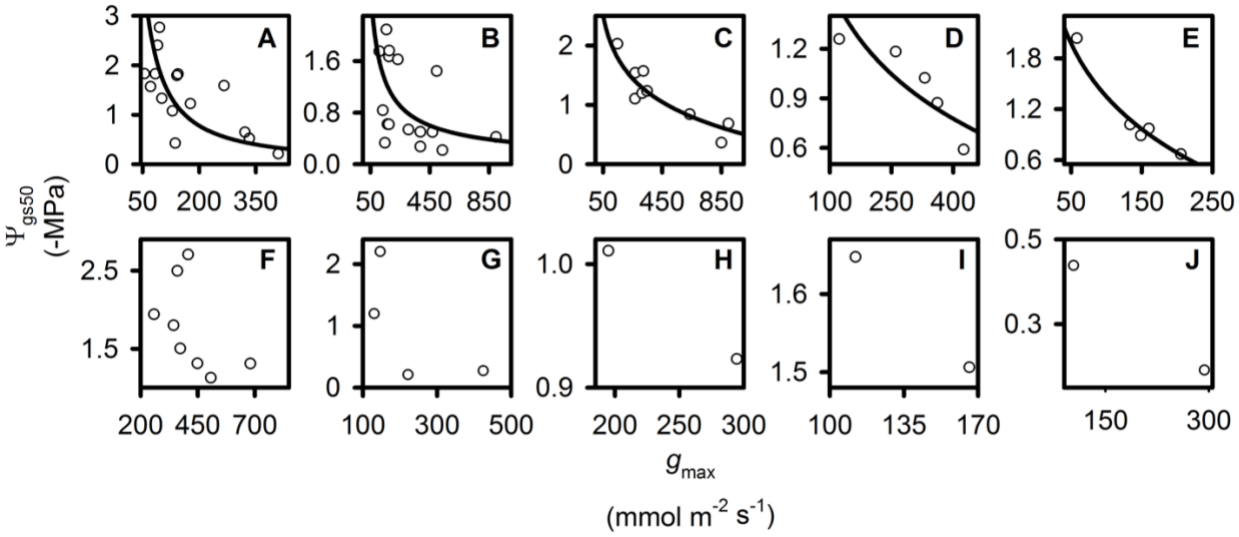

Figure 2.3: Testing hypothesized rationales for the stomatal safety-efficiency trade-off.

Relationships of maximum stomatal conductance (g_{max}) and the leaf water potential at 50% stomatal closure (Ψ_{gs50}) with (A) and (B) stomatal size (s; n = 12 species for which data were available); (C) and (D) osmotic potential at full turgor (π_o; n = 13 species for which data were available); and (E) and (F) leaf mass per area (LMA; n = 15 species). Lines are standard major axes for untransformed or log-transformed data, i.e., for linear or power law fits, depending on which showed a stronger fit. Phylogenetic least squares regression r values for panels (A)-(F) respectively were -0.56, 0.61, -0.82, 0.73, -0.61, and 0.56 (P= 0.0009-0.04). The g_{max} and Ψ_{gs50} values were derived from fitted curves (Supplementary Figure 1). Source data are provided as a Source Data file.

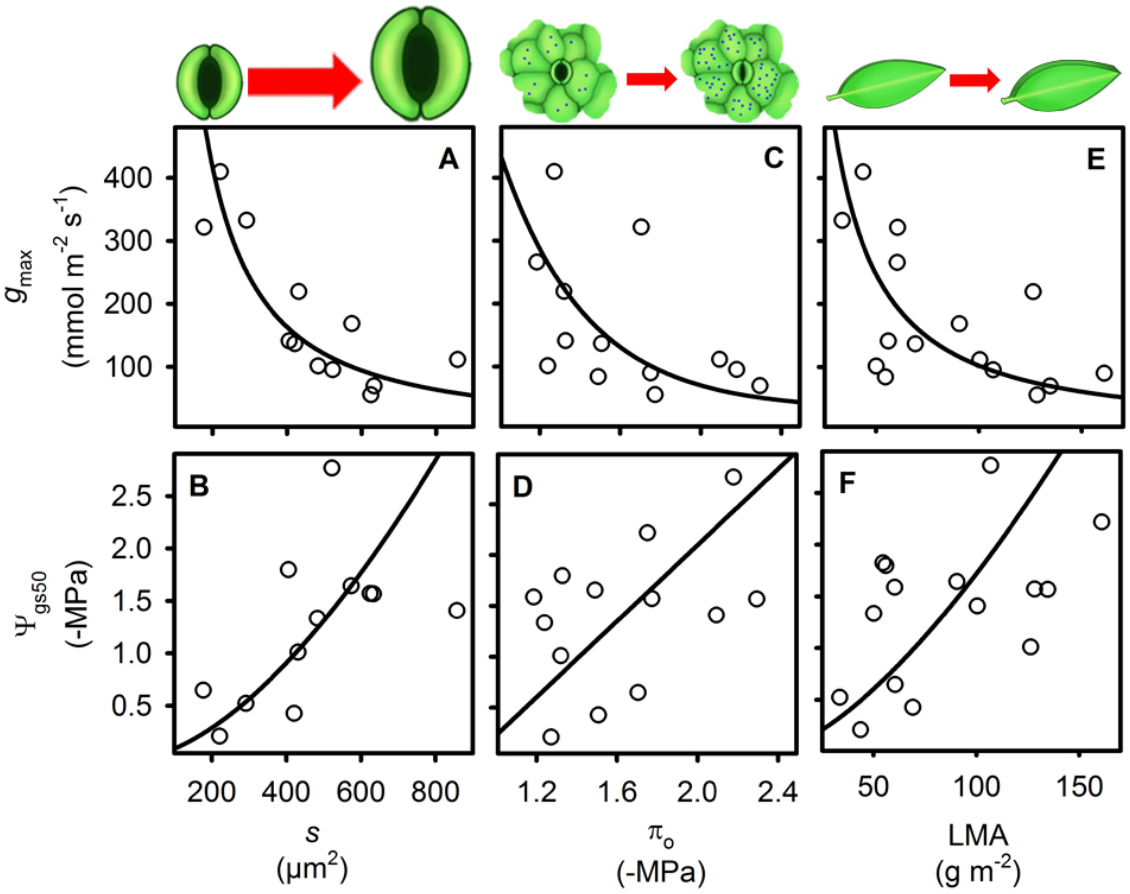

Figure 2.4: Testing for a benefit in plant hydraulic design of a stomatal efficiency-safety trade-off.

(A) contour plot shows modelled light saturated photosynthetic rate (A; units μmol m^{-2} s^{-1}) for simulated species with combinations of maximum stomatal conductance (g_{max}) and sensitivity to stomatal closure (Ψ_{gs50}) under high water availability, i.e., soil water (Ψ_{soil}) of 0 MPa; species with higher g_{max} had higher A whereas species with sensitive stomatal closure, i.e., .higher (lower numerical values of) Ψ_{gs50} had reduced A; (B) modelled stem water potential (Ψ_{stem}; units: MPa) for these simulated species under low water availability, i.e., Ψ_{soil} of -1.2 MPa; species with higher g_{max} had steeper declines in Ψ_{stem}, whereas species with higher (lower numerical values of) Ψ_{gs50} were protected from dehydration stress. The g_{max} vs Ψ_{gs50} trade-off for the 15 California species positioned these species in the optimal zone, with high enough g_{max} to achieve moderate to high values of A under high water availability, and sensitive enough stomatal closure (i.e., low enough numerical values of Ψ_{gs50}) to avoid hydraulic damage during drought. See Methods for model description and parameterization, and Supplementary Figure 3 for additional simulations, including of impacts on leaf water potential. Source data are provided as a Source Data file.

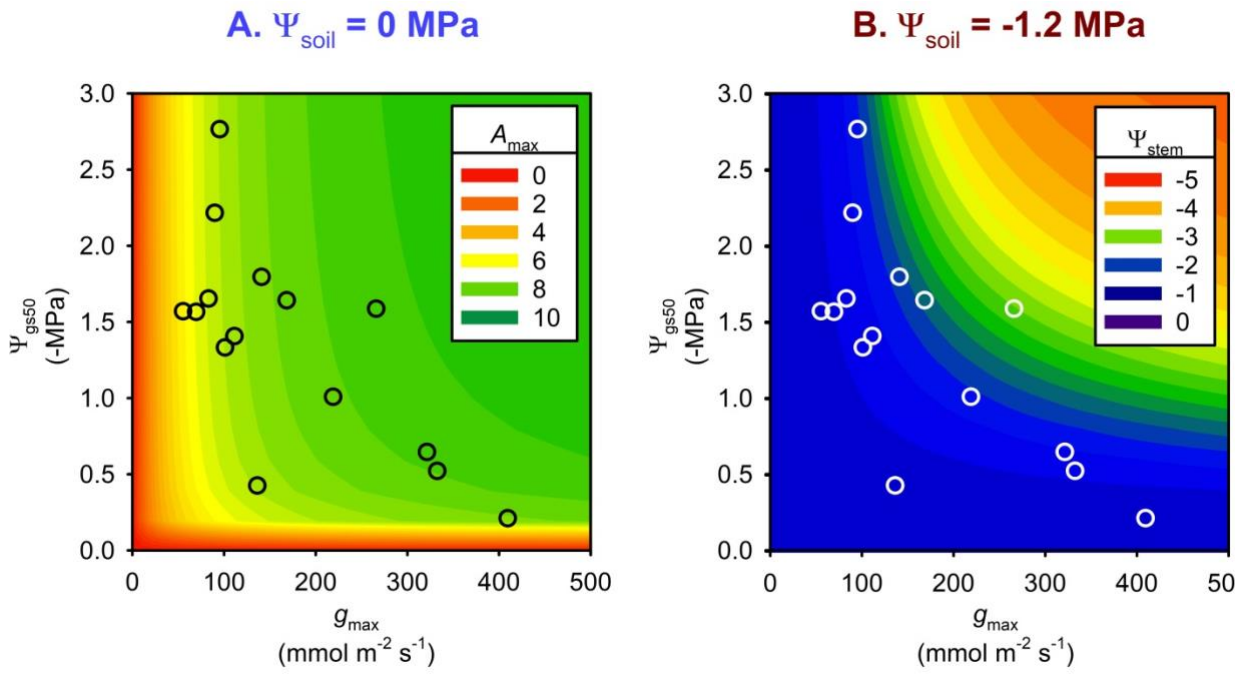

2.6 References

1 Anderegg, W. R. L. *et al.* Plant water potential improves prediction of empirical stomatal models. *Plos One* **12**, 17 (2017).

2 Hetherington, A. M. & Woodward, F. I. The role of stomata in sensing and driving environmental change. *Nature* **424**, 901-908 (2003).

3 Lin, Y. S. *et al.* Optimal stomatal behaviour around the world. *Nature Climate Change* **5**, 459-464 (2015).

4 Franks, P. J. & Farquhar, G. D. The mechanical diversity of stomata and its significance in gas-exchange control. *Plant Physiol* **143**, 78-87 (2007).

5 McElwain, J. C., Yiotis, C. & Lawson, T. Using modern plant trait relationships between observed and theoretical maximum stomatal conductance and vein density to examine patterns of plant macroevolution. *New Phytologist* **209**, 94-103 (2016).

6 Wong, S. C., Cowan, I. R. & Farquhar, G. D. Stomatal conductance correlates with photosynthetic capacity. *Nature* **282**, 424 (1979).

7 Tyree, M. T. & Zimmerman, M. H. *Xylem structure and the ascent of sap*. 2 edn, (Springer-Verlag Berlin Heidelberg, 2002).

8 Martin-StPaul, N., Delzon, S. & Cochard, H. Plant resistance to drought depends on timely stomatal closure. *Ecology Letters* **20**, 1437-1447 (2017).

9 Aasamaa, K. & Sober, A. Responses of stomatal conductance to simultaneous changes in two environmental factors. *Tree Physiol* **31**, 855-864, doi:10.1093/treephys/tpr078 (2011).

10 Aasamaa, K. & Sõber, A. Stomatal sensitivities to changes in leaf water potential, air humidity, CO2 concentration and light intensity, and the effect of abscisic acid on the

sensitivities in six temperate deciduous tree species. *Environmental and Experimental Botany* **71**, 72-78, doi:https://doi.org/10.1016/j.envexpbot.2010.10.013 (2011).

11 Jones, H. G. *Plants and microclimate: a quantitative approach to environmental plant physiology*. (Cambridge university press, 2013).

12 Bartlett, M. K., Klein, T., Jansen, S., Choat, B. & Sack, L. The correlations and sequence of plant stomatal, hydraulic, and wilting responses to drought. *Proceedings of the National Academy of Sciences of the United States of America* **113**, 13098-13103 (2016).

13 Christoffersen, B. O. *et al.* Linking hydraulic traits to tropical forest function in a size-structured and trait-driven model (TFS v.1-Hydro). *Geoscientific Model Development* **9**, 4227-4255 (2016).

14 Klein, T. The variability of stomatal sensitivity to leaf water potential across tree species indicates a continuum between isohydric and anisohydric behaviours. *Functional Ecology* **28**, 1313-1320 (2014).

15 Skelton, R. P., West, A. G. & Dawson, T. E. Predicting plant vulnerability to drought in biodiverse regions using functional traits. *Proceedings of the National Academy of Sciences of the United States of America* **112**, 5744-5749 (2015).

16 Dupont-Prinet, A. *et al.* Physiological mechanisms underlying a trade-off between growth rate and tolerance of feed deprivation in the European sea bass *Dicentrarchus labrax*. *The Journal of Experimental Biology* **213**, 1143-1152 (2010).

17 Grime, J. P. *Plant strategies and vegetation processes*. (John Wiley & Sons Ltd, 1979).

18 Torrao, G., Fontes, T., Coelho, M. & Rouphail, N. Integrated indicator to evaluate vehicle performance across: safety, fuel efficiency and green domains. *Accident Analysis and Prevention* **92**, 153-167 (2016).

19 Gleason, S. M. *et al.* Weak tradeoff between xylem safety and xylem-specific hydraulic efficiency across the world's woody plant species. *New Phytologist* **209**, 123-136 (2016).

20 Hacke, U. G., Sperry, J. S., Wheeler, J. K. & Castro, L. Scaling of angiosperm xylem structure with safety and efficiency. *Tree Physiology* **26**, 689-701 (2006).

21 Scoffoni, C. & Sack, L. The causes and consequences of leaf hydraulic decline with dehydration. *Journal of Experimental Botany* **68**, 4479-4496 (2017).

22 Manzoni, S. *et al.* Hydraulic limits on maximum plant transpiration and the emergence of the safety–efficiency trade-off. *New Phytologist* **198**, 169-178 (2013).

23 Silvertown, J., Araya, Y. & Gowing, D. Hydrological niches in terrestrial plant communities: a review. *Journal of Ecology* **103**, 93-108 (2015).

24 de Boer, H. J. *et al.* Optimal allocation of leaf epidermal area for gas exchange. *New Phytologist* **210**, 1219-1228 (2016).

25 Drake, P. L., Froend, R. H. & Franks, P. J. Smaller, faster stomata: scaling of stomatal size, rate of response, and stomatal conductance. *Journal of Experimental Botany* **64**, 495-505 (2013).

26 Aasamaa, K., Sober, A. & Rahi, M. Leaf anatomical characteristics associated with shoot hydraulic conductance, stomatal conductance and stomatal sensitivity to changes of leaf water status in temperate deciduous trees. *Australian Journal of Plant Physiology* **28**, 765-774 (2001).

27 DeMichele, D. W. & Sharpe, P. J. H. An analysis of the mechanics of guard cell motion. *Journal of Theoretical Biology* **41**, 77-96, doi:https://doi.org/10.1016/0022-5193(73)90190-2 (1973).

28 Lawson, T. & Blatt, M. R. Stomatal size, speed, and responsiveness impact on photosynthesis and water use efficiency. *Plant Physiol* **164**, 1556-1570 (2014).

29 Franks, P. J. Use of the pressure probe in studies of stomatal function. *Journal of Experimental Botany* **54**, 1495-1504 (2003).

30 Nonami, H. & Schulze, E. D. Cell water potential, osmotic potential, and turgor in the epidermis and mesophyll of transpiring leaves: Combined measurements with the cell pressure probe and nanoliter osmometer. *Planta* **177**, 35-46 (1989).

31 Brodribb, T. J. & Holbrook, N. M. Stomatal closure during leaf dehydration, correlation with other leaf physiological traits. *Plant Physiol* **132**, 2166-2173 (2003).

32 Hao, G. Y., Sack, L., Wang, A. Y., Cao, K. F. & Goldstein, G. Differentiation of leaf water flux and drought tolerance traits in hemiepiphytic and non-hemiepiphytic Ficus tree species. *Functional Ecology* **24**, 731-740 (2010).

33 Li, S. *et al.* Leaf gas exchange performance and the lethal water potential of five European species during drought. *Tree Physiology* **36**, 179-192 (2016).

34 Meinzer, F. C. *et al.* Mapping "hydroscapes' along the iso- to anisohydric continuum of stomatal regulation of plant water status. *Ecology Letters* **19**, 1343-1352 (2016).

35 Chapin, F. S. The mineral nutrition of wild plants. *Annual Review of Ecology and Systematics* **11**, 233-260 (1980).

36 Orians, G. H. & Solbrig, O. T. A cost-income model of leaves and roots with special reference to arid and semiarid areas. *American Naturalist* **111**, 677-690 (1977).

37 Wright, I. J. *et al.* The worldwide leaf economics spectrum. *Nature* **428**, 821-827 (2004).

38 Osborne, C. P. & Sack, L. Evolution of C_4 plants: a new hypothesis for an interaction of CO_2 and water relations mediated by plant hydraulics. *Philosophical Transactions of the Royal Society B-Biological Sciences* **367**, 583-600 (2012).

39 Brodribb, T. J., McAdam, S. A., Jordan, G. J. & Martins, S. C. Conifer species adapt to low-rainfall climates by following one of two divergent pathways. *Proceedings of the National Academy of Sciences* **111**, 14489-14493 (2014).

40 Martins, S. C. V., McAdam, S. A. M., Deans, R. M., DaMatta, F. M. & Brodribb, T. J. Stomatal dynamics are limited by leaf hydraulics in ferns and conifers: results from simultaneous measurements of liquid and vapour fluxes in leaves. *Plant, Cell & Environment* **39**, 694-705, doi:10.1111/pce.12668 (2016).

41 McAdam, S. A. & Brodribb, T. J. Separating active and passive influences on stomatal control of transpiration. *Plant Physiol* **164**, 1578-1586 (2014).

42 Hochberg, U., Rockwell, F. E., Holbrook, N. M. & Cochard, H. Iso/anisohydry: a plant-environment interaction rather than a simple hydraulic trait. *Trends Plant Sci* **23**, 112-120, doi:10.1016/j.tplants.2017.11.002 (2018).

43 Martínez-Vilalta, J. & Garcia-Forner, N. Water potential regulation, stomatal behaviour and hydraulic transport under drought: deconstructing the iso/anisohydric concept. *Plant, Cell & Environment* **40**, 962-976, doi:10.1111/pce.12846 (2017).

44 Mencuccini, M., Manzoni, S. & Christoffersen, B. Modelling water fluxes in plants: from tissues to biosphere. *New Phytologist* **222**, 1207-1222, doi:10.1111/nph.15681 (2019).

45 Guyot, G., Scoffoni, C. & Sack, L. Combined impacts of irradiance and dehydration on leaf hydraulic conductance: insights into vulnerability and stomatal control. *Plant Cell and Environment* **35**, 857-871 (2012).

46 Rodriguez-Dominguez, C. M. *et al.* Most stomatal closure in woody species under moderate drought can be explained by stomatal responses to leaf turgor. *Plant Cell and Environment* **39**, 2014-2026, doi:10.1111/pce.12774 (2016).

47 Scoffoni, C. *et al.* The causes of leaf hydraulic vulnerability and its influence on gas exchange in Arabidopsis thaliana. *Plant Physiol* (2018).

48 Lawson, T. & Vialet-Chabrand, S. Speedy stomata, photosynthesis and plant water use efficiency. *New Phytologist* **0**, doi:doi:10.1111/nph.15330 (2015).

49 Damour, G., Simonneau, T., Cochard, H. & Urban, L. An overview of models of stomatal conductance at the leaf level. *Plant, Cell & Environment* **33**, 1419-1438 (2010).

50 Nolan, R. H. *et al.* Differences in osmotic adjustment, foliar abscisic acid dynamics, and stomatal regulation between an isohydric and anisohydric woody angiosperm during drought. *Plant, cell & environment* **40**, 3122-3134 (2017).

51 Holloway-Phillips, M. M. & Brodribb, T. J. Minimum hydraulic safety leads to maximum water-use efficiency in a forage grass. *Plant, cell & environment* **34**, 302-313 (2011).

52 Franks, P. J., Berry, J. A., Lombardozzi, D. L. & Bonan, G. B. Stomatal function across temporal and spatial scales: deep-time trends, land-atmosphere coupling and global models. *Plant Physiol* **174**, 583-602, doi:10.1104/pp.17.00287 (2017).

53 Schulze, E.-D., Kelliher, F. M., Körner, C., Lloyd, J. & Leuning, R. Relationships among maximum stomatal conductance, ecosystem surface conductance, carbon assimilation rate, and plant nitrogen nutrition: a global ecology scaling excercise. *Annual Review of Ecology and Systematics* **25**, 629-662, doi:10.1146/annurev.es.25.110194.003213 (1994).

54 Kennedy, D. *et al.* Implementing plant hydraulics in the community land model, version 5. *Journal of Advances in Modeling Earth Systems* **11**, 485-513 (2019).

55 John, G. P., Henry, C. & Sack, L. Leaf rehydration capacity: associations with other indices of drought tolerance and environment. *Plant, Cell & Environment* **41**, 2638-2653 (2018).

56 Poorter, H., Bühler, J., van Dusschoten, D., Climent, J. & Postma, J. A. Pot size matters: a meta-analysis of the effects of rooting volume on plant growth. *Functional Plant Biology* **39**, 839-850 (2012).

57 Nardini, A., Peda, G. & La Rocca, N. Trade-offs between leaf hydraulic capacity and drought vulnerability: morpho-anatomical bases, carbon costs and ecological consequences. *New Phytologist* **196**, 788-798, doi:10.1111/j.1469-8137.2012.04294.x (2012).

58 Pasquet-Kok, J., Creese, C. & Sack, L. Turning over a new 'leaf': multiple functional significances of leaves versus phyllodes in Hawaiian Acacia koa. *Plant Cell and Environment* **33**, 2084-2100, doi:10.1111/j.1365-3040.2010.02207.x (2010).

59 Duursma, R. A. *et al.* On the minimum leaf conductance: its role in models of plant water use, and ecological and environmental controls. *New Phytologist* **221**, 693-705, doi:10.1111/nph.15395 (2019).

60 Grubb, P. J. Trade-offs in interspecific comparisons in plant ecology and how plants overcome proposed constraints. *Plant Ecology & Diversity* **9**, 3-33 (2016).

61 Scoffoni, C. *et al.* Outside-Xylem Vulnerability, Not Xylem Embolism, Controls Leaf Hydraulic Decline during Dehydration. *Plant Physiol* **173**, 1197-1210, doi:10.1104/pp.16.01643 (2017).

62 Burnham, K. P. & Anderson, D. R. *Model Selection and Multimodel Inference*. (2002).

63 Sack, L. & Buckley, T. N. The developmental basis of stomatal density and flux. *Plant Physiol* **171**, 2358-2363 (2016).

64 Cardoso, A. A., Randall, J. M. & McAdam, S. A. Hydraulics Regulate Stomatal Responses to Changes in Leaf Water Status in the Fern Athyrium filix-femina. *Plant Physiol* **179**, 533-543 (2019).

65 Sperry, J. S., Adler, F. R., Campbell, G. S. & Comstock, J. P. Limitation of plant water use by rhizosphere and xylem conductance: results from a model. *Plant Cell and Environment* **21**, 347-359 (1998).

66 Farquhar, G. D., von Caemmerer, S. & Berry, J. A. A biochemical model of photosynthetic CO_2 assimilation in leaves of C_3 species. *Planta* **149**, 78-90 (1980).

67 Peña-Rojas, K., Aranda, X. & Fleck, I. Stomatal limitation to CO_2 assimilation and down-regulation of photosynthesis in *Quercus ilex* resprouts in response to slowly imposed drought. *Tree Physiology* **24**, 813-822 (2004).

68 R: a language and environment for statistical computing (2008).

69 Sokal, R. R. a. R., F.J. *Biometry: the principles and practice of statistics in biological research.* 3 edn, (W.H. Freeman and Co., 1995).

70 Warton, D. I., Wright, I. J., Falster, D. S. & Westoby, M. Bivariate line-fitting methods for allometry. *Biological Reviews* **81**, 259-291 (2006).

71 Zanne, A. E. *et al.* Three keys to the radiation of angiosperms into freezing environments. *Nature* **506**, 89-92 (2014).

72 Webb, C. *Phylomatic v3*, <http://phylodiversity.net/phylomatic/> (2012).

73 Freckleton, R., Harvey, P. & Pagel, M. Phylogenetic analysis and comparative data: A test and review of evidence. *The American Naturalist* **160**, 712-726 (2002).

74 Garland, T., Bennett, A. F. & Rezende, E. L. Phylogenetic approaches in comparative physiology. *Journal of Experimental Biology* **208**, 3015 (2005).

75 Trueba, S. *et al.* Thresholds for leaf damage due to dehydration: declines of hydraulic function, stomatal conductance and cellular integrity precede those for photochemistry. *The New phytologist*, doi:10.1111/nph.15779 (2019).

76 Gindaba, J., Rozanov, A. & Negash, L. Response of seedlings of two *Eucalyptus* and three deciduous tree species from Ethiopia to severe water stress. *Forest Ecology and Management* **201**, 121-131 (2004).

77 Brodribb, T. J., Holbrook, N. M., Edwards, E. J. & Gutierrez, M. V. Relations between stomatal closure, leaf turgor and xylem vulnerability in eight tropical dry forest trees. *Plant Cell and Environment* **26**, 443-450 (2003).

78 Tombesi, S., Nardini, A., Farinelli, D. & Palliotti, A. Relationships between stomatal behavior, xylem vulnerability to cavitation and leaf water relations in two cultivars of Vitis vinifera. *Physiologia Plantarum* **152**, 453-464 (2014).

79 Ganthaler, A. & Mayr, S. Dwarf shrub hydraulics: two *Vaccinium* species (*Vaccinium myrtillus*, *Vaccinium vitis-idaea*) of the European Alps compared. *Physiologia Plantarum* **155**, 424-434 (2015).

3. Chapter 3: Foliar water uptake: relationship to leaf structure in native California species

3.1 Introduction

Leaf traits have important influences on the adaptation of species to climate and ecological niches, and are thus associated with species' distributions and their ongoing responses to climate change. Yet, while a rich literature has focused on leaf traits that influence economics of gas exchange and leaf longevity[1,2], the mechanistic basis for other critical physiological leaf traits are still in discovery phase. Plant foliar surface water uptake (FWU) has been reported in a wide diversity of plants[3], but its relationship to cuticular and lamina tissue properties have not been elucidated. Previous studies have shown that foliar water uptake is slow yet substantial over long periods, and thus rehydration of leaves may occur at night, during fog or rainfall events, and may enable rapid photosynthetic activity early in the day, or transiently when air is humid especially when soil is dry. Thus, FWU has potentially strong adaptive value under a wide range of environmental conditions, from arid or high salinity systems to fog-, rain- and cloud forests dominated by species with high hydraulic sensitivity, to Mediterranean climate species[3]. We aimed to determine the potential for the association of FWU with leaf structural traits, including trichomes, across a diverse species set, and potentially with species' native climate. The quantification of foliar water uptake as a transport efficiency can be accomplished through measurement of its hydraulic conductance (K_{surf}). We measured K_{surf} for leaves in fog chambers for 12 species grown in a greenhouse common garden (Table 1), comprised by paired species with contrasting trichome abundances from six California woody genera with diverse leaves and adapted to a wide range of aridity in their native habitat.

K_{surf} can be measured using the time constant for water uptake based on initial and final leaf water potentials, and the leaf capacitance[4,5]. Previous studies have reported a decline in K_{surf}

with time after initial exposure to surface moisture[3-5]. We refined the calculation of K_{surf} to account for the effect that, as the leaf rehydrates, the capacitance would decline, due to the dilution of solutes, and thus we derived an improved estimate accounting for declining capacitance (Appendix 1).

We further analyzed the causality of K_{surf} by considering the first constraint to surface rehydration of the leaf, i.e., vapor uptake into the dehydrated leaf through the stomata, or liquid water across the cuticularized epidermis. Recent studies have attributed K_{surf} to stomatal vapor uptake[4,6-8] based on experiments showing K_{surf} was modulated by hormones that influence stomatal aperture[4]. Yet, liquid movement across cuticle in highly humid environments has also been proposed[9-12]. We thus tested whether K_{surf} could be accounted for by vapor uptake through closed stomata by comparing values with minimum epidermal conductance in dehydrated leaves (g_{min}), and for operating stomatal conductance in light saturated leaves (g_{op}).

We additionally hypothesized that K_{surf} would depend on trichome number and size. Leaf trichomes are found on 30% of vascular land plant species[13], tend to be correlated with drought stress and elevation[14,15,16,17], and play many roles affecting water use, light absorption and temperature, and thereby photosynthetic efficiency, transpiration rates and leaf water status, as well as vulnerability to herbivores. and herbivore deterrence[18,19,20,21,22,23,24,12,25-31]. Several recent studies have suggested that leaf hairs may play multiple, and opposite causal influences on K_{surf}. These studies have suggested that multicellular (living) hair showing improved water uptake, whereas species possessing unicellular (dead) hair reducing water uptake due to a hydrophobic surface above the leaf lamina[32,33]. Yet, studies applied different approaches and the association of K_{surf} with leaf hairs has not been assessed quantitatively across multiple species. We thus tested the association of K_{surf} with trichome density and size, and the proportion of living to dead trichomes, as well as with derived traits, including trichome surface area and volume per leaf area.

We also tested whether K_{surf} would be related to leaf structural and pressure-volume parameters. We hypothesized that K_{surf} would be related to leaf capacitance, and traits that contribute to capacitance per leaf area including leaf thickness and leaf mass per area. Such an association would be expected if leaves with high water storage would benefit from higher K_{surf}, to restore stored water; in that case, K_{surf} would be related to leaf thickness, and potentially leaf mass per area and leaf water mass per area. We also tested and other pressure-volume parameters, such as turgor loss point. If leaf osmotic potential is a driving force for K_{surf} water uptake, then we would expect a higher K_{surf} to correspond to a more negative osmotic potential, within and across species. We also tested the hypothesis that species with high light-saturated photosynthetic gas exchange, and associated traits such as nitrogen per mass (N_{mass}) , percent nitrogen per area (N_{area}), Chlorophyll per area (Chl_{area}), Chlorophyll per mass (Chl_{mass}), Chlorophyll: nitrogen ratio (Chl/N), and carbon isotopic composition ($\partial\ ^{13}C$) would be associated with high K_{surf}. This would be the case if K_{surf} might play a role in enabling species with high gas exchange rates to recover after rainfall, and thus contribute to their ability to "avoid" drought with rapid gas exchange after short rainfall events.

Finally, we tested whether K_{surf} varied across species in association with climatic aridity and/or drought tolerance traits hypothesizing that species adapted to water stress would have greater foliar water uptake to benefit from atmospheric recharge as an alternative to root rehydration, especially those species with greater water storage, or dependency for survival on stored water.

3.2 Results

The dynamics of leaf surface hydraulic conductance (K_{surf})

Across all species, K_{surf} as calculated with a constant capacitance was highly correlated with K_{surf} accounting for the shift in capacitance with rehydration (for 1h, 8h and 24h, r = 0.85-0.95 for K_{surf}' vs K_{surf}; P <0.001; Tables S1, S2, S3 and S10); Thus, data reported in the main text are corrected for the capacitance shift (K_{surf}'), with the noncorrected values and their correlations presented in the supplement (Tables S1 and S2). For all species, K_{surf}' declined with time (Fig. 1), comparing the first hour, the first 8 hours and 24 hours (Fig. 2; Tables S1, S2 and S9). Across species, K_{surf} was correlated when considered for the first 1h, 8h and 24 h (Table S10; r = 0.66-0.85 and P = <0.001 to 0.05 for relationships between $K_{surf,1h}$, $K_{surf,8h}$ and $K'_{surf,24h}$, and $K'_{surf,1h}$, $K'_{surf,8h}$ and $K'_{surf,24h}$)

We found strong variation in $K'_{surf,1h}$ across the 12 species of native California trees, shrubs and vines (Fig. 1; Tables S1 and S9), including strong variation within and among genera. $K'_{surf,1h}$ ranged from 0.03 mmol m^{-2} MPa^{-1} s^{-1} for *Vitis girdiana* to 0.52 mmol m^{-2} MPa^{-1} s^{-1} for *Salvia apiana*; at 8h ranged from 0.01 mmol m^{-2} MPa^{-1} s^{-1} for *Vitis girdiana* to 0.1 mmol m^{-2} MPa^{-1} s^{-1} for *Clematis lasiantha* and at 24h ranged from 0.008 mmol m^{-2} MPa^{-1} s^{-1} for *Vitis girdiana* to 0.07 mmol m^{-2} MPa^{-1} s^{-1} for *Clematis lasiantha*.

Variation across species in K_{surf} independent of g_{min} and g_{op}, and cannot be explained by stomatal vapor uptake

Across species, $K'_{surf,1h}$ and $K'_{surf,24h}$ was correlated with g_{min} and $K'_{surf,1h}$was correlated with g_{op}, and K_{surf} at all times was higher than both (Fig 2; Table S10). $K'_{surf,1h}$, when considered in units of "stomatal conductance" (i.e., mmol m^{-2} s^{-1}), by considering the driving force for transpiration, was across species 135-285-fold higher than g_{min} (on average 211-fold) and 2914-3592-fold (on average, 3253-fold) greater than g_{op}, i.e., the stomatal conductance of well-illuminated leaves (Fig. 2c).

Variation among species in leaf water relations, structure and gas exchange

We found pronounced variation in many leaf traits across and/or within the six genera (Tables S1 and S9). Considering pressure volume and other water relations traits, we found 5-fold variation among species in SWC, 3-fold in π_o, 2-fold in π_{tlp}, 15% difference in RWC_{tlp}, 24% difference in RWC_{tlp_sym}, 3-fold in elastic modulus, 8-fold in mod_{sym}, 2-fold in C_{tlp}, 3-fold in C_{ft}, 2-fold in C_{tlp_sym}, 4-fold in C_{ft_sym}, 4-fold in C_{ft_abs}, 4-fold in g_{min}, and 4-fold in t60_t.

Species also varied strongly in leaf morphology. Species varied 161-fold in LA, 2-fold in LT, 8-fold in LMA, 3-fold in SWMA (Tables S1 and S9).

Species also varied strongly in gas exchange, with 8-fold variation among species in g_{op}, and 3-fold variation in $A_{max.}$ (Tables S1 and S9).

Species varied strongly in leaf trichome traits (Figs 3-7; Tables S1 and S9). Species varied 937- to 960-fold in TD_{ad} and TD_{ab}; 440-fold in TL_{ad} and 21-fold in TL_{ab}; 28- to 40-fold in Td_{tip_ad}, Td_{base_ad}, and $Td_{central\_ad}$; 2- to 11-fold in Td_{tip_ab}, Td_base_ab, and Td_central_ab; 9-fold in $CSA_{central\_ad}$, and 47-fold variation among species in $CSA_{central\_ab}$; 200,629-fold in TV_{ad} and 13-fold in TV_{ab}; 3089-fold in TBALA, 12155-fold in TCALA, 11615-fold in TSALA, 8711-fold in TVLA, 13-fold variation among species in TBA, 16-fold variation among species in TSA.

Testing the association of $K'_{surf,1h}$ with leaf water relations and structural traits

We found that $K'_{surf,1h}$ was related to leaf capacitance, which was one of the determinants in its calculation (Tables S2 and S10). Thus, $K'_{surf,1h}$ was positively related to CFT_{abs} (r =0.61; P =0.003) and C_{tlp} (r =0.48; P =0.01).

For three genera (*Clematis, Encelia, Salvia*), the species with higher TD had higher K'_{surf}1h, whereas for two genera (*Arctostaphylos* and *Vitis*), the species with lower TD had higher

K'_{surf}1h (Fig. 1; Table S1). Two genera (*Clematis* and *Encelia*) had higher K'_{surf}8h for the species with higher TD, and three genera (*Arctostaphylos, Salvia,* and *Vitis*) had lower K'_{surf}8h for species with higher TD. Three genera (*Clematis, Encelia, Salvia*) had higher K'_{surf}24h for the species with higher TD, and two genera (*Arctostaphylos* and *Vitis*) had lower K'_{surf}24h for species with higher TD.

Across species, $K'_{surf,1h}$ was related to leaf trichome density (Table S11). Thus, $K'_{surf,1h}$ was positively correlated with TD_{ab} (r =0.79; P =0.0002), TD_{ad} (r =0.72; P =.001), and TD_{tot} (r =0.77; P =0.0004; Figure 8A). $K'_{surf,1h}$ was also related to stomatal traits. Thus, $K'_{surf,1h}$ was positively related to SD_{ab} (r =.45; P =0.02), SD_{ad} (r =0.43; P =0.03) and SD_{tot} (r =0.56; P =0.01; Figure 8B)

Testing the association of $K'_{surf,1h}$ with leaf gas exchange and nutrient composition

We found that $K'_{surf,1h}$ was related to leaf gas exchange (Table S10). Thus, $K'_{surf,1h}$ was positively related to A_{max} (r =0.50; P =0.01) and g_{op} (r =0.63; P =0.03)

Testing the association of K_{surf} with climate

K_{surf} values were independent of species' native climate (Table S10). No correlations were observed between K_{surf}, K'_{surf} at 1h or 8h or 24h with any of the tested climatic variables.

3.3 Discussion

We found strong foliar water uptake in the diverse 12 species of native California trees, shrubs and vines within six genera. The rates of foliar water uptake were within the range of those of previous studies[3-7,12,26,51,52]. Further our analyses showed that foliar water uptake declined with time, due to a decline in the hydraulic conductance to foliar water uptake (K_{surf}). Our findings demonstrated that K_{surf} could not be accounted for by vapor uptake through the stomata, in

contrast to the hypotheses proposed in previous studies[4,6]. Further, we demonstrated novel linkages of K_{surf} with leaf structure. We found that K_{surf} was strong in all species, independent of the climate of species' native distribution.

The dynamics of leaf surface hydraulic conductance (K_{surf})

Our analyses enabled a novel determination of K_{surf}, accounting for the shift in capacitance that would occur as leaves dehydrate (K_{surf}). We found that across all species, K_{surf} as calculated with a constant capacitance was highly correlated with K_{surf} . K_{surf} declined with time (Fig. 1), comparing the first hour, the first 8 hours and 24hours. This decline of K_{surf} with time has been reported in previous studies[4,6,53]. The decline of K_{surf} with time implies a shift in the properties of water uptake, potentially implicating either a chance in the uptake properties of cuticle and/or permeability of cell membranes in rehydrating cells, which may arise due to changes in aquaporin expression or activity[54].

Variation across species in K_{surf} cannot be explained by stomatal vapor uptake

Across species, $K'_{surf,1h}$ was statistically associated with both g_{min} and g_{op}, and was substantially higher than both (Fig 2). Our analysis of K_{surf}, considered in units of "stomatal conductance" (i.e., mmol m^{-2} s^{-1}), in comparison with operating stomatal conductance is the first to our knowledge and showed a substantially higher uptake conductance than was found under illuminated leaves during the day. Thus, given that stomata would have been closed in the dark, humid conditions, we find that K_{surf} could not be accounted for by stomatal vapor uptake. Given that stomatal architecture prevents liquid water uptake, the high K_{surf} values measured must depend on liquid uptake through the cuticle. Our conclusion is at odds with previous studies that concluded that K_{surf} was principally determined by vapor uptake through stomata, based on studies that showed

that K_{surf} was sensitive to hormones that would modulate stomatal aperture, such as abscisic acid, which closes stomata, and fusicoccin, which opens stomata[4,6]. Yet, that study estimated K_{surf} based on a capacitance value from a pressure-volume curve on leaves that were not treated with these substances; previous work shows that leaf capacitance would also be responsive to these compounds[55], which would have explained the apparent responses of K_{surf}; thus, those studies do not conclusively show that K_{surf} is responsive to stomatal aperture changes. Indeed, the uptake of water across the cuticle is consistent with studies that show that cuticular conductance increases dramatically with humidity[9].

Linkage of $K'_{surf,1h}$ with leaf structural, water relations and epidermal traits

$K'_{surf,1h}$ differed across species, and between species with more and fewer trichomes within genera. Notably, in three genera the higher $K'_{surf,1h}$ was found for the species with more trichomes and in three genera the lower $K'_{surf,1h}$ for the species with more trichomes. This finding indicates that in certain species trichomes may increase $K'_{surf,1h}$, yet, in other species, however, trichomes may reduce $K'_{surf,1h}$. This difference may relate to the hydrophobicity of the trichomes[32]. Notably, across all species, $K'_{surf,1h}$ was related to trichome density, a pattern arising from the two species with highest trichome densities, *Encelia* and *Salvia*, which also had highest $K'_{surf,1h}$.

Independence of $K'_{surf,1h}$ from the native climate of species' distributions

We found that all species showed substantial $K'_{surf,1h}$, and that $K'_{surf,1h}$ was not related to mean climate variables for species' distributions, despite species having been selected from across an aridity gradient. Yet, $K'_{surf,1h}$ was related to leaf time to death after stomatal closure, implying that species that depend on stored water to survive dry periods benefit from a high $K'_{surf,1h}$ to recharge their water storage. This role for $K'_{surf,1h}$ merits further investigation.

3.4 Methods

Plant material

Fully developed leaves of 12 species of native California trees and shrubs were used in this study. Species were chosen based on phylogenetic relatedness and their presence of hair. Plants were cultivated in a greenhouse common garden at the UCLA Plant Growth Center from February 2019 to July 2020. 15 individual seedlings of each species were acquired in 1 L pots (Rancho Santa Ana Botanic Garden; Claremont, CA), and randomized within each of 10 blocks containing one individual of each species spread across five greenhouse benches in two greenhouse rooms. Plants were acclimated 12–18 months prior to initial measurements, developing canopies of mature leaves under the similar external conditions. Plants were carefully monitored for root expansion and repotted into 5 gallon pots when roots filled the pots. Potting soil (18.75% washed plaster sand, 18.75% sandy loam, 37.5% grower grade peat moss, 12.5% horticultural grade perlite, 12.5% coarse vermiculite; Therm-O-Rock West, Inc., Chandler, AZ) was autoclaved prior to use. Plants were irrigated every second day with 200–250 ppm 20:20:20 NPK fertilizer. Daily irradiance ranged up to 1400 μmol m^{-2} s^{-1} (LI-250 light meter; LI-COR Biosciences, Lincoln, NE, USA), while mean minimum, mean and maximum values for temperature, 15.8°C, 19.8°C, 24.5°C; for relative humidity 31.6%, 61.4%, 93.0% over the course of our experiments (HOBO Micro Station with Smart Sensors; Onset, Bourne, MA, USA).

Leaf rehydration through the epidermal surface

For rehydration kinetics, five branches of each species were collected in the evening, enclosed in a dark bag and transported back to the laboratory to be rehydrated overnight. Excised branches were bench dried over a fan to different water potentials (0.48-2.2 ±.002 MPa) and placed into dark bags with wet paper towels to allow for water potential equilibrium among all

leaves on the branch. Leaf water potential (Ψ_{leaf}) was measured to determine the level hydration using a pressure (Plant Moisture Stress pressure chamber model 1000; PMS Instrument Co., Albany, OR, USA). Prior to starting rehydration experiments, leaves were substantially dried and leaf water potential was later confirmed to be within to be ≥80% of turgor loss point; branches bearing leaves with a less negative water potential than described were allowed to continue drying. Eight leaves per individual per species were selected for measurement on each shoot. Two leaves were measured for initial water potential (Ψ_i). These leaves were selected from the top and bottom of the branch. After confirmation of initial leaf water potential, leaves were collected from the middle of the shoot for rehydration. The kinetics of water absorption via the leaf surface was analyzed using a custom "fog chamber"[6]. The chamber was comprised of two stacked polystyrene foam coolers. The bottom cooler was used as a compartment to feed the fog source into the top cooler. The fog source was an ultrasonic humidifier producing room temperature submicron fog droplets. Prior to fog exposure, leaves had their petioles sealed with hot candle wax to prevent further water loss after excision. Leaves were individually suspended in the fog chamber with no contact among leaves. Three leaves were excised from the branch and rehydrated Ψ_{leaf} after 1, 8 and 24 hours (Ψ_1, Ψ_8 and Ψ_{24}). Only one measurement per leaf was made to avoid changes in absorptive properties. Leaves exposed to the fog chamber were patted with napkins at each time point, at least 3 hours after the first time point and at least 10 hours after the second time point to prevent water collecting on the surface. Species of *Arctostaphylos* and *Monardella* had leaves too small to be suspended in the fog chamber and were instead rehydrated from wax sealed stem segments with at least 8 leaves.

Following these measurements, the leaf surface area was determined by analyzing the scanned material with ImageJ software (ImageJ 1.45s National Institutes of Health, Bethesda,

MD, USA). Then, leaves were oven-dried at >70ºC for two weeks and the final dry weight was recorded.

Determination of pressure-volume curves, leaf structure and turgor loss point

We constructed pressure volume curves for an additional set of 12 woody and non-woody species. Mature individuals of each species grown in the plant growth center of the University of California, Los Angeles (minimum, mean and maximum values for temperature, 15.8°C, 19.8°C, 24.5°C; for relative humidity 31.6%, 61.4%, 93.0%; and for irradiance 1.2, 31.4, 1336 µmol photons m^{-2} s^{-1}). Leaf pressure volume curve parameters were determined using the bench drying method[34]. Shoots with full developed sun leaves from six individuals were harvested in the afternoon of the day prior to measurements and transported to the lab in plastic bags with wet paper towels. From each shoot, two nodes were recut under deionized water, and shoots were rehydrated overnight under plastic. From the plotted curves; we determined osmotic potential at full turgor (π_o) and water potential at turgor loss point (π_{tlp}), RWC at turgor loss point (RWC_{tlp}), modulus of elasticity (ε), capacitance at turgor loss point (C_{tlp}), leaf area (LA) and capacitance at full turgor (C_{ft}). One leaf from each of six individuals were used for measurements. Due to limited availability of individuals, we constructed pressure volume curve parameters for two leaves of three individuals of *Clematis lasiantha*. When “plateau effects” were detected during early dehydration, these measurements were excluded before estimation of pressure-volume parameters[35].

Leaf structure was measured for 4 leaves on each of 5 individual plants of each species. Leaf area was measured using a flatbed scanner and imageJ. Leaf mass was measured using a digital analytic balance. Leaf thickness was measured using digital calipers. Leaf mass per area was determined as the ratio of leaf mass to area.

Determination of minimal conductance and leaf drought survival time

We measured minimum epidermal conductance (g_{min}) for 6 leaves per individual per species for each species. After rehydrating individual leaves for > 8 hours, we measured saturated leaf mass (± 0.01 mg; MS205DU; Mettler Toledo, OH) and area (flatbed scanner; ImageJ software version 1.42q; National Institutes of Health). Leaves were suspended by their petioles over a fan for 30 minutes to 2 hours to force stomatal closure, and then weighed at 15-minute intervals for at least 2 hours, after which leaf area was measured again. We collected ambient temperature and relative humidity at 30 second intervals using a weather station (HOBO Micro Station with Smart Sensors; Onset, Bourne, MA, USA). After measurements, leaves were oven dried for three days at 70º C and weighed for dry mass, and g_{min} calculated from the minimum epidermal transpiration rate divided by mole fraction vapor pressure deficit and by the twice the mean projected leaf area[36].

We estimated leaf survival time due to dehydration after stomatal closure, using the g_{min} measurements and values for leaf saturated water content (SWC; units g g^{-1}) and leaf mass per area (LMA; units g m^{-2}). We calculated the time to reach relative water content of 60% ($t_{60\%}$; units h), previously recognized as a threshold for damage or lethality[37-39].

$$t_{60\%} = \frac{\mathrm{SWC} \times \mathrm{LMA} \times 60\%}{g_{\min} \times 18.0 \times \mathrm{VPD} \times 2} \quad (2)$$

where 18.0 g mol^{-1} is the molar mass of water, and water loss was assumed to occur from both leaf faces. A VPD of 2.5 kPa (at atmospheric pressure = 101.3 kPa; mole-fraction = 0.025 mol mol^{-1}) was used for calculations, though species comparisons would be robust to other values. The leaf saturated water mass per area (SWMA; units g m^{-2}) was calculated as the product of SWC and LMA.

Gas exchange measurements

Leaf gas exchange measurements were taken using a Portable Photosynthesis System (LI-COR 6400; LI-COR Inc, Lincoln, NE, USA). For three to five individuals of each species, Measurements of Photosynthetic rate (A_{max}), Conductance to H_2O (g_{op}), Transpiration rate (E), Vapor pressure deficit based on Leaf temperature (VPD), Temperature of leaf thermocouple (T_{leaf}), Intercellular CO^2 concentration (Ci), and Leaf water potential (Ψ) were taken from 10:00-14:00, and averaged for each species. Measurements were taken at saturating light (1,000 µmol/m2/s) after a 10-min acclimation period with the leaf in the chamber at vapor pressure deficit <1 kPa. Intrinsic water use efficiency (A_{max}/g_{op}) was determined as the ratio of A_{max} to g_{op}.

Measurement of trichome traits

Leaf hair traits were measured on images of the adaxial and abaxial surfaces one leaf from each of three individuals of each species (except *Monardella macrantha*) from the synchrotron at The Advanced Light Source – Lawrence Berkeley National Laboratory (Beamline 8.3.2). We measured trichome density (TD), trichome length (TL) and the diameters of trichomes at the base (Td_{base}), midpoint ($Td_{central}$) and tip (Td_{tip}). Trichomes were measured of different types; data were combined in this study. We calculated trichome central cross sectional area ($CSA_{central}$) as $\pi \times (0.5 \times Td_{central})^2$. We calculated trichome basal area (TBA) as $\pi \times (0.5 \times Td_{base})^2$. We calculated trichome volume (TV) and trichome surface area (TSA) by considering the trichome as a conical frustrum[40], and with volume = $1/3 \times \pi \times TL \times (0.5 \times Td_{base})^2 + 0.5 \times Td_{base} \times 0.5 \times Td_{tip} \times (0.5 \times Td_{tip})^2$ and surface area = $\pi \times (0.5 \times Td_{base} + 0.5 \times Td_{tip}) \times [(0.5 \times Td_{base} - 0.5 \times Td_{tip})^2 + TL^2]^{0.5}$. We calculated trichome central area per leaf area (TCALA) as $TD \times CSA_{central}$, trichome basal area per leaf area (TBALA) as TD × TBA, trichome volume per leaf area (TVLA) as TD × TV,

and trichome surface area per leaf area (TSALA) as TD × TSA. We also calculated total trichome density (TD_{tot}) on abaxial and adaxial surfaces of each leaf.

Measurements of leaf composition and nutrient analysis

Nutrient data were obtained from 4 leaves each from 5 individual plants of 11 species. Leaves were oven dried at 70°C for at least 72 hours. Liquid nitrogen was then poured over the leaves as they were ground with a mortar and pestle into a fine powder. 3-4mg of material were weighed into tin 4 × 6 capsules and were sent to the Center for Stable Isotope Biogeochemistry at the University of California, Berkeley. Carbon isotope ratio (δ13C) was measured by dual isotope analysis with an Elemental Analyzer interfaced to a mass spectrometer, along with the percent of nitrogen in the sample. Nitrogen per leaf mass (N_{mass}; mg g-1) was determined as the mass nitrogen in the sample (mg) per the mass of the sample (g). Nitrogen per leaf area (N_{area}; g m^{-2}) was determined as N_{mass} multiplied by LMA. Chl_{area} was measured with a SPAD meter. Chl_{mass} was determined as the quotient of Chl_{area} and LMA. Chl/N was determined as the quotient of Chl_{area} and N_{area}.

Analyses of relationships to climate

Occurrence records were downloaded using the '*rgbif*' package[41] and filtered to keep herbarium records since 1950 and remove incomplete (latitude or longitude missing) and duplicated records, non-natural occurrences (e.g., records from botanical gardens or planted urban trees)[41]. We extracted 30 environmental variables from open-access raster layers, relating to air temperature (WorldClim, CRU[42]), precipitation (WorldClim[42]), aridity (CGIAR-CSI, NCAR-UCAR[43]) and soil characteristics (ISRIC Soilgrids[44]) (see Table S1 for all variables). The raster layers with the same resolution were stacked using the stack function from the 'raster' package[45]

and the environmental variables for each occurrence record were extracted using the extract function from the '*dismo*' package[46]. Due to their coarse resolution, these environmental variables are effective in characterizing large scale patterns but do not reflect differences in microclimate, i.e., temperature, water and nutrient availability, irradiance and soil composition[47]. The MAT, MAP, AI, and PET data were extracted at each coordinate for each species using ArcMap, and averaged for each species (Table 1).

Statistics

Results of analyses of variance for traits measured for 12 native California woody species within six genera. Results are presented for three ANOVAs: (1) repeated-measures ANOVA testing differences in foliar surface hydraulic conductance measured at three times (1, 8 and 24h), testing for variation among species, and among time intervals, and within species and time intervals; (2) nested ANOVA testing differences in traits among genera, and between species within genera, and within (Minitab 21; State College, PA, USA).

To test species' trait-trait and trait-environment relationships while explicitly accounting for species relatedness, we performed phylogenetic generalized least-squares analyses (PGLS[48,49]) using the *pgls* function from the '*caper*' package[50] with lambda (λ) optimized using maximum likelihood. Analysis of variance were performed for untransformed and log transformed data, to test for either approximately linear or non-linear (i.e., approximate power law) relationships respectively.

3.5 Appendix

I. Inferring leaf surface conductance from rehydration kinetics, with dynamic capacitance

The rate of increase of total water content (W_t, mol) during rehydration is the rate of flow into the leaf, *F*, or

$$\frac{dW_t}{dt} = F = K\Delta\psi = -K\psi\,, \qquad (A1)$$

where *K* is the conductance for rehydration and Ψ is the water potential; Ψ is the difference between turgor pressure (*P*) and osmotic pressure (π):

$$\psi = P - \pi\ . \qquad (A2)$$

To a reasonable approximation (Bartlett et al. 2012), *P* can be modeled as a linear function of symplastic relative water content (*r*), between full turgor (*r* =1) and the turgor loss point (*r* = *r*′), and at full turgor *P* equals osmotic pressure at full turgor, π_o:

$$P = \pi_o \frac{r - r'}{1 - r'}\,. \qquad (A3)$$

Assuming no change in leaf osmotic content, osmotic pressure is π_o divided by symplastic relative water content:

$$\pi = \frac{\pi_o}{r}\,. \qquad (A4)$$

Applying A4 and A3 to A2 gives water potential as

$$\psi = \pi_o \left(\frac{r - r'}{1 - r'} - \frac{1}{r}\right). \qquad (A5)$$

Applying A5 to A1 gives

$$\frac{dW_t}{dt} = -K\pi_o\left(\frac{r-r'}{1-r'} - \frac{1}{r}\right). \qquad \text{(A6)}$$

To link W_t and r, note that r is given by

$$r = \frac{W}{W_o}, \qquad \text{(A7)}$$

where W is symplastic water content, W_o is symplastic water content at full turgor, and W is related to W_t as

$$W = W_t - W_a = W_t - a_f W_{to}, \qquad \text{(A8)}$$

where W_a is apoplastic water content, and a_f is apoplastic fraction of leaf water content at full turgor ($a_f = W_a/W_{to}$, where W_{to} is total leaf water content at full turgor). The rate of change of symplastic water content is thus

$$\frac{dW}{dt} = \frac{dW}{dW_t}\frac{dW_t}{dt} = -K\pi_o\left(\frac{r-r'}{1-r'} - \frac{1}{r}\right). \qquad \text{(A9)}$$

Expressed in terms of r, this is

$$\frac{dr}{dt} = \frac{dr}{dW}\frac{dW}{dt} = -\frac{K\pi_o}{W_o}\left(\frac{r-r'}{1-r'} - \frac{1}{r}\right). \qquad \text{(A10)}$$

The quantity in parentheses on the right hand side can be written as a ratio of polynomials in r:

$$\frac{dr}{dt} = -\frac{K\pi_o}{W_o}\left(\frac{(r-r')r-(1-r')}{(1-r')r}\right) = -\frac{K\pi_o}{(1-r')W_o}\cdot\left\{\frac{r^2-[r']r-[1-r']}{r}\right\}. \qquad \text{(A11)}$$

Note that A11 is correct only above the turgor loss point; below TLP, $P = 0$, so that

$$\frac{dr}{dt} = -\frac{K\pi_o}{W_o}\left(-\frac{1}{r}\right) = -\frac{K\pi_o}{(1-r')W_o}\left(-\frac{1-r'}{r}\right). \qquad \text{(A12)}$$

Integrating A11 and A12 and assuming *K* is constant gives

$$-\frac{1}{1-r'}\int_{t=0}^{t=t*} rdr + \int_{t=t*}^{t=t_f} \frac{rdr}{r^2 - r'r - (1-r')} = -\frac{K\pi_o}{(1-r')W_o}\int_{t=0}^{t=t_f} dt\ , \qquad \text{(A13)}$$

where t_f is the time at which final water potential is measured and t^* is the first time between t = 0 and $t = t_f$ at which Ψ is equal to or greater than the TLP; if Ψ is above the TLP at t = 0, then t^* = 0, and if y is below the TLP at $t = t_f$, then $t^* = t_f$. *K* is assumed constant. The integral on the right is simply

$$-\frac{K\pi_o}{(1-r')W_o}t_f\ . \qquad \text{(A14)}$$

The integral at far left is

$$-\frac{1}{2}\left(\frac{r^{*2} - r_i^2}{1-r'}\right)\ , \qquad \text{(A15)}$$

where r_i and r^* are the values of r at t = 0 and t^*, respectively. To solve the second integral on the left, complete the square in the denominator by adding and subtracting $r'^2/4$:

$$\int \frac{rdr}{r^2 - r'r - (1-r')} = \int \frac{rdr}{r^2 - r'r + \frac{1}{4}r'^2 - \frac{1}{4}r'^2 - (1-r')}$$

$$= \int \frac{rdr}{\left(r - \frac{1}{2}r'\right)^2 - \sqrt{\frac{1}{4}r'^2 + 1 - r'}^2}\ . \qquad \text{(A16)}$$

Substituting $u = r - r'/2$ and defining the radical as $z = \sqrt{\frac{1}{4}r'^2 + 1 - r'}$ gives

$$\int \frac{rdr}{\left(r-\frac{1}{2}r'\right)^2-\sqrt{\frac{1}{4}r'^2+1-r'}^2}=\int \frac{u+\frac{1}{2}r'}{u^2-z^2}du\,. \qquad \text{(A17)}$$

The integrand can be decomposed by partial fractions, thus:

$$\frac{u+\frac{1}{2}r'}{u^2-z^2}=\frac{u+\frac{1}{2}r'}{(u-z)(u+z)}=\frac{A}{u-z}+\frac{B}{u+z}=\frac{A(u+z)+B(u-z)}{(u-z)(u+z)}$$
$$=\frac{(A+B)u+(A-B)z}{(u-z)(u+z)}\,. \qquad \text{(A18)}$$

By inspection, $A + B = 1$ and $A - B = r'/2z$, giving $B = -r'/4z + 1/2$ and $A = +r'/4z + 1/2$, and making the integral

$$\int \frac{u+\frac{1}{2}r'}{u^2-z^2}du=\left(\frac{r'}{4z}+\frac{1}{2}\right)\int\frac{du}{u-z}-\left(\frac{r'}{4z}-\frac{1}{2}\right)\int\frac{du}{u+z}\,, \qquad \text{(A19)}$$

whose solution (with limits of integration u^* and u_f, corresponding to t^* and t_f, respectively) is

$$\left(\frac{r'}{4z}+\frac{1}{2}\right)\ln\left|\frac{u_f-z}{u^*-z}\right|-\left(\frac{r'}{4z}-\frac{1}{2}\right)\ln\left|\frac{u_f+z}{u^*+z}\right|\,. \qquad \text{(A20)}$$

Reversing the substitution as $r = u + r'/2$ and combining with the solutions to the other integrals gives

$$-\frac{1}{2}\left(\frac{r^{*2}-r_i^2}{1-r'}\right)+\left(\frac{r'}{4z}+\frac{1}{2}\right)\ln\left|\frac{r_f-\frac{1}{2}r'-z}{r^*-\frac{1}{2}r'-z}\right|-\left(\frac{r'}{4z}-\frac{1}{2}\right)\ln\left|\frac{r_f-\frac{1}{2}r'+z}{r^*-\frac{1}{2}r'+z}\right|$$
$$=-\frac{K\pi_o}{(1-r')W_o}t_f\,, \qquad \text{(A21)}$$

Note that applying ψ=0 (and r=1) to the solution for r as a function of ψ (A37 below) gives

$$1 = \frac{1}{2}r'\left(1 + \sqrt{1 + \frac{4(1-r')}{r'^2}}\right). \qquad \text{(A22)}$$

thus

$$1 - \frac{1}{2}r' = \frac{1}{2}r'\sqrt{1 + \frac{4(1-r')}{r'^2}} = \sqrt{\frac{1}{4}r'^2 + 1 - r'} = z \qquad \text{(A23)}$$

Applying $z = 1 - r'/2$ to A21 eliminates z from the solution, giving

$$-\frac{1}{2}\left(\frac{r^{*2} - r_i^2}{1-r'}\right) + \left(\frac{r'}{4\left(1-\frac{1}{2}r'\right)} + \frac{1}{2}\right)\ln\left|\frac{r_f - \frac{1}{2}r' - \left(1-\frac{1}{2}r'\right)}{r^* - \frac{1}{2}r' - \left(1-\frac{1}{2}r'\right)}\right| - \left(\frac{r'}{4\left(1-\frac{1}{2}r'\right)} - \frac{1}{2}\right)\ln\left|\frac{r_f - \frac{1}{2}r' + \left(1-\frac{1}{2}r'\right)}{r^* - \frac{1}{2}r' + \left(1-\frac{1}{2}r'\right)}\right| = -\frac{K\pi_o}{(1-r')W_o}t_f\,. \qquad \text{(A24)}$$

This can be simplified to

$$-\frac{1}{2}\left(\frac{r^{*2} - r_i^2}{1-r'}\right) + \left(\frac{1}{2-r'}\right)\ln\left|\frac{r_f - 1}{r^* - 1}\right| + \left(\frac{1-r'}{2-r'}\right)\ln\left|\frac{r_f + 1 - r'}{r^* + 1 - r'}\right| = -\frac{K\pi_o}{(1-r')W_o}t_f\,, \qquad \text{(A25)}$$

and finally to

$$-\frac{1}{2}\left(\frac{r^{*2} - r_i^2}{1-r'}\right) + \left(\frac{1}{2-r'}\right)\ln\left|\left(\frac{r_f - 1}{r^* - 1}\right)\left(\frac{r_f + 1 - r'}{r^* + 1 - r'}\right)^{1-r'}\right| = -\frac{K\pi_o}{(1-r')W_o}t_f\,. \qquad \text{(A26)}$$

Solving for K gives

$$K = \frac{W_o}{2\pi_o t_f}\left(r^{*2} - r_i^2\right) - \frac{W_o}{\pi_o t_f}\left(\frac{1-r'}{2-r'}\right)\ln\left|\left(\frac{r_f - 1}{r^* - 1}\right)\left(\frac{r_f + 1 - r'}{r^* + 1 - r'}\right)^{1-r'}\right|. \qquad \text{(A27)}$$

An additional simplification is possible, as follows. Note that differentiating A5 gives

$$\frac{d\psi}{dr} = \pi_o\left(\frac{1}{1-r'} + \frac{1}{r^2}\right) = \frac{\pi_o(r^2 + 1 - r')}{(1-r')r^2}\,. \qquad \text{(A28)}$$

By definition, capacitance $C \equiv dr/d\psi$, so C is the inverse of A28:

$$C \equiv \frac{dr}{d\psi} = \frac{(1-r')r^2}{\pi_o(r^2 + 1 - r')}\,. \qquad \text{(A29)}$$

At full turgor, $r = 1$, so capacitance at full turgor (C_{FT}) is

$$C_{FT} = \frac{1}{\pi_o}\left(\frac{1-r'}{2-r'}\right). \qquad \text{(A30)}$$

Applying A30 to A27 gives the general solution for K as

$$K = \frac{W_o}{t_f}\left(\frac{r^{*2} - r_i^2}{2\pi_o} - C_{FT}\ln\left|\left(\frac{r_f - 1}{r^* - 1}\right)\left(\frac{r_f + 1 - r'}{r^* + 1 - r'}\right)^{1-r'}\right|\right). \qquad \text{(A31)}$$

For rehydration curves that start at or above the TLP, $r^* = r_i$, giving the solution as

$$K = -\frac{W_o C_{FT}}{t_f}\ln\left|\left(\frac{1-r_f}{1-r_i}\right)\left(\frac{r_f + 1 - r'}{r_i + 1 - r'}\right)^{1-r'}\right|. \qquad \text{(A32)}$$

For rehydration curves that start below and end above the TLP, $r^* = r'$, giving the solution as

$$K = \frac{W_o}{t_f}\left(\frac{r'^2 - r_i^2}{2\pi_o} - C_{FT}\ln\left|\left(\frac{1-r_f}{1-r'}\right)(r_f + 1 - r')^{1-r'}\right|\right). \qquad \text{(A33)}$$

For hydration curves that end below the TLP, $r^* = r_f$, and the solution is

$$K = \frac{W_o}{t_f}\left(\frac{r_f^2 - r_i^2}{2\pi_o}\right). \qquad \text{(A34)}$$

To apply A31-A34 using values of final and initial water potential during rehydration curves (ψ_f and ψ_i, respectively), r_f and r_i can be found from ψ_f and ψ_i by inverting A5 to give a quadratic in r:

$$0 = r^2 - \left(\frac{\psi}{\pi_o}(1 - r') + r'\right)r - (1 - r'), \qquad \text{(A35)}$$

whose solution is

$$r = \frac{1}{2}\left(\frac{\psi}{\pi_o}(1 - r') + r'\right)\left(1 \mp \sqrt{1 + \frac{4(1 - r')}{\left(\frac{\psi}{\pi_o}(1 - r') + r'\right)^2}}\right). \qquad \text{(A36)}$$

To identify the correct root, note that $r = 1$ when $\psi = 0$, whereas the negative root would make $r < r'/2$; thus the positive root is the correct one, and r_f and r_i are found by applying $\psi = \psi_f$ and $\psi = \psi_i$, respectively, to A37 if $\psi > -\pi_o$ (i.e., above TLP), or A38 if $\psi \leq -\pi_o$ (below TLP):

$$r = \frac{1}{2}\left(\frac{\psi}{\pi_o}(1 - r') + r'\right)\left(1 + \sqrt{1 + \frac{4(1 - r')}{\left(\frac{\psi}{\pi_o}(1 - r') + r'\right)^2}}\right), \qquad \text{(A37)}$$

$$r = -\frac{\pi_o}{\psi}. \qquad \text{(A38)}$$

II. Converting liquid-phase leaf surface conductances for rehydration from a saturated atmosphere into equivalent vapor-phase conductances

Water flow between the leaf and its external surroundings, F, can be expressed either as a product of a hydraulic conductance (K_{surf}) and a water potential difference ($\Delta\psi$), or as a vapor-phase conductance (g_{surf}) and a water vapor mole fraction difference (Δw):

$$F = K_{surf}\Delta\psi = g_{surf}\Delta w\,. \qquad (A39)$$

Thus, g_{surf} and K_{surf} are related as

$$\therefore\ g_{surf} = K_{surf}\frac{\Delta\psi}{\Delta w}\,. \qquad (A40)$$

Assuming that the leaf and air are at exactly the same temperature, and that the air is saturated with water vapor, then the water potential of the air is zero, giving $\Delta\psi = 0 - \psi_{leaf} = -\psi_{leaf}$ and $\Delta w = w_{sat}(T_{leaf}) - w_{leaf}(\Psi_{leaf})$, where $w_{sat}(T)$ is the saturated water vapor mole fraction at the temperature T. The equilibrium relationship between liquid water with a water potential ψ and an adjacent atmosphere with actual and saturated water vapor mole fractions w and w_{sat}, respectively, all at a temperature T_K (kelvins), is

$$\psi = \frac{RT_K}{V_w}\ln\frac{w}{w_{sat}}\,, \qquad (A41)$$

where R is the gas constant (8.314462 Pa m^3 mol^{-1} K^{-1}), V_w is the molar volume of liquid water ($1.8\cdot10^{-5}$ m^3 mol^{-1}), ψ is given in Pa, and w is given in mol mol^{-1}. This gives w as

$$w = w_{sat}\cdot\exp\left(\frac{\psi V_w}{RT_K}\right). \qquad (A42)$$

Δw is thus

$$\Delta w = w_{sat} - w_{leaf} = w_{sat}\cdot\left(1 - \exp\left(\frac{\psi_{leaf}V_w}{RT_{leaf,K}}\right)\right). \qquad (A43)$$

where $T_{leaf,K}$ is the leaf temperature in kelvins. At sea level, w_{sat} is given by

$$w_{sat} = \frac{611.2}{101325} \cdot \exp\left(\frac{17.62 \cdot T_{leaf,C}}{243.12 + T_{leaf,C}}\right). \qquad \text{(A44)}$$

At 25°C, w_{sat} = 0.031187 mol mol^{-1}, and the quantity $V_w/(RT_{leaf,K})$ in A43 is 7.2611·10^{-9} Pa^{-1} = 0.0072611 MPa^{-1} . Applying this to A40 gives

$$g_{surf} = \frac{-K_{surf}\psi_{leaf}}{0.031187 \cdot \left(1 - \exp\left(0.0072611 \cdot \psi_{leaf}\right)\right)}. \qquad \text{(A45)}$$

where K_{surf} is in units of mol m^{-2} s^{-1} MPa^{-1}, ψ_{leaf} (≤ 0) is in MPa, and g_{surf} is in units of mol m^{-2} s^{-1}. For ψ_{leaf} not too far from zero, the argument in the exponential in the denominator is quite close to zero, in which case the denominator is approximately equal to minus the argument (because $e^x \approx x + 1$ for $x \approx 0$, so $1 - e^x \approx -x$), or

$$g_{surf} \approx \frac{K_{surf}\psi_{leaf}}{0.031187 \cdot 0.0072611 \cdot \psi_{leaf}} = 4416 \cdot K_{surf}. \qquad \text{(A46)}$$

If K_{surf} is given in mmol m^{-2} s^{-1} MPa^{-1}, then $g_{surf} \approx 4.416 \cdot K_{surf}$.

3.6 Figures

Figure 3.1: Hydraulic conductance to foliar surface water uptake

Hydraulic conductance to foliar surface water uptake, corrected for changing capacitance, for leaves exposed to fog in chambers for 1, 8 or 24 hours, of twelve Californian species, two species differing in trichome abundance within each of six genera.

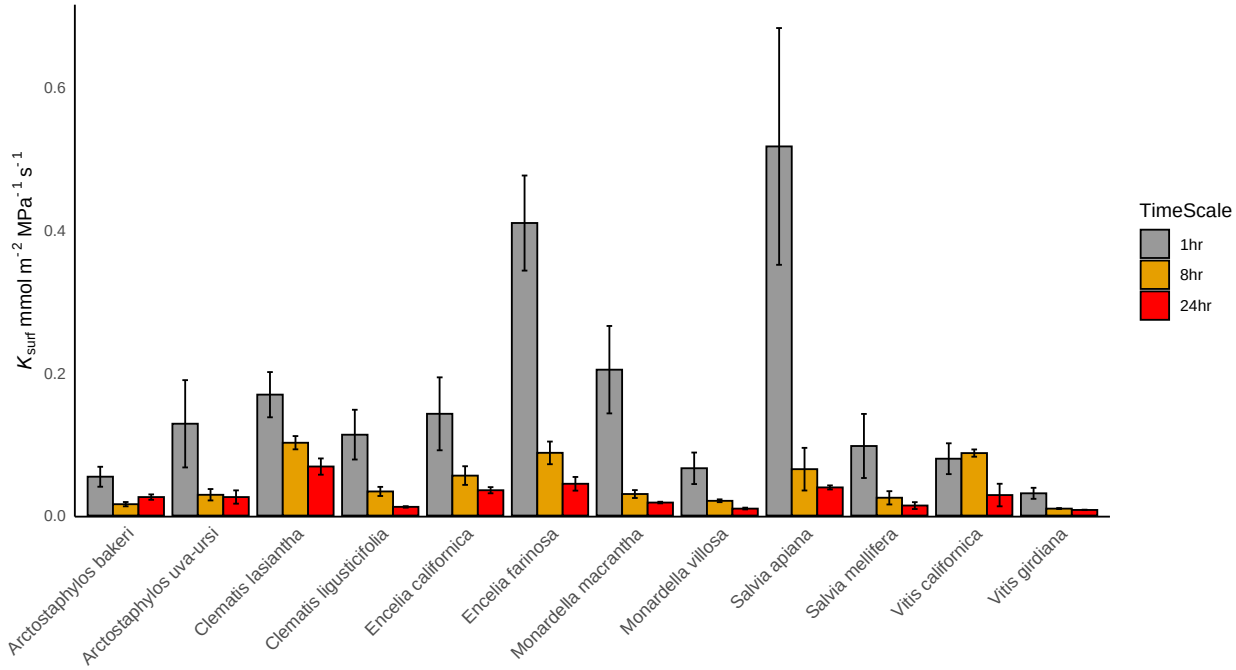

Figure 3.2: Relationships of foliar surface hydraulic conductance

Relationships of foliar surface hydraulic conductance, corrected for changing capacitance $K'_{surf,1h}$ and $K'_{surf,24h}$ (A and B respectively) to minimum surface conductance to diffusion (g_{min}) and of $K'_{surf,1h}$ with operating stomatal conductance at mid-day under light saturating conditions (g_{op}). Plotted lines are regressions (r = 0.62, 0.68, 0.63 and in panels A, B and C; P = 0.031, 0.014, 0.029). Ksurf is reported in units of hydraulic conductance (left y-axis) and units of diffusion conductance (right y-axis), enabling comparison with surface conductances to diffusion. Note that Ksurf values are much larger than gmin values and gop values in the same units; all points are above the 1:1 line plotted in each figure, though that line is not distinct from the x-axis in panels A and B; it is the lower line in panel C.

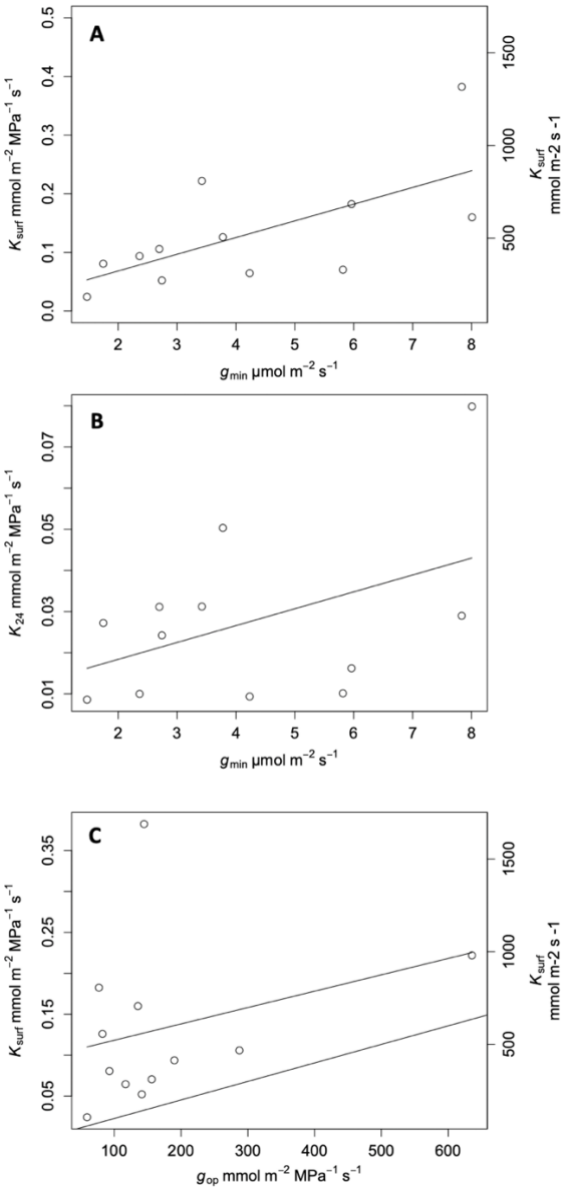

Figure 3.3: Micrographs of abaxial leaf surfaces

Micrographs of abaxial leaf surfaces for two species within each of three Californian genera, with the species on the left having denser trichomes than that on the right.

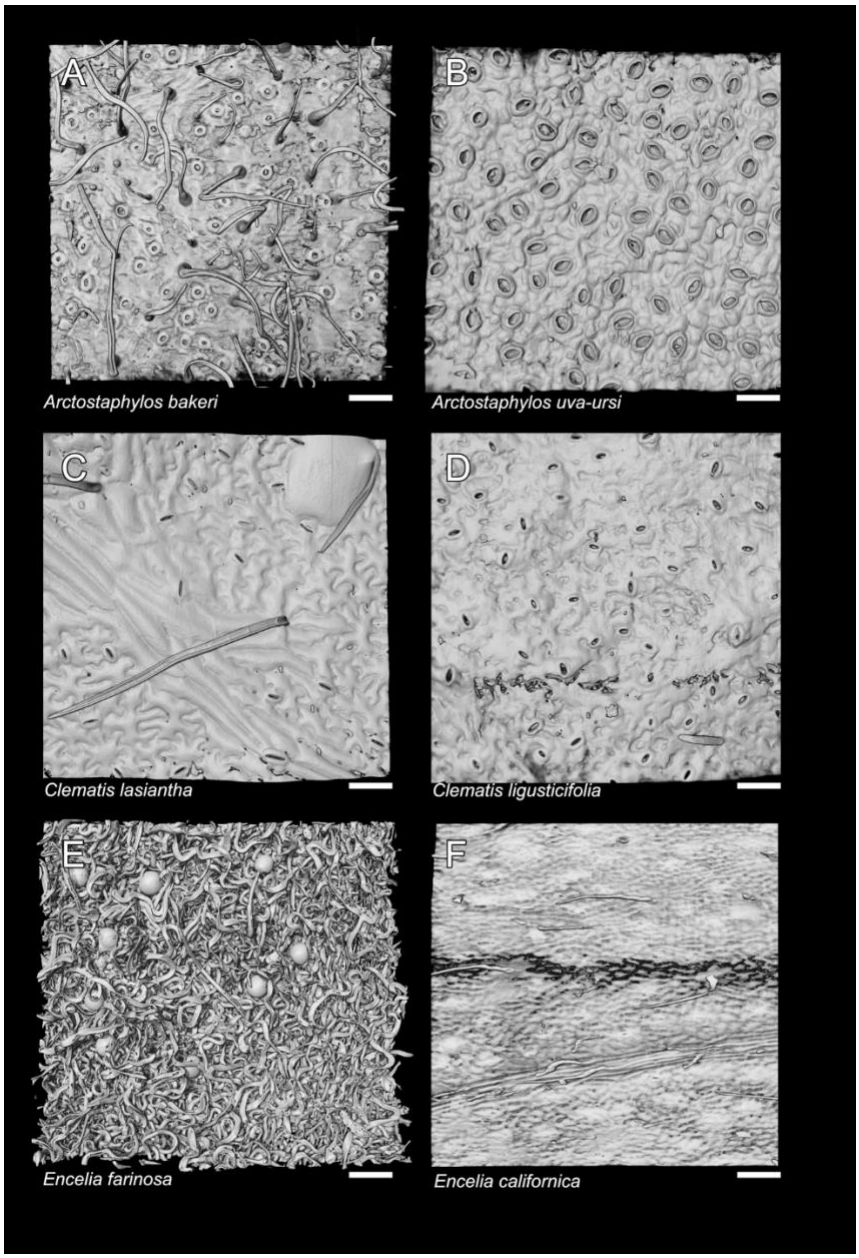

Figure 3.4: Micrographs of abaxial leaf surfaces

Micrographs of abaxial leaf surfaces for species within each of three Californian genera, with the species on the left having denser trichomes than that on the right. (Image not available for *Monardella macrantha*).

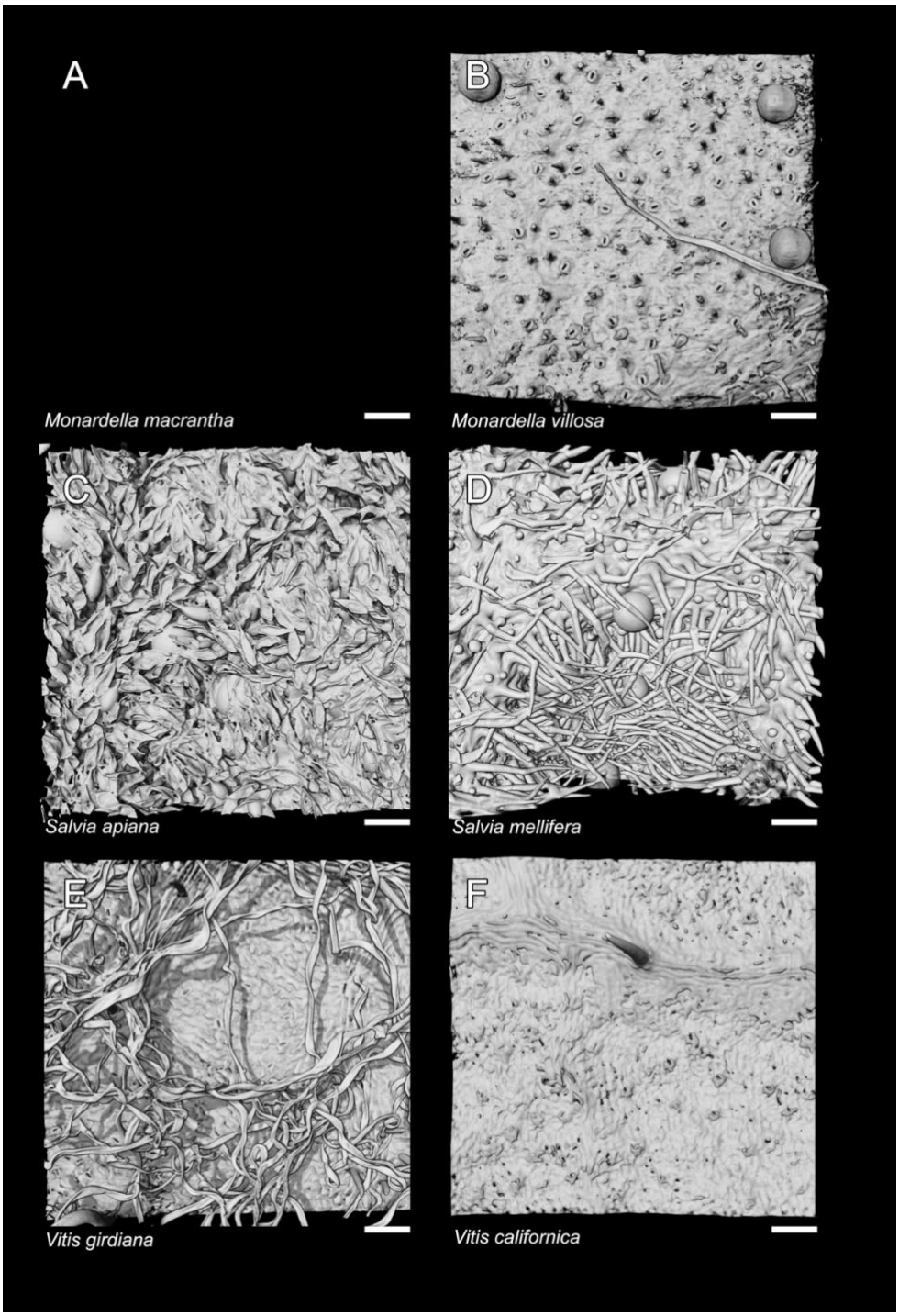

Figure 3.5: Micrographs of adaxial leaf surfaces

Micrographs of adaxial leaf surfaces for two species within each of three Californian genera, with the species on the left having denser trichomes than that on the right.

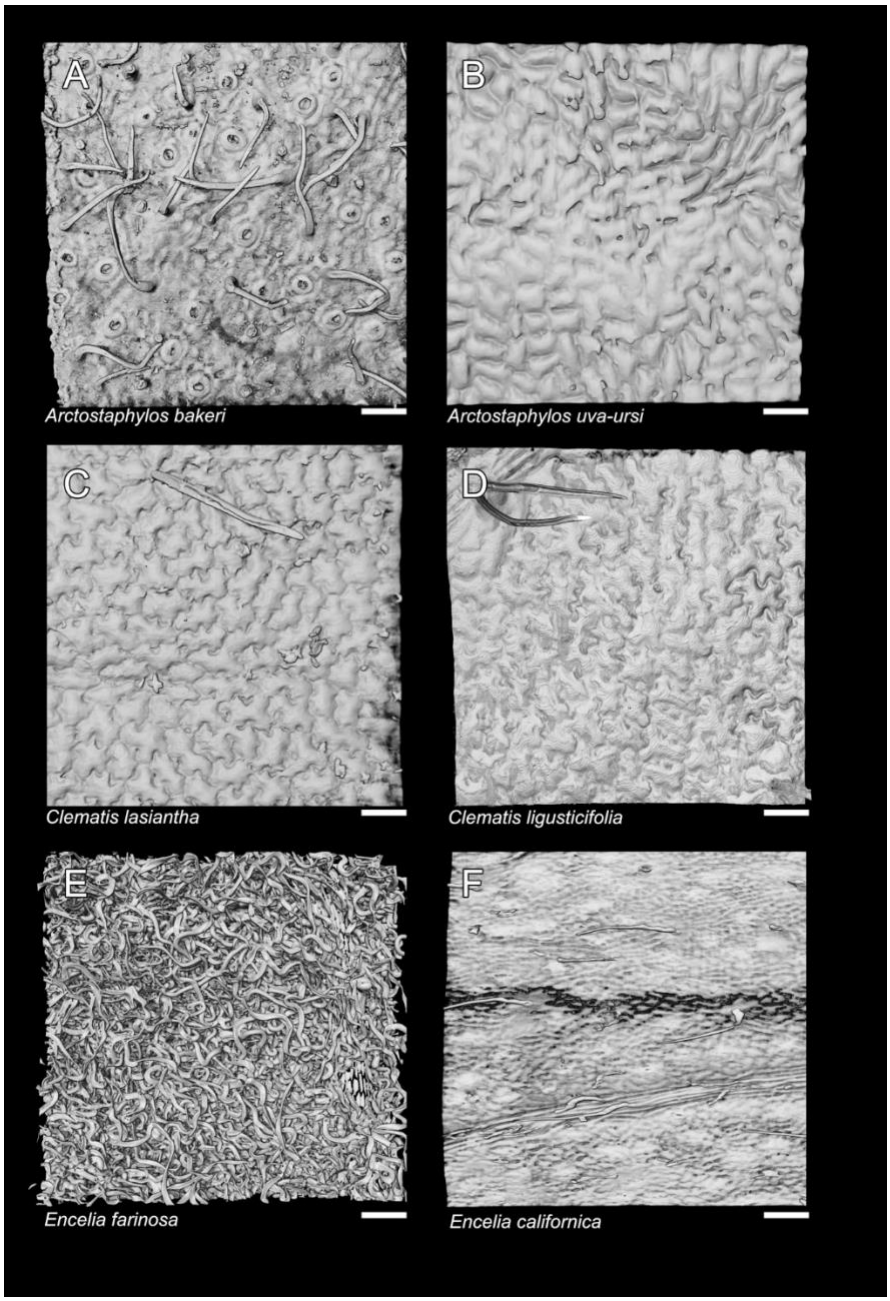

Figure 3.6: Micrographs of adaxial leaf surfaces for species

Micrographs of adaxial leaf surfaces for species within each of three Californian genera, with the species on the left having denser trichomes than that on the right. (Image not available for *Monardella macrantha*).

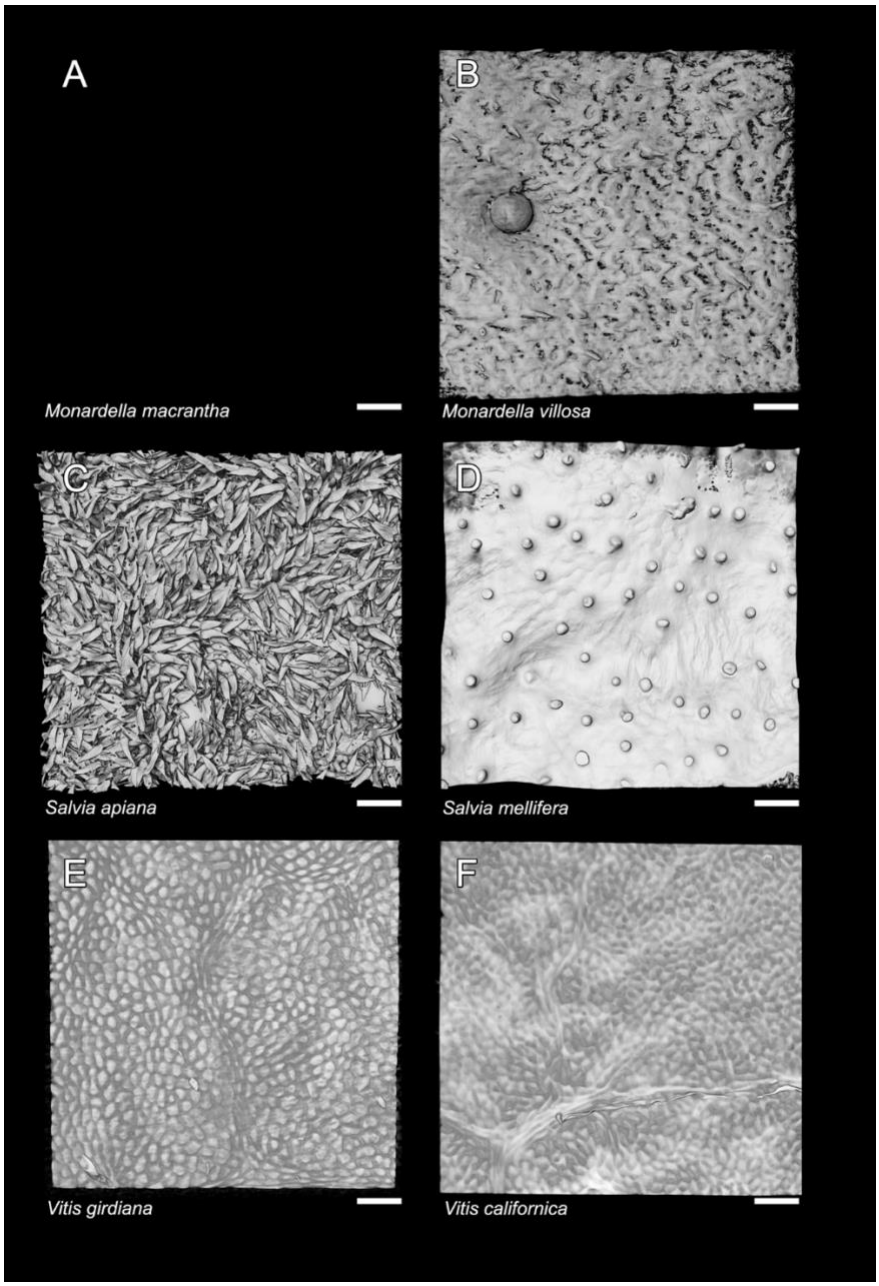

Figure 3.7: Variation across species in leaf trichome traits for twelve species within six Californian genera

Variation across species in leaf trichome traits for twelve species within six Californian genera, with a species with abundant trichomes (orange) and less abundant trichomes (grey). Panel A, trichome density, total for both leaf surfaces (TD); Panel B, trichome length, averaged for both surfaces (TL); Panel C, trichome surface area per leaf area, total for both surfaces (TSALA); Panel D, trichome basal area per leaf area (TBALA); Panel E, trichome volume per leaf area (TVLA).

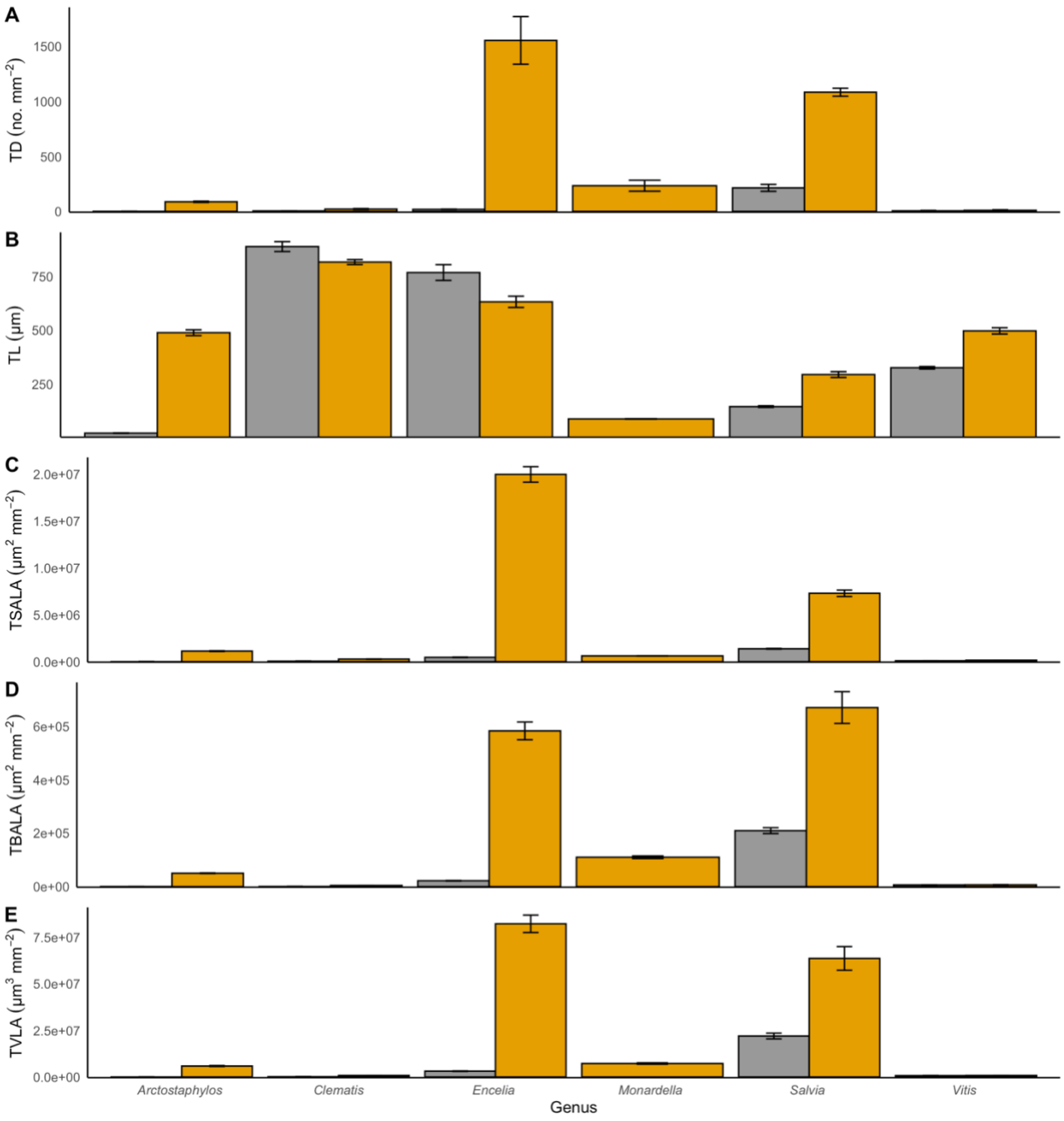

Figure 3.8: Relationships of foliar surface hydraulic conductance

Relationships of foliar surface hydraulic conductance, corrected for changing capacitance (K_{surf}) at 1h with trichome density per leaf area (total both surfaces, panel A) and stomatal density (total both surfaces, panel B).

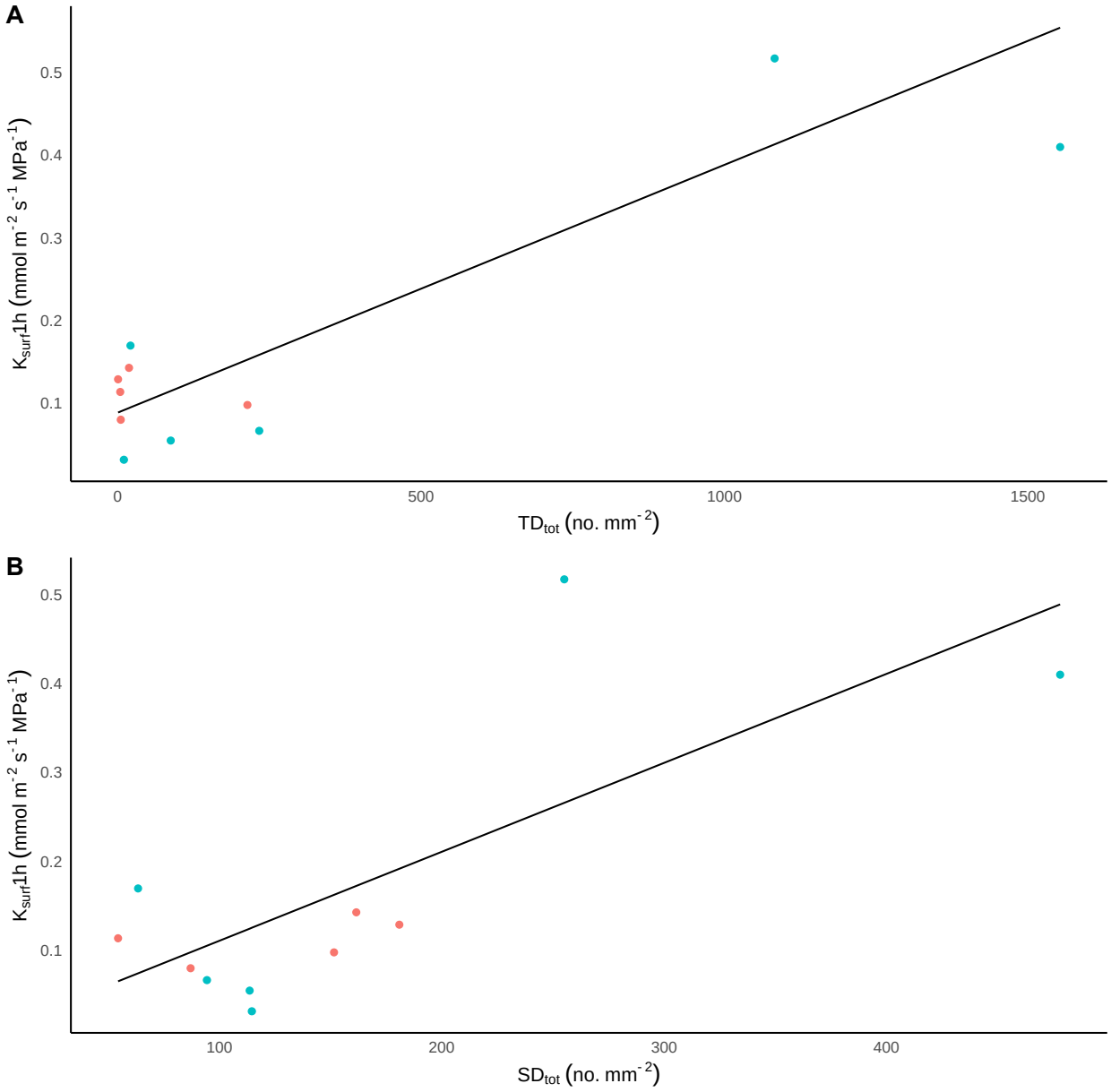

Figure 3.9: Relationships of light-saturated rate of photosynthesis (A_{max}) with foliar surface hydraulic conductance

Relationships of light-saturated rate of photosynthesis (A_{max}) with foliar surface hydraulic conductance, corrected for changing capacitance at 1h ($K_{surf,1h}$; panel A); leaf nitrogen concentration per mass (N_{mass}) with foliar surface hydraulic conductance, corrected for changing capacitance at 8h ($K_{surf,8h}$; panel B), and nitrogen concentration per leaf area (N_{area}) with foliar surface hydraulic conductance, corrected for changing capacitance at 24h ($K_{surf,24h}$; panel C).

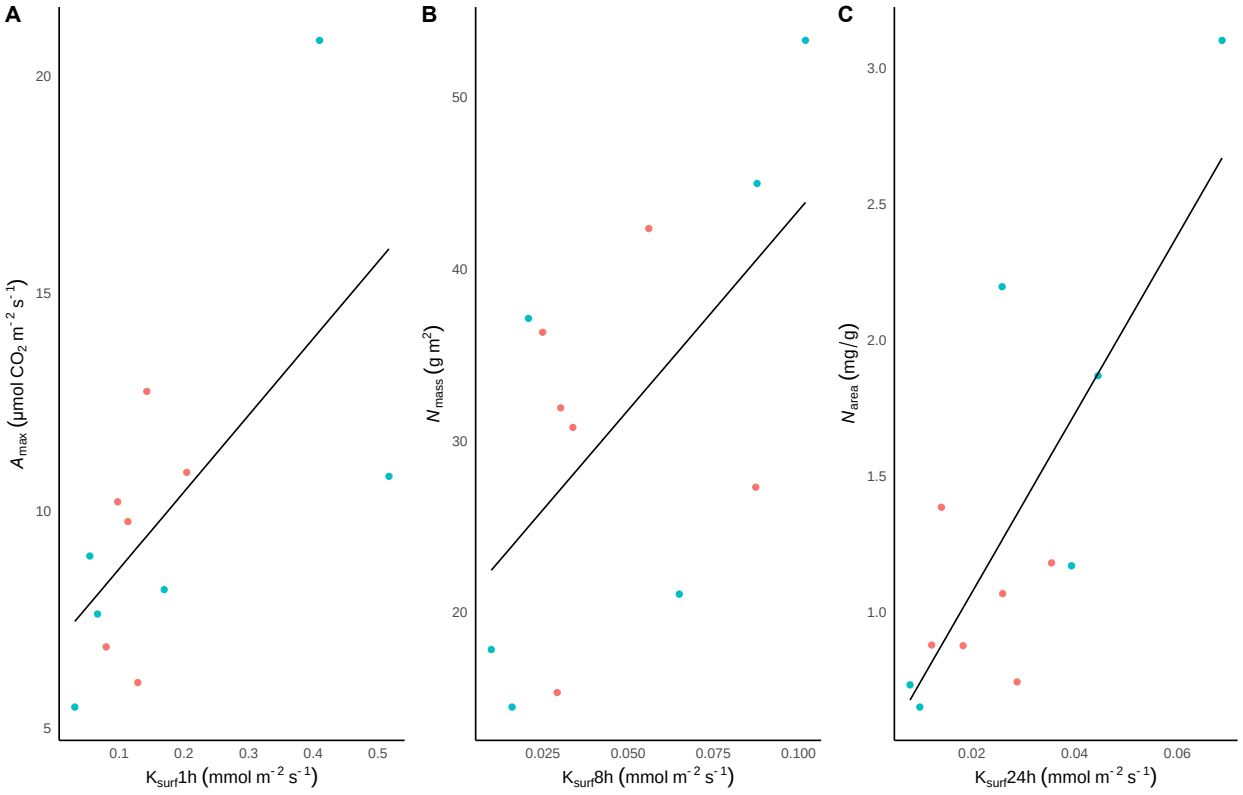

Table 3.1: Diverse study species tested for foliar water uptake conductance and its association with leaf structure

Diverse study species tested for foliar water uptake conductance and its association with leaf structure, including two species within six native California genera differing in leaf trichome abundance and type, and varying strongly in structure and native climate distribution. We present species, native vegetation type, type of indumentum and hair type, trichome density, leaf mass per area, leaf area, mean annual temperature, mean annual precipitation.

1: V. Thomas Parker, Michael C. Vasey & Jon E. Keeley 2012, *Arctostaphylos uva-ursi*, in Jepson Flora Project (eds.) Jepson eFlora https://ucjeps.berkeley.edu/eflora/eflora_display.php?tid=49161, accessed on August 18, 2021.

2: V. Thomas Parker, Michael C. Vasey & Jon E. Keeley 2012, Arctostaphylos bakeri subsp. bakeri, in Jepson Flora Project (eds.) Jepson eFlora, https://ucjeps.berkeley.edu/eflora/eflora_display.php?tid=49161, accessed on August 18, 2021.

3: Ehleringer, J., & Cook, C. (1987). Leaf Hairs in Encelia (Asteraceae). American Journal of Botany, 74(10), 1532-1540. doi:10.2307/2444047

4: Andrew C. Sanders, Mark A. Elvin & Mark S. Brunell 2012, Monardella macrantha, in Jepson Flora Project (eds.) Jepson eFlora, https://ucjeps.berkeley.edu/eflora/eflora_display.php?tid=33939, accessed on August 18, 2021.

5: Andrew C. Sanders, Mark A. Elvin & Mark S. Brunell 2012, Monardella villosa, in Jepson Flora Project (eds.) Jepson eFlora, https://ucjeps.berkeley.edu/eflora/eflora_display.php?tid=33939, accessed on August 18, 2021.=

6: Deborah Engle Averett 2012, Salvia apiana, in Jepson Flora Project (eds.) Jepson eFlora, https://ucjeps.berkeley.edu/eflora/eflora_display.php?tid=43038, accessed on August 18, 2021.

7: Citation for this treatment: Deborah Engle Averett 2012, Salvia mellifera, in Jepson Flora Project (eds.) Jepson eFlora, https://ucjeps.berkeley.edu/eflora/eflora_display.php?tid=43071, accessed on August 18, 2021.

8: Eric B. Wada & M. Andrew Walker 2012, Vitis californica, in Jepson Flora Project (eds.) Jepson eFlora, https://ucjeps.berkeley.edu/eflora/eflora_display.php?tid=48407, accessed on August 18, 2021.

9: Eric B. Wada & M. Andrew Walker 2012, Vitis girdiana, in Jepson Flora Project (eds.) Jepson eFlora, https://ucjeps.berkeley.edu/eflora/eflora_display.php?tid=48417, accessed on August 18, 202

Genus	Species	Family	Vegetation Type	Indumentum	Hair Type	TD_{tot} (no mm^2)	LMA ($g\ m^{-2}$)	LA (cm^2)	MAT (°C)	MAP (mm)
Arctostaphylos	*uva-ursi*	Ericaceae	Chaparral	sparsely puberulent[1]	simple	0.63 ± 0.32	69.73 ± 9.39	1.46 ± 0.35	3.85	846
Arctostaphylos	*bakeri spp. bakeri*	Ericaceae	Chaparral	papillate, scabrous[2]	glandular	36.39 ± 2.7	151.68 ± 11.16	4.4 ± 0.23	13.8	1041
Clematis	*ligusticifolia*	Ranunculaceae	Wetland	glabrous	-	3.76 ± 0.7	28.6 ± 5.29	20.4 ± 0.12	9.24	411
Clematis	*lasiantha*	Ranunculaceae	Chaparral	minute	simple	16.99 ± 4.52	58.16 ± 6.92	4.97 ± 0.28	14.8	645
Encelia	*californica*	Asteraceae	Coastal scrub	glabrous to sparsely and minutely strigose or bristly[3]	multicellular	10.24 ± 1.41	27.89 ± 2.46	18.6 ± 0.08	17.1	358
Encelia	*farinosa*	Asteraceae	Coastal scrub/desert	silver- or gray-tomentose[3]	multicellular	592.74 ± 149.31	41.54 ± 2.35	55.7 ± 0.1	20.5	227
Monardella	*macrantha*	Lamiaceae	Chaparral	glabrous[4]	-		27.49 ± 7.02	0.76 ± 0.37	12.1	571
Monardella	*villosa*	Lamiaceae	Chaparral	abaxially woolly[5]	glandular	156.13 ± 36.61	17.56 ± 1.4	1.86 ± 0.33	13.8	770
Salvia	*mellifera*	Lamiaceae	Chaparral	dense abaxially[6]	non-glandular and glandular	165.16 ± 26.74	38.17 ± 6.15	5.28 ± 0.74	16.3	436
Salvia	*apiana*	Lamiaceae	Chaparral	densely appressed[7]	non-glandular and glandular	545.78 ± 16.33	55.6 ± 1.99	22.1 ± 0.18	16.5	388
Vitis	*californica*	Vitaceae	Streamside	tomentose[8]	simple	4.52 ± 0.75	27.28 ± 4.07	123 ± 0.1	15.1	751
Vitis	*girdiana*	Vitaceae	Streamside	tomentose[9]	simple	8.16 ± 3.91	41.14 ± 4.66	95.6 ± 0.08	17.0	330

3.7 References

1 Wright, I. J. *et al.* The worldwide leaf economics spectrum. *Nature* **428**, 821-827, doi:10.1038/nature02403 (2004).

2 Sack, L., Cowan, P. D., Jaikumar, N. & Holbrook, N. M. The 'hydrology' of leaves: co-ordination of structure and function in temperate woody species. *Plant Cell Environ.* **26**, 1343-1356, doi:10.1046/j.0016-8025.2003.01058.x (2003).

3 Berry, Z. C., Emery, N. C., Gotsch, S. G. & Goldsmith, G. R. Foliar water uptake: Processes, pathways, and integration into plant water budgets. *Plant, Cell & Environment* **42**, 410-423, doi:https://doi.org/10.1111/pce.13439 (2019).

4 Guzmán-Delgado, P., Laca, E. & Zwieniecki, M. A. Unravelling foliar water uptake pathways: The contribution of stomata and the cuticle. *Plant, Cell & Environment* **44**, 1728-1740, doi:https://doi.org/10.1111/pce.14041 (2021).

5 Bryant, C. *et al.* Foliar water uptake via cork warts in mangroves of the Sonneratia genus. *Plant, Cell & Environment* **44**, 2925-2937, doi:https://doi.org/10.1111/pce.14129 (2021).

6 Guzmán-Delgado, P., Mason Earles, J. & Zwieniecki, M. A. Insight into the physiological role of water absorption via the leaf surface from a rehydration kinetics perspective. *Plant Cell Environ* **41**, 1886-1894, doi:10.1111/pce.13327 (2018).

7 Eichert, T., Kurtz, A., Steiner, U. & Goldbach, H. E. Size exclusion limits and lateral heterogeneity of the stomatal foliar uptake pathway for aqueous solutes and water-suspended nanoparticles. *Physiol Plant* **134**, 151-160, doi:10.1111/j.1399-3054.2008.01135.x (2008).

8 Burkhardt, J., Basi, S., Pariyar, S. & Hunsche, M. Stomatal penetration by aqueous solutions – an update involving leaf surface particles. *New Phytol.* **196**, 774-787, doi:https://doi.org/10.1111/j.1469-8137.2012.04307.x (2012).

9 Kerstiens, G. Cuticular water permeability and its physiological significance. *J. Exp. Bot.* **47**, 1813-1832, doi:10.1093/jxb/47.12.1813 (1996).

10 Kerstiens, G. Water transport in plant cuticles: an update. *J Exp Bot* **57**, 2493-2499, doi:10.1093/jxb/erl017 (2006).

11 Riederer, M. & Schreiber, L. Protecting against water loss: analysis of the barrier properties of plant cuticles. *J Exp Bot* **52**, 2023-2032, doi:10.1093/jexbot/52.363.2023 (2001).

12 Limm, E. B., Simonin, K. A., Bothman, A. G. & Dawson, T. E. Foliar water uptake: a common water acquisition strategy for plants of the redwood forest. *Oecologia* **161**, 449-459, doi:10.1007/s00442-009-1400-3 (2009).

13 Uzelac, B., Stojičić, D. & Budimir, S. in *Plant Cell and Tissue Differentiation and Secondary Metabolites: Fundamentals and Applications* (eds Kishan Gopal Ramawat, Halina Maria Ekiert, & Shaily Goyal) 1-37 (Springer International Publishing, 2019).

14 Smith, W. K. & Nobel, P. S. Influences of seasonal changes in leaf morphology on water-use efficiency for three desert broadleaf shrubs. *Ecology* **58**, 1033-1043, doi:10.2307/1936923 (1977).

15 De Micco, V. & Aronne, G. Occurrence of morphological and anatomical adaptive traits in young and adult plants of the rare mediterranean cliff species primula palinuri petagna. *The Scientific World Journal* **2012**, 471814, doi:10.1100/2012/471814 (2012).

16 Perez-Estrada, L. B., Cano-Santana, Z. & Oyama, K. Variation in leaf trichomes of Wigandia urens: environmental factors and physiological consequences. *Tree Physiology* **20**, 629-632 (2000).

17 Amada, G., Onoda, Y., Ichie, T. & Kitayama, K. Influence of leaf trichomes on boundary layer conductance and gas-exchange characteristics in *Metrosideros polymorpha* (*Myrtaceae*). *Biotropica* **49**, 482-492, doi:10.1111/btp.12433 (2017).

18 Kenzo, T., Yoneda, R., Azani, M. A. & Majid, N. M. Changes in leaf water use after removal of leaf lower surface hairs on *Mallotus macrostachyus* (*Euphorbiaceae*) in a tropical secondary forest in Malaysia. *J. For. Res.* **13**, 137-142, doi:10.1007/s10310-008-0062-z (2008).

19 Ehleringer, J. R. & Björkman, O. Pubescence and leaf spectral characteristics in a desert shrub, Encelia farinosa. *Oecologia* **36**, 151-162, doi:10.1007/bf00349805 (1978).

20 Ehleringer, J. The influence of water stress and temperature on leaf pubescence development in *Encelia farinosa*. *Am. J. Bot.* **69**, 670-675, doi:doi:10.1002/j.1537-2197.1982.tb13306.x (1982).

21 Ripley, B. S., Pammenter, N. W. & Smith, V. R. Function of leaf hairs revisited: The hair layer on leaves *Arctotheca populifolia* reduces photoinhibition, but leads to higher leaf temperatures caused by lower transpiration rates. *Journal of Plant Physiology* **155**, 78-85, doi:https://doi.org/10.1016/S0176-1617(99)80143-6 (1999).

22 Wuenscher, J. E. Effect of leaf hairs of *Verbascum thapsus* on leaf energy exchange. *New Phytol.* **69**, 65-+, doi:10.1111/j.1469-8137.1970.tb04050.x (1970).

23 Parkhurst, D. F. Effects of *Verbascum thapsus* leaf hairs on heat and mass transfer reassessment. *New Phytol.* **76**, 453-457, doi:10.1111/j.1469-8137.1976.tb01481.x (1976).

24 Schreuder, M. D. J., Brewer, C. A. & Heine, C. Modelled influences of non-exchanging trichomes on leaf boundary layers and gas exchange. *Journal of Theoretical Biology* **210**, 23-32, doi:10.1006/jtbi.2001.2285 (2001).

25 Franke, W. Mechanisms of foliar penetration of solutions. *Annual Review of Plant Physiology* **18**, 281-&, doi:10.1146/annurev.pp.18.060167.001433 (1967).

26 Benzing, D. H., Seemann, J. & Renfrow, A. The foliar epidermis in *Tillandsioideae* (*Bromeliaceae*) and its role in habitat selection. *Am. J. Bot.* **65**, 359-365, doi:10.2307/2442278 (1978).

27 Dalin, P., Agren, J., Bjorkman, C., Huttunen, P. & Karkkainen, K. *Leaf trichome formation and plant resistance to herbivory*. (Springer, Po Box 17, 3300 Aa Dordrecht, Netherlands, 2008).

28 Gassmann, A. J. & Hare, J. D. Indirect cost of a defensive trait: variation in trichome type affects the natural enemies of herbivorous insects on *Datura wrightii*. *Oecologia* **144**, 62-71, doi:10.1007/s00442-005-0038-z (2005).

29 Givnish, T. J., Sytsma, K. J., Smith, J. F. & Hahn, W. J. Thorn-like prickles and heterophylly in *Cyanea*: adaptations to extinct avian browsers on Hawaii? *Proceedings of the National Academy of Sciences* **91**, 2810-2814, doi:10.1073/pnas.91.7.2810 (1994).

30 Hanley, M. E., Lamont, B. B., Fairbanks, M. M. & Rafferty, C. M. Plant structural traits and their role in anti-herbivore defence. *Perspect. Plant Ecol. Evol. Syst.* **8**, 157-178, doi:10.1016/j.ppees.2007.01.001 (2007).

31 Seelmann, L., Auer, A., Hoffmann, D. & Schausberger, P. Leaf pubescence mediates intraguild predation between predatory mites. *Oikos* **116**, 807-817, doi:10.1111/j.2007.0030-1299.15895.x (2007).

32 Fernández, V. *et al.* Wettability, polarity, and water absorption of holm oak leaves: effect of leaf side and age. *Plant Physiol.* **166**, 168-180, doi:10.1104/pp.114.242040 (2014).

33 Schreel, J. D. M. *et al.* Identifying the pathways for foliar water uptake in beech (Fagus sylvatica L.): a major role for trichomes. *The Plant Journal* **103**, 769-780, doi:https://doi.org/10.1111/tpj.14770 (2020).

34 Sack, L. & Pasquet-Kok, J. *Leaf pressure-volume curve parameters*, <http://prometheuswiki.org/tiki-index.php?page=Leaf%20pressure-volume%20curve%20parameters> (2011).

35 Kubiske, M. E. & Abrams, M. D. Pressure-volume relationships in non-rehydrated tissue at various water deficits. *Plant, Cell & Environment* **13**, 995-1000, doi:https://doi.org/10.1111/j.1365-3040.1990.tb01992.x (1990).

36 Scoffoni, C., Rawls, M., McKown, A., Cochard, H. & Sack, L. Decline of Leaf Hydraulic Conductance with Dehydration: Relationship to Leaf Size and Venation Architecture. *Plant Physiol.* **156**, 832, doi:10.1104/pp.111.173856 (2011).

37 Oppenheimer, H. R. & Leshem, B. Critical thresholds of dehydration in leaves ofNerium oleander L. *Protoplasma* **61**, 302-321, doi:10.1007/BF01248987 (1966).

38 Chen, T., Starns, J. J. & Rotello, C. M. A violation of the conditional independence assumption in the two-high-threshold model of recognition memory. *Journal of Experimental Psychology: Learning, Memory, and Cognition* **41**, 1215-1222, doi:10.1037/xlm0000077 (2015).

39 John, G. P., Henry, C. & Sack, L. Leaf rehydration capacity: associations with other indices of drought tolerance and environment. *Plant, Cell & Environment* **41**, 2638-2653 (2018).

40 Weisstein, E. W. *"Conical Frustum."*, <https://mathworld.wolfram.com/ConicalFrustum.html> (2022).

41 *rgbif: Interface to the Global Biodiversity Information Facility API*. v. 3.3.0 (2020).

42 Hijmans, R. J., Cameron, S. E., Parra, J. L., Jones, P. G. & Jarvis, A. Very high resolution interpolated climate surfaces for global land areas. *Int. J. Climatol.* **25**, 1965-1978, doi:10.1002/joc.1276 (2005).

43 Zomer, R. J., Trabucco, A., Bossio, D. A. & Verchot, L. V. Climate change mitigation: A spatial analysis of global land suitability for clean development mechanism afforestation and reforestation. *Agriculture, Ecosystems & Environment* **126**, 67-80, doi:https://doi.org/10.1016/j.agee.2008.01.014 (2008).

44 Hengl, T. *et al.* SoilGrids250m: Global gridded soil information based on machine learning. *PLoS One* **12**, e0169748, doi:10.1371/journal.pone.0169748 (2017).

45 Hijmans, R. J. *et al.* (Version, 2013).

46 Hijmans, R. J., Phillips, S., Leathwick, J., Elith, J. & Hijmans, M. R. J. Package 'dismo'. *Circles* **9**, 1-68 (2017).

47 Perez, T. M. & Feeley, K. J. Weak phylogenetic and climatic signals in plant heat tolerance. *Journal of Biogeography* **48**, 91-100, doi:https://doi.org/10.1111/jbi.13984 (2021).

48 Harmon, L. J. *Phylogenetic comparative methods*. (Independent, 2019).

49 Freckleton, R. P., Harvey, P. H. & Pagel, M. Phylogenetic analysis and comparative data: a test and review of evidence. *Am Nat* **160**, 712-726, doi:10.1086/343873 (2002).

50 Orme, D. *et al.* The caper package: comparative analysis of phylogenetics and evolution in R. *R package version* **5**, 1-36 (2013).

51 Benz, B. W. & Martin, C. E. Foliar trichomes, boundary layers, and gas exchange in 12 species of epiphytic *Tillandsia* (*Bromeliaceae*). *Journal of Plant Physiology* **163**, 648-656, doi:https://doi.org/10.1016/j.jplph.2005.05.008 (2006).

52 Berry, Z. C., White, J. C. & Smith, W. K. Foliar uptake, carbon fluxes and water status are affected by the timing of daily fog in saplings from a threatened cloud forest. *Tree Physiology* **34**, 459-470, doi:10.1093/treephys/tpu032 (2014).

53 Fuenzalida, T. *et al.* Shoot surface water uptake enables leaf hydraulic recovery in Avicennia marina. *New Phytol.* **224**, doi:10.1111/nph.16126 (2019).

54 Maurel, C. Aquaporins and water permeability of plant membranes. *Annu. Rev. Plant Physiol. Plant Molec. Biol.* **48**, 399-429, doi:10.1146/annurev.arplant.48.1.399 (1997).

55 Turner, N. C. Use of the Pressure Chamber in Membrane Damage Studies. *J. Exp. Bot.* **27**, 1085-1092, doi:10.1093/jxb/27.5.1085 (1976).

4. Chapter 4: Diverse effects of leaf hairs on gas exchange in native California species

4.1 Introduction

The leaf's surface is the locus for a multitude of physiological processes important in plant vitality and responses to the environment. Stomata are pores in the leaf epidermis, enabling CO_2 uptake at the cost of the loss of water vapor [1]. Leaf hairs (trichomes) also play important roles in plant function, including reflecting light, taking up water and/or slowing transpiration via a thicker boundary layer. The multiple functions of leaf trichomes can explain several contradictory trends observed across floras. For example, some have hypothesized that leaf trichome density tends to be higher for species adapted to drought stress, and yet many species of wet places also bear pubescence[1]. To date, there are no physiological studies highlighting comparative differences between species with and without trichomes across genera. Given climate change, it is increasingly urgent to clarify the role(s) of leaf trichomes both to model gas exchange and function accurately, and their roles on the climate system[2].

We focused on the potential association of leaf trichomes with climatic aridity and with leaf gas exchange. Previous studies found that the presence of hair on the leaf surface may lead to a thicker leaf boundary layer [3-9]. Yet, the impact of the reduced boundary layer may depend on the species and context. If stomatal conductance remains the same, then the reduction of boundary layer conductance would reduce overall conductance, and the transpiration rate for a given vapor pressure deficit driving force, and given this reduced conductance influences transpiration more strongly than carbon uptake, trichomes may thereby increase water use efficiency[3,6,10,11]. Alternatively, leaf trichomes may play a negligible role in influencing gas exchange. Recently, phenotypic differences within a species have been studied to characterize physiological response [11]. Populations of *Metrosideros polymorpha* express a varying phenotype across an elevation

gradient, with hairier individuals at higher elevations. Yet, populations differed only marginally in gas exchange and WUE across populations[11].

We tested for variation in gas exchange, nutrient concentrations and water use efficiency across 12 species in six genera of native California species, with species varying strongly in trichome density and morphology within each genus. We hypothesized that across species trichome density and morphology would be associated with climate, and that species with greater trichome abundance, surface area and/or volume per leaf area would show associated variation in stomatal conductance and photosynthetic rate under light saturated conditions, and in instantaneous and integrated water use efficiency.

4.2 Results

Variation in leaf trichome density and morphology across species

Species varied strongly in trichome abundance and dimensions (Figs 1-5; Table S1). Species varied 937- to 960-fold in TD_{ad} and TD_{ab}; 440-fold in TL_{ad} and 21-fold in TL_{ab}; 28- to 40-fold in Td_{tip_ad}, Td_{base_ad}, and $Td_{central\_ad}$; 2- to 11-fold in Td_{tip_ab}, Td_{base_ab}, and $Td_{central\_ab}$; 9-fold in $CSA_{central\_ad}$, and 47-fold variation among species in $CSA_{central\_ab}$; 200,629-fold in TV_{ad} and 13-fold in TV_{ab}; 3089-fold in TBALA, 12155-fold in TCALA, 11615-fold in TSALA, 8711-fold in TVLA, 13-fold variation among species in TBA, 16-fold variation among species in TSA.

We also found strong variation across the species pairs within genera in all measured leaf trichome traits. The species with more abundant trichomes within genera had higher values for TD_{ad}, TD_{ab}, TD_{tot}, $TCALA_{ad}$, $TBALA_{ad}$, $TVLA_{ad}$, $TSALA_{ad}$, (repeated measures ANOVA; $P = 0.006$-0.039, Table S9) but not for TL_{ad}, Td_tip_{ad}, Td_{base_ad}, $Td_{central\_ad}$, $CSA_{central\_ad}$, TBA_{ad}, TV_{ad}, TSA_{ad}, TL_{ab}, Td_{tip_ab}, Td_{base_ab}, $Td_{central\_ab}$, $CSA_{central\_ab}$, TBA_{ab}, TV_{ab}, TSA_{ab}, $TCALA_{ab}$, $TBALA_{ab}$, $TVLA_{ab}$, and $TSALA_{ab}$ ($P > 0.05$).

Variation in leaf stomatal density and morphology across species

We found strong variation across species within genera in all measured leaf stomatal traits (Table S1; $P = 0.001$ to $P < 0.05$, ANOVA), but no association with leaf trichomes on average within genera (repeated measures ANOVA; $P > 0.05$). Species varied 249-fold in SD_{ad}, 4-fold in SD_{ab} and 8-fold in SD_{tot}; 67-fold in gcl_{ad} and 3-fold in gcl_{ab}; and 49-fold in gcw_{ad} and 4-fold in gcw_{ab}.

Variation in leaf gas exchange and nutrient and isotope composition across species

We found strong variation across species within genera in gas exchange traits (Fig. 6; Table S1; $P < 0.001$ to $P < 0.01$, ANOVA), but no association with leaf trichomes on average within genera (repeated measures ANOVA; $P > 0.05$). Species varied 7-fold in g_{op}, 3-fold in A_{max}, and 2-fold in A_{max}/g_{op}.

We found strong variation across species within genera in leaf composition ($P < 0.001$, ANOVA), but no association with leaf trichomes on average within genera (repeated measures ANOVA; $P > 0.05$). Species varied 8-fold in *LMA,* 3-fold in N_{mass}, 4-fold in N_{area}, ranged from -28 to -36 ‰ in *∂13C*

Relationships of trichome, stomatal and gas exchange traits with climate variables

Across species, trichome abundance and morphology traits were related to climatic aridity (Figure 7; Table S4). Thus, across species, numerous trichome traits were related to mean annual temperature (MAT): TD_{ab}, Td_{tip_ad}, Td_{base_ad}, $Td_{central\_ad}$, TD_{tot}, TL_{ab}, TL_{ad}, $CSA_{central\_ad}$, TBA_{ad}, TSA_{ab}, TSA_{ad}, TV_{ad} ($r = 0.39$-0.82; $P < 0.001$ to $P = 0.041$). Further, numerous trichome traits were related to aridity index (AI): TD_{ab}, Td_{base_ad}, $Td_{central\_ad}$, TD_{tot}, TL_{ab}, TL_{ad}, TBA_{ad}, TSA_{ad},

TV_{ad} (r = -0.38 to -0.46; P = 0.022-0.04). Numerous trichome traits were related to potential evapotranspiration (PET): TD_{ab}, TD_{ad}, Td_{tip_ad}, Td_{base_ad}, $Td_{central\_ad}$, TD_{tot}, TL_{ab}, TL_{ad}, $CSA_{central\_ad}$, TBA_{ad}, TSA_{ab}, TSA_{ad}, TV_{ad}, SD_{ad} (r = 0.42-0.76; P <0.001 to 0.03). Numerous trichome traits were related to the maximum temperature of the warmest month (MTWM): TD_{ab}, TD_{ad}, Td_{tip_ad}, Td_{base_ad}, $Td_{central\_ad}$, TD_{tot}, TL_{ab}, TL_{ad}, $CSA_{central\_ad}$, TBA_{ad}, TSA_{ab}, TSA_{ad}, TV_{ad}, SD_{ad} (r = 0.42-0.65; P = 0.0036-0.044). Additionally, across species, SD_{tot} was negatively related to mean annual precipitation (r = -0.41; P = 0.033).

Across species, gas exchange traits were related to climatic aridity (Figure 8). A_{max} was negatively related to aridity index (r = -0.43; P = 0.03) and positively to PET (r = 0.49; P = 0.017); g_{op} was positively related to PET (r = 0.40; P = 0.036), and A_{max} and g_{op} with MTWM (r = 0.57 and 0.46 respectively (P = 0.0075 and 0.021).

Tests for association of gas exchange with trichome and stomatal morphology and leaf composition

Greater trichome abundance was not associated with higher gas exchange between species within genera, on average (ANOVA, P > 0.05; Table S9). For two genera (*Arctostaphylos* and *Encelia*), the species with higher TD had higher g_{op}; for three genera (*Clematis*, *Salvia* and *Vitis*) the species with higher TD had lower g_{op}. For three genera (*Arctostaphylos*, *Encelia* and *Salvia*) the species with higher TD had higher A_{max}; for two genera (*Clematis* and *Vitis*), the species with higher TD had lower A_{max} (Fig. 6).

Across species, g_{op} and A_{max} were positively correlated with TD_{ab}, TD_{ad}, and TD_{tot} (r = 0.63-0.83; P = 0.0014-0.023) (Table S11; Fig. 9). Across species, g_{op} and A_{max} were positively correlated with SD_{ad}, SD_{ab}, and SD_{tot} (r = 0.66-0.94; P = 0.00002-0.007) (Table S11; Fig. 9)

Tests for association of water use and nitrogen use efficiency with with trichome and stomatal morphology and leaf composition

Greater trichome abundance was not associated with higherwater use efficiency between species within genera, on average (ANOVA, $P > 0.05$; Table S9). For three genera (*Clematis*, *Salvia* and *Vitis*), the species with higher TD had higher A_{max} / g_{op}; for two genera (*Arctostaphylos* and *Encelia*), the species with higher TD had lower A_{max} / g_{op}. For four genera (*Clematis*, *Encelia*, *Salvia* and *Vitis*), the species with higher TD had higher ∂13C; for one genus (*Arctostaphylos*), the species with higher TD had lower ∂13C.

Across species, A_{max} / g_{op} was negatively correlated with SD_{ad} ($r = -0.61$; $P = 0.046$). Neither A_{max}/g_{op} or ∂13C was statistically associated with trichome traits ($P > 0.05$).

4.3 Methods

Plant material

Twelve species of native California trees and shrubs were selected, with two species within each genus, one with substantially higher trichome density than the other (Table 1). Plants were cultivated in a greenhouse common garden at the UCLA Plant Growth Center from February 2019 to July 2020. 15 individual seedlings of each species were acquired in 1 L pots (Rancho Santa Ana Botanic Garden; Claremont, CA), and randomized within each of 10 blocks containing one individual of each species spread across five greenhouse benches in two greenhouse rooms. Plants were acclimated 12–18 months prior to initial measurements to establish similar external conditions across individuals and species, and to ensure canopies of mature leaves. Plants were carefully monitored for root expansion and repotted when roots filled the pots. Potting soil (18.75% washed plaster sand, 18.75% sandy loam, 37.5% grower grade peat moss, 12.5% horticultural grade perlite, 12.5% coarse vermiculite; Therm-O-Rock West, Inc., Chandler, AZ) was autoclaved

prior to use. Plants were irrigated every second day with 200–250 ppm 20:20:20 NPK fertilizer. Daily irradiance ranged up to 1400 μmol m^{-2} s^{-1} (LI-250 light meter; LI-COR Biosciences, Lincoln, NE, USA), while mean minimum, mean and maximum values for temperature were 22.1, 23.9, and 25.2 °C and relative humidity were 47.3%, 60.1%, and 72.8% in the greenhouse (HOBO Micro Station with Smart Sensors; Onset, Bourne, MA, USA).

Gas exchange measurements

Leaf gas exchange measurements were taken using a Portable Photosynthesis System (LI-COR 6400; LI-COR Inc, Lincoln, NE, USA). For three to five individuals of each species, Measurements of Photosynthetic rate (A_{max}), Conductance to H_2O (g_{op}), Transpiration rate (E), Vapor pressure deficit based on Leaf temperature (VPD), Temperature of leaf thermocouple (T_{leaf}), Intercellular CO^2 concentration (Ci), and Leaf water potential (Ψ) were taken from 10:00-14:00, and averaged for each species. Measurements were taken at saturating light (1,000 μmol/m2/s) after a 10-min acclimation period with the leaf in the chamber at vapor pressure deficit <1 kPa. Intrinsic water use efficiency (A_{max}/g_{op}) was determined as the ratio of A_{max} to g_{op}.

Measurements of leaf structure, composition, and nutrient analysis

Leaf structure was measured for 4 leaves on each of 5 individual plants of each species. Leaf area was measured using a flatbed scanner and imageJ. Leaf mass was measured using a digital analytic balance. Leaf thickness was measured using digital calipers. Leaf mass per area was determined as the ratio of leaf mass to area.

Leaf hair traits were measured on images of the adaxial and abaxial surfaces one leaf from each of three individuals of each species (except *Monardella macrantha*) from the synchrotron at The Advanced Light Source – Lawrence Berkeley National Laboratory (Beamline

8.3.2). We measured trichome density (TD), trichome length (TL) and the diameters of trichomes at the base (Td_{base}), midpoint ($Td_{central}$) and tip (Td_{tip}). Trichomes were measured of different types; data were combined in this study. We calculated trichome central cross sectional area ($CSA_{central}$) as $\pi \times (0.5 \times Td_{central})^2$. We calculated trichome basal area (TBA) as $\pi \times (0.5 \times Td_{base})^2$. We calculated trichome volume (TV) and trichome surface area (TSA) by considering the trichome as a conical frustrum[12], and with volume = $1/3 \times \pi \times TL \times (0.5 \times Td_{base})^2 + 0.5 \times Td_{base} \times 0.5 \times Td_{tip} \times (0.5 \times Td_{tip})^2$ and surface area = $\pi \times (0.5 \times Td_{base} + 0.5 \times Td_{tip}) \times [(0.5 \times Td_{base} - 0.5 \times Td_{tip})^2 + TL^2]^{0.5}$. We calculated trichome central area per leaf area (TCALA) as TD × $CSA_{central}$, trichome basal area per leaf area (TBALA) as TD × TBA, trichome volume per leaf area (TVLA) as TD × TV, and trichome surface area per leaf area (TSALA) as TD × TSA. We also calculated total trichome density (TD_{tot}) on abaxial and adaxial surfaces of each leaf.

Nutrient and isotope composition data were obtained from 4 leaves combined from each of 5 individual plants of 11 of the species, excluding *Clematis lasiantha* due to lack of material during sampling on January 16, 2021. Leaves were oven dried at 70°C for at least 72 hours. Liquid nitrogen was then poured over the leaves, and these were ground with a mortar and pestle into a fine powder. 3-4mg of material were weighed into tin 4 × 6 capsules and analyzed at the Center for Stable Isotope Biogeochemistry at the University of California, Berkeley. Carbon isotope ratio ($\delta^{13}C$) was measured by dual isotope analysis with an Elemental Analyzer interfaced to a mass spectrometer, along with the percent of nitrogen in the sample. Nitrogen per leaf mass (N_{mass}; mg g-1) was determined as the mass nitrogen in the sample (mg) per the mass of the sample (g). Nitrogen per leaf area (N_{area}; g m^{-2}) was determined as N_{mass} multiplied by LMA.

Climate data

Occurrence records were downloaded using the '*rgbif*' package[13] and filtered to keep

herbarium records since 1950 and remove incomplete (latitude or longitude missing) and duplicated records, non-natural occurrences (e.g., records from botanical gardens or planted urban trees)[13]. We extracted 30 environmental variables from open-access raster layers, relating to air temperature (WorldClim, CRU[14]), precipitation (WorldClim[14]), aridity (CGIAR-CSI, NCAR-UCAR[15]) and soil characteristics (ISRIC Soilgrids[16]) (see Table S1 for all variables). The raster layers with the same resolution were stacked using the stack function from the '*raster*' package[17] and the environmental variables for each occurrence record were extracted using the extract function from the '*dismo*' package[18]. Due to their coarse resolution, these environmental variables are effective in characterizing large scale patterns but do not reflect differences in microclimate, i.e., temperature, water and nutrient availability, irradiance and soil composition[19]. The MAT, MAP, AI, and PET data were extracted at each coordinate for each species using ArcMap, and averaged for each species (Table 1).

Statistics

Results of analyses of variance for traits measured for 12 native California woody species within six genera. Results are presented for three ANOVAs: (1) repeated-measures ANOVA testing differences in foliar surface hydraulic conductance measured at three times (1, 8 and 24h), testing for variation among species, and among time intervals, and within species and time intervals; (2) nested ANOVA testing differences in traits among genera, and between species within genera, and within (Minitab 21; State College, PA, USA).

To test species' trait relationships while explicitly accounting for species relatedness, we performed phylogenetic generalized least-squares analyses (PGLS[20,21]) using the *pgls* function from the '*caper*' package[22] with lambda (λ) optimized using maximum likelihood. Analysis of

variance were performed for untransformed and log transformed data, to test for either approximately linear or non-linear (i.e., approximate power law) relationships respectively.

4.4 Discussion

We found that across 11 species in six genera, greater trichome abundance and higher light-saturated rates of gas exchange associated with drier and warmer conditions. Notably, despite this overall pattern, genera differed in the association of trichome traits with climate. Further, genera differed in whether the species with more abundant trichomes had higher g_{op}, A_{max} and water use efficiency.

These results are consistent with an overall adaptive function of leaf trichomes in arid climates. One potential advantage includes reflectance of high irradiance[23] which may allow leaves to avoid high temperatures and excess light stress; future analyses will test for this impact. Another function of the trichomes may be to increase the leaf boundary layer, which would potentially increase A_{max} / g_{op} under the conditions of natural gas exchange. We did not find such an association when gas exchange was measured under light saturated conditions in a photosynthesis system; in this system the boundary layer would be disrupted by the fan. In future work, the boundary layer conductance can be estimated using models to determine its variation under natural windspeeds, and the potential influence on water use efficiency can be better constrained. Finally, trichome traits may influence leaf water uptake (see Chapter 2) or resistance to herbivory.

The finding that overall species of more arid climates had higher gas exchange rates is consistent with species showing an “avoidance” response[24] , which would allow mitigation of the shorter growing season with rapid gas exchange when water is available. Whether the trichomes

contribute to this avoidance response requires testing using integrated models to consider the influence of reflectance and boundary layer effects on gas exchange.

Overall, we found that species were highly diverse in trichome abundance and morphology and that trichome traits were associated in evolution with both gas exchange and species' climate distribution. These findings highlight the important role of leaf surface traits in evolutionary adaptation and their potential contribution to species habitat and climate specialization.

Table 4.1: Diverse study species tested for foliar water uptake conductance and its association with leaf structure

Diverse study species tested for foliar water uptake conductance and its association with leaf structure, including two species within six native California genera differing in leaf trichome abundance and type, and varying strongly in structure and native climate distribution. We present species, native vegetation type, type of indumentum and hair type, trichome density, leaf mass per area, leaf area, mean annual temperature, mean annual precipitation.

1: V. Thomas Parker, Michael C. Vasey & Jon E. Keeley 2012, *Arctostaphylos uva-ursi*, in Jepson Flora Project (eds.) Jepson eFlora https://ucjeps.berkeley.edu/eflora/eflora_display.php?tid=49161, accessed on August 18, 2021.

2: V. Thomas Parker, Michael C. Vasey & Jon E. Keeley 2012, Arctostaphylos bakeri subsp. bakeri, in Jepson Flora Project (eds.) Jepson eFlora, https://ucjeps.berkeley.edu/eflora/eflora_display.php?tid=49161, accessed on August 18, 2021.

3: Ehleringer, J., & Cook, C. (1987). Leaf Hairs in Encelia (Asteraceae). American Journal of Botany, 74(10), 1532-1540. doi:10.2307/2444047

4: Andrew C. Sanders, Mark A. Elvin & Mark S. Brunell 2012, Monardella macrantha, in Jepson Flora Project (eds.) Jepson eFlora, https://ucjeps.berkeley.edu/eflora/eflora_display.php?tid=33939, accessed on August 18, 2021.

5: Andrew C. Sanders, Mark A. Elvin & Mark S. Brunell 2012, Monardella villosa, in Jepson Flora Project (eds.) Jepson eFlora, https://ucjeps.berkeley.edu/eflora/eflora_display.php?tid=33939, accessed on August 18, 2021.=

6: Deborah Engle Averett 2012, Salvia apiana, in Jepson Flora Project (eds.) Jepson eFlora, https://ucjeps.berkeley.edu/eflora/eflora_display.php?tid=43038, accessed on August 18, 2021.

7: Citation for this treatment: Deborah Engle Averett 2012, Salvia mellifera, in Jepson Flora Project (eds.) Jepson eFlora, https://ucjeps.berkeley.edu/eflora/eflora_display.php?tid=43071, accessed on August 18, 2021.

8: Eric B. Wada & M. Andrew Walker 2012, Vitis californica, in Jepson Flora Project (eds.) Jepson eFlora, https://ucjeps.berkeley.edu/eflora/eflora_display.php?tid=48407, accessed on August 18, 2021.

9: Eric B. Wada & M. Andrew Walker 2012, Vitis girdiana, in Jepson Flora Project (eds.) Jepson eFlora, https://ucjeps.berkeley.edu/eflora/eflora_display.php?tid=48417, accessed on August 18, 202

Genus	Species	Family	Vegetation Type	Indumentum	Hair Type	TD_{tot} (no mm^2)	LMA ($g\ m^{-2}$)	LA (cm^2)	MAT (°C)	MAP (mm)
Arctostaphylos	*uva-ursi*	Ericaceae	Chaparral	sparsely puberulent[1]	simple	0.63 ± 0.32	69.73 ± 9.39	1.46 ± 0.35	3.85	846
Arctostaphylos	*bakeri spp. bakeri*	Ericaceae	Chaparral	papillate, scabrous[2]	glandular	36.39 ± 2.7	151.68 ± 11.16	4.4 ± 0.23	13.8	1041
Clematis	*ligusticifolia*	Ranunculaceae	Wetland	glabrous	-	3.76 ± 0.7	28.6 ± 5.29	20.4 ± 0.12	9.24	411
Clematis	*lasiantha*	Ranunculaceae	Chaparral	minute	simple	16.99 ± 4.52	58.16 ± 6.92	4.97 ± 0.28	14.8	645
Encelia	*californica*	Asteraceae	Coastal scrub	glabrous to sparsely and minutely strigose or bristly[3]	multicellular	10.24 ± 1.41	27.89 ± 2.46	18.6 ± 0.08	17.1	358
Encelia	*farinosa*	Asteraceae	Coastal scrub/desert	silver- or gray-tomentose[3]	multicellular	592.74 ± 149.31	41.54 ± 2.35	55.7 ± 0.1	20.5	227
Monardella	*macrantha*	Lamiaceae	Chaparral	glabrous[4]	-		27.49 ± 7.02	0.76 ± 0.37	12.1	571
Monardella	*villosa*	Lamiaceae	Chaparral	abaxially woolly[5]	glandular	156.13 ± 36.61	17.56 ± 1.4	1.86 ± 0.33	13.8	770
Salvia	*mellifera*	Lamiaceae	Chaparral	dense abaxially[6]	non-glandular and glandular	165.16 ± 26.74	38.17 ± 6.15	5.28 ± 0.74	16.3	436
Salvia	*apiana*	Lamiaceae	Chaparral	densely appressed[7]	non-glandular and glandular	545.78 ± 16.33	55.6 ± 1.99	22.1 ± 0.18	16.5	388
Vitis	*californica*	Vitaceae	Streamside	tomentose[8]	simple	4.52 ± 0.75	27.28 ± 4.07	123 ± 0.1	15.1	751
Vitis	*girdiana*	Vitaceae	Streamside	tomentose[9]	simple	8.16 ± 3.91	41.14 ± 4.66	95.6 ± 0.08	17.0	330

4.5 Figures

Figure 4.1: Micrographs of abaxial leaf surfaces for two species within each of three Californian genera

Micrographs of abaxial leaf surfaces for two species within each of three Californian genera, with the species on the left having denser trichomes than that on the right.

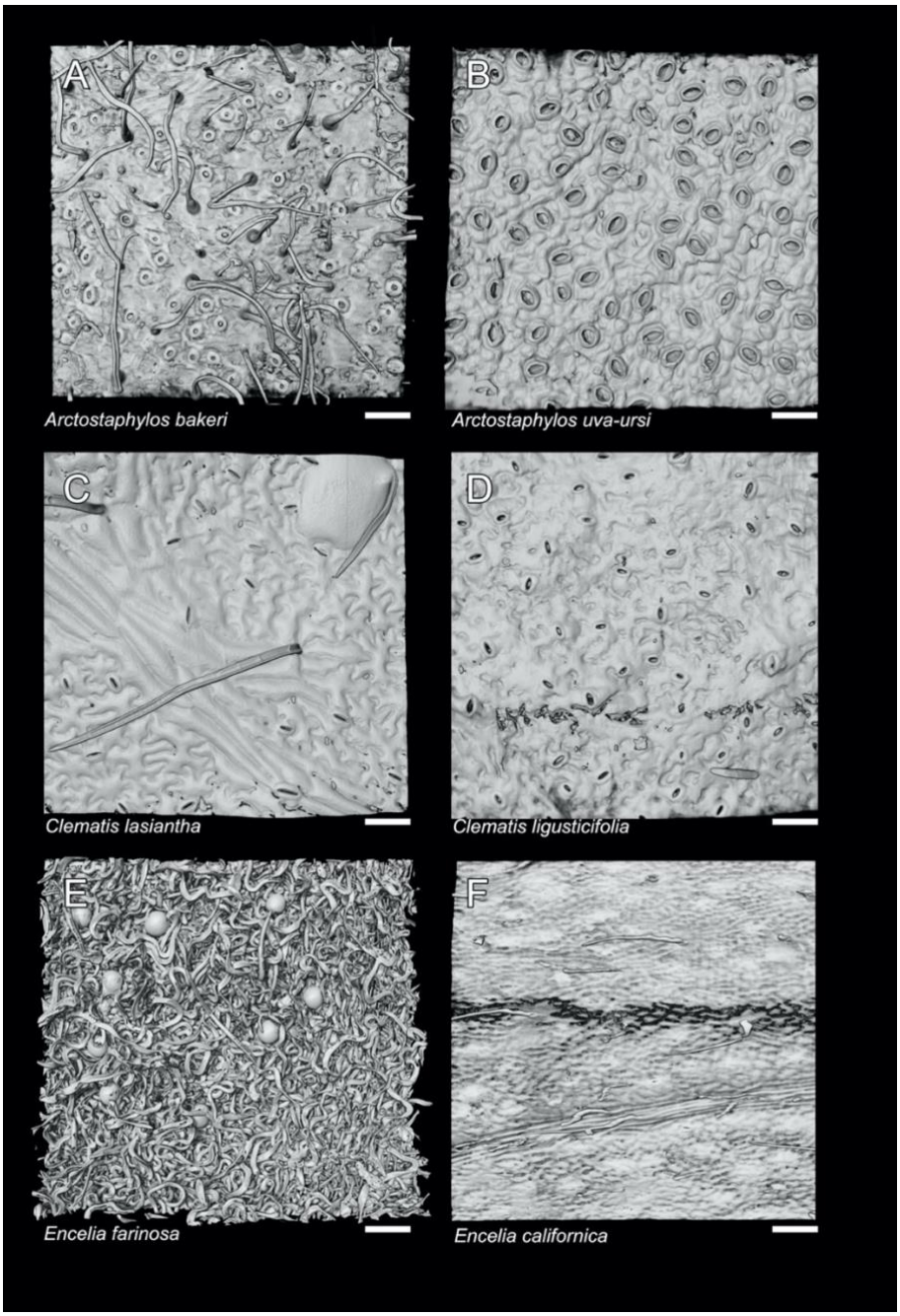

Figure 4.2: Micrographs of abaxial leaf surfaces for two species within each of three Californian genera

Micrographs of abaxial leaf surfaces for two species within each of three Californian genera, with the species on the left having denser trichomes than that on the right. (Image not available for *Monardella macrantha*).

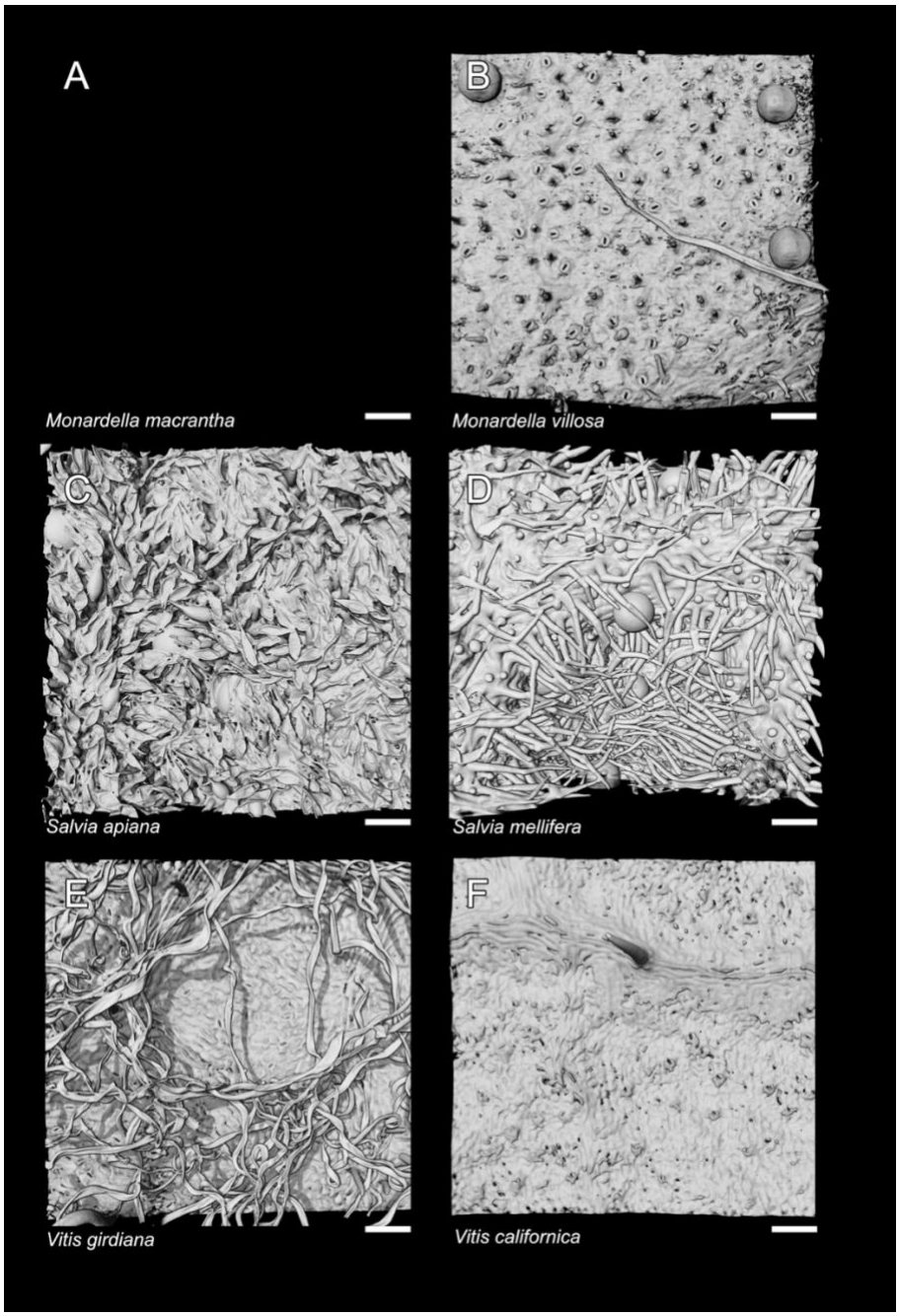

Figure 4.3: Micrographs of adaxial leaf surfaces for two species within each of three Californian genera

Micrographs of adaxial leaf surfaces for two species within each of three Californian genera, with the species on the left having denser trichomes than that on the right.

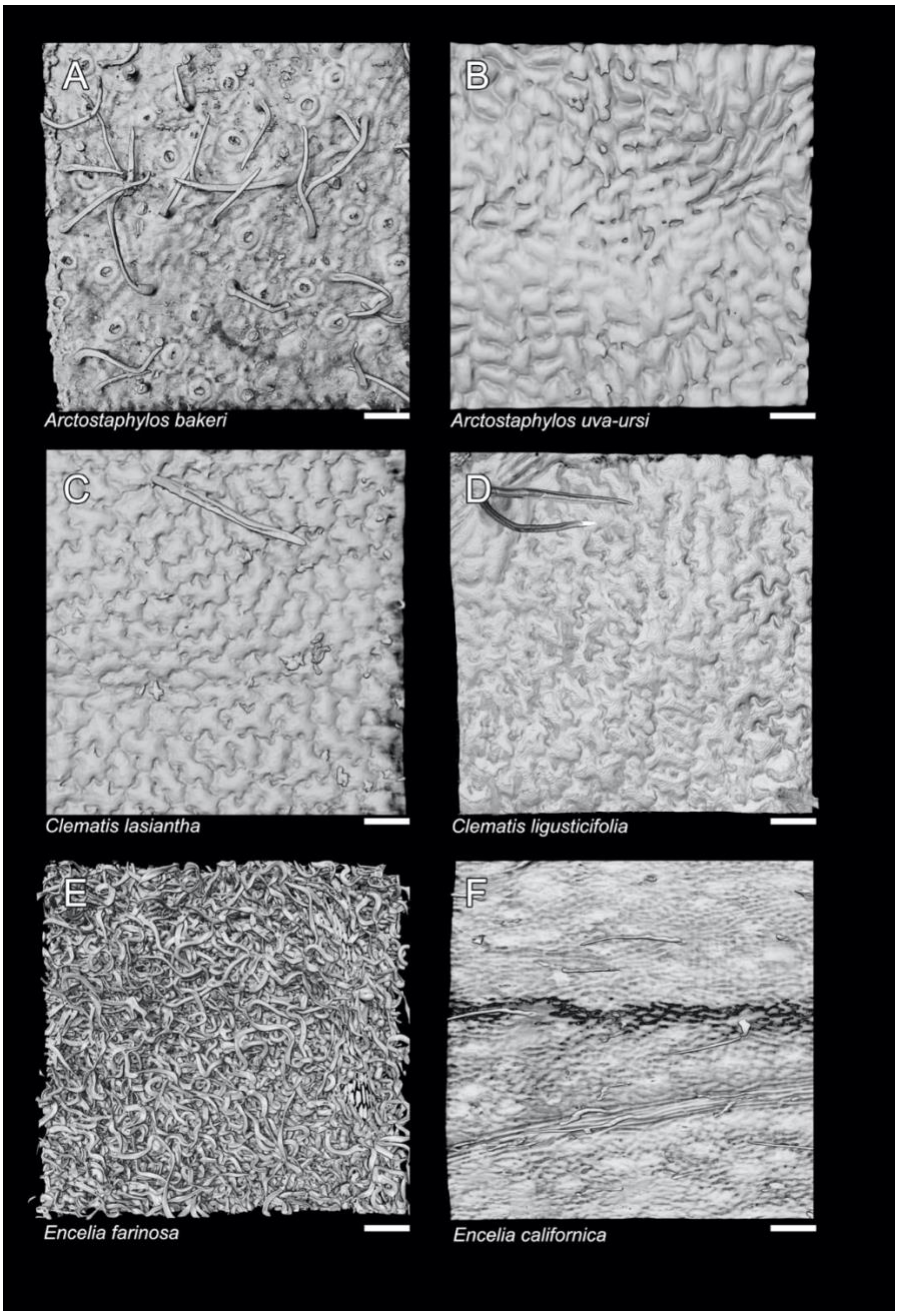

Figure 4.4: Micrographs of adaxial leaf surfaces for species within each of three Californian genera

Micrographs of adaxial leaf surfaces for species within each of three Californian genera, with the species on the left having denser trichomes than that on the right. (Image not available for *Monardella macrantha*).

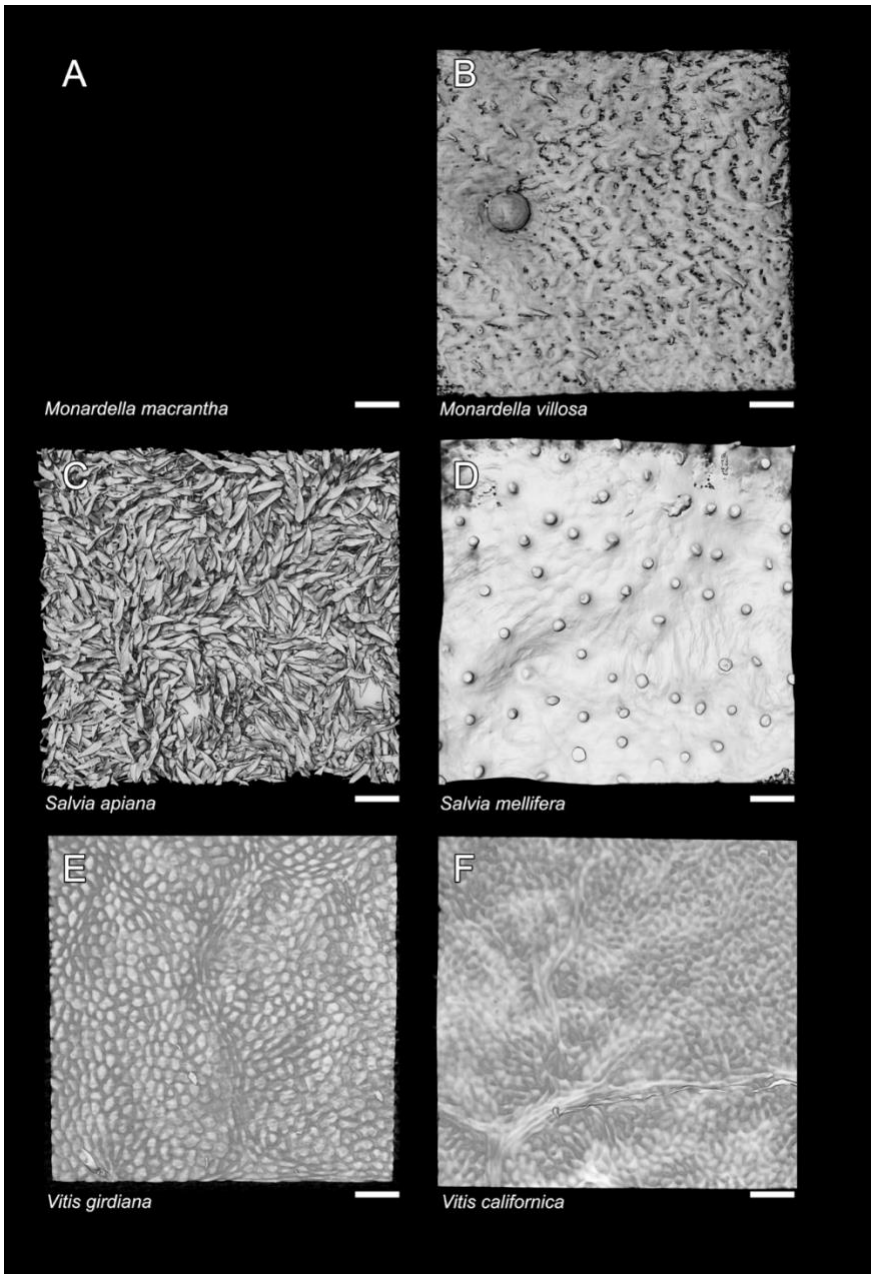

Figure 4.5: Variation across species in leaf trichome traits for twelve species within six Californian genera

Variation across species in leaf trichome traits for twelve species within six Californian genera, with a species with abundant trichomes (orange) and less abundant trichomes (grey). Panel A, trichome density, total for both leaf surfaces (TD); Panel B, trichome length, averaged for both surfaces (TL); Panel C, trichome surface area per leaf area, total for both surfaces (TSALA); Panel D, trichome basal area per leaf area (TBALA); Panel E, trichome volume per leaf area (TVLA).

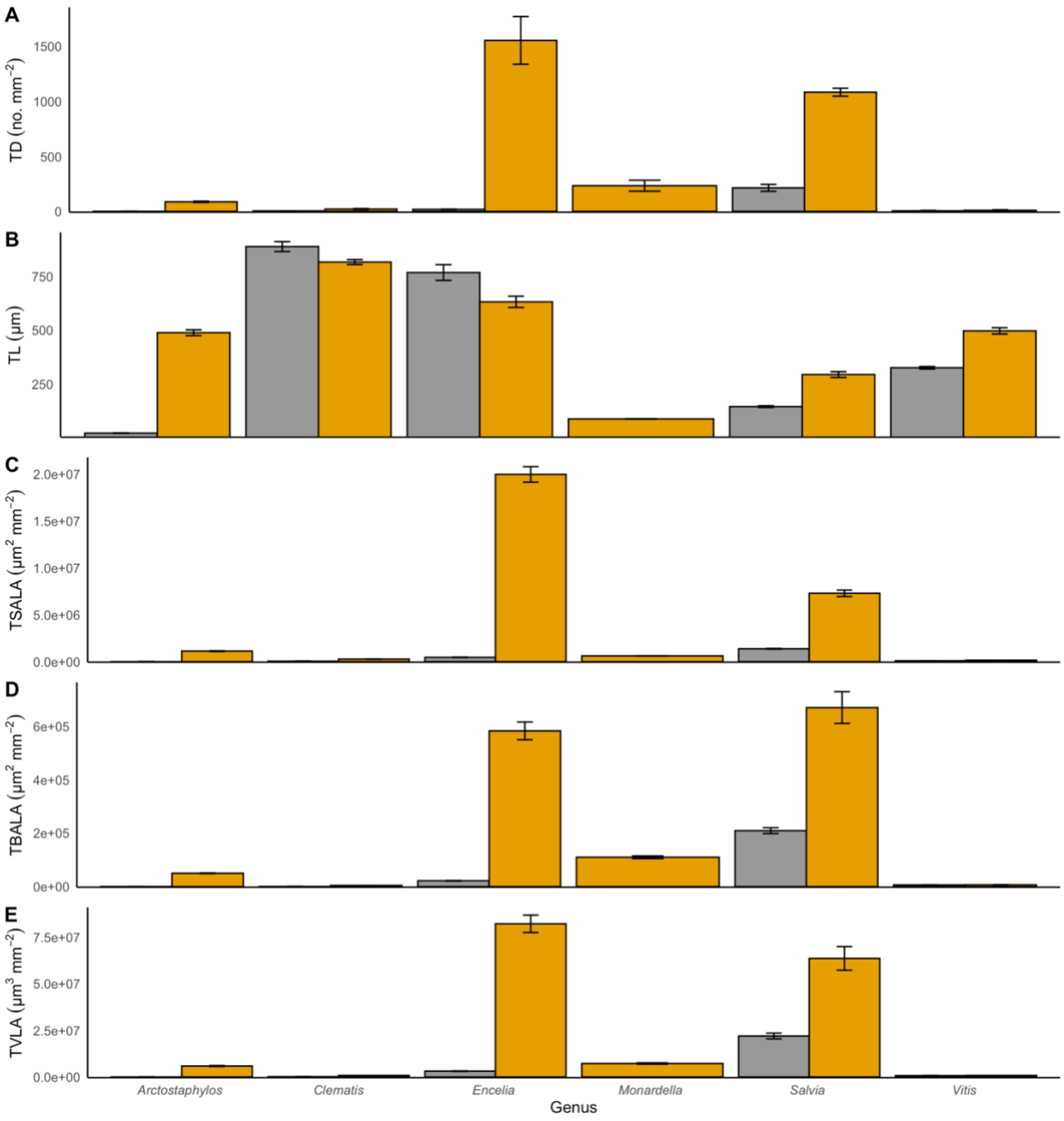

Figure 4.6: Variation across species in leaf gas exchange and water use efficiency traits for twelve species within six Californian genera

Variation across species in leaf gas exchange and water use efficiency traits for twelve species within six Californian genera, with a species with abundant trichomes (orange) and less abundant trichomes (grey). Panel A, light saturated photosynthetic rate per leaf area (A_{max}); Panel B, operating mid-day stomatal conductance (g_{op}); Panel C, intrinsic water use efficiency (A_{max}: g_{op}); Panel D, leaf carbon isotope composition (∂13C).

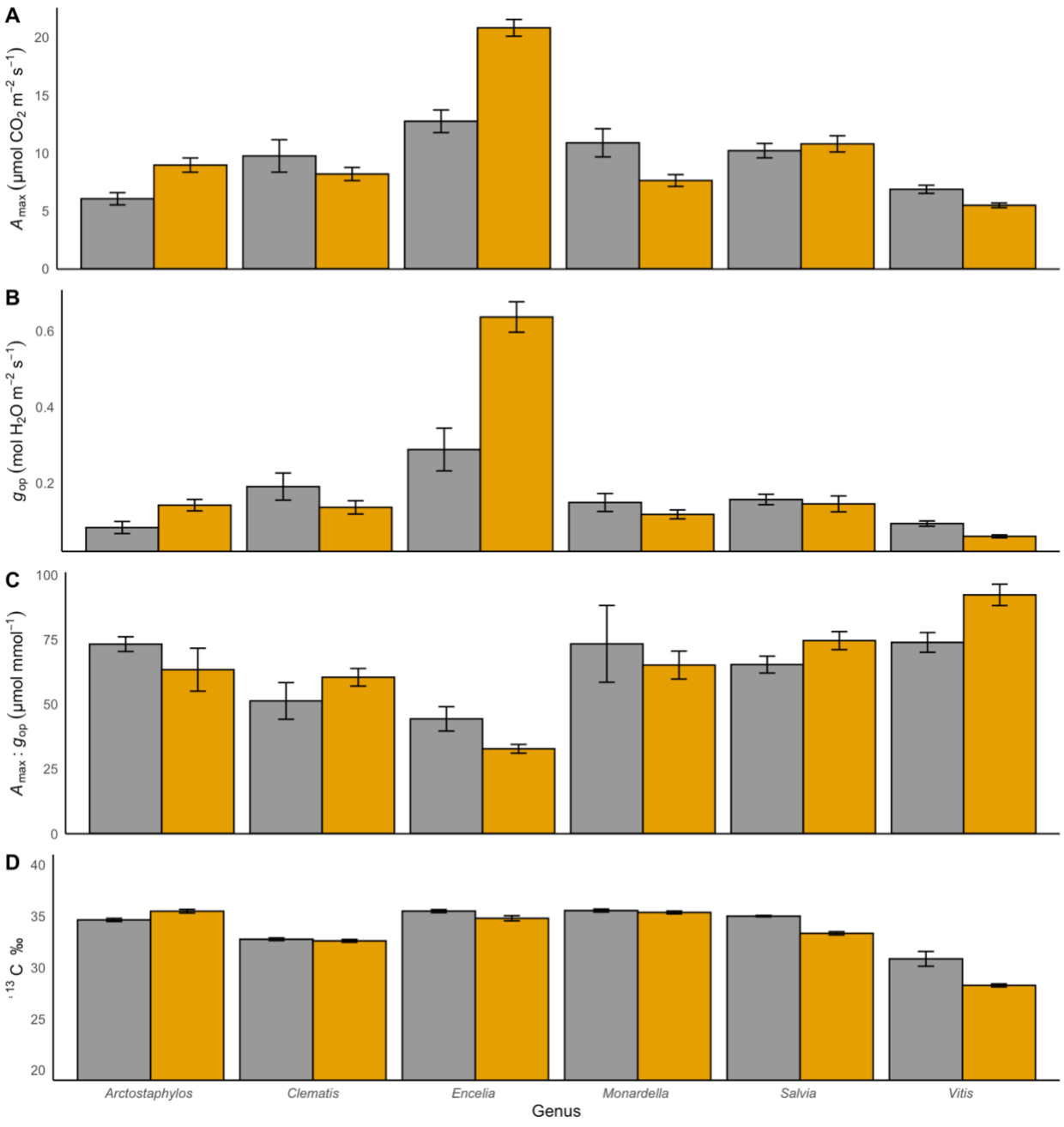

Figure 4.7: Relationships of total trichome density per leaf area (both leaf surfaces) with climate variables

Relationships of total trichome density per leaf area (both leaf surfaces) with climate variables, mean annual temperature (MAT), potential evapotranspiration (PET) and aridity index (AI; lower numbers represent greater aridity). for twelve species within six Californian genera, with a species with abundant trichomes (orange) and less abundant trichomes (blue). Plotted regression lines are significant at r = 0.63-0.73; P = 0.009-0.039 (phylogenetic least-squares regression).

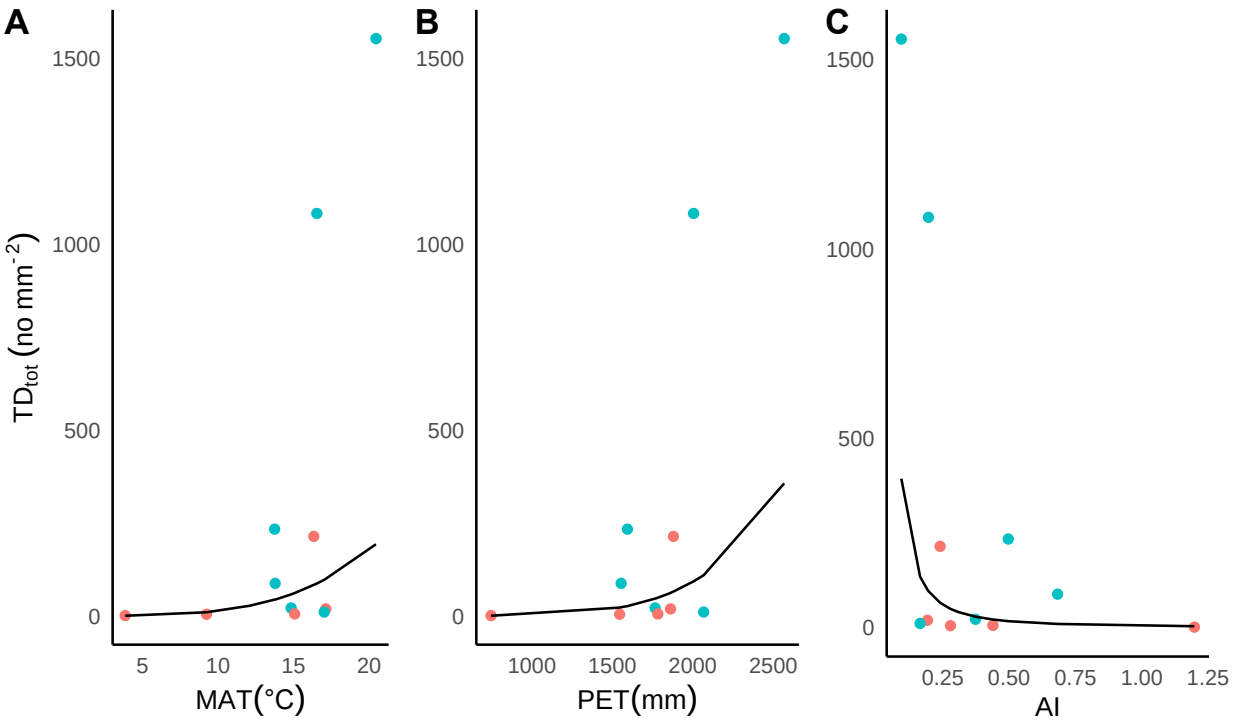

Figure 4.8: Relationships of gas exchange variables with climate variables for twelve species within six Californian genera

Relationships of gas exchange variables with climate variables for twelve species within six Californian genera, with a species with abundant trichomes (orange) and less abundant trichomes (blue). Panel A, operating mid-day stomatal conductance (g_{op}) and potential evapotranspiration (PET); Panel B, light saturated photosynthetic rate per leaf area (A_{max}) with PET; and Panel C, A_{max} with aridity index (AI; lower numbers represent greater aridity). Plotted regression lines are significant at r = 0.40-0.49; P = 0.017-0.03 (phylogenetic least-squares regression).

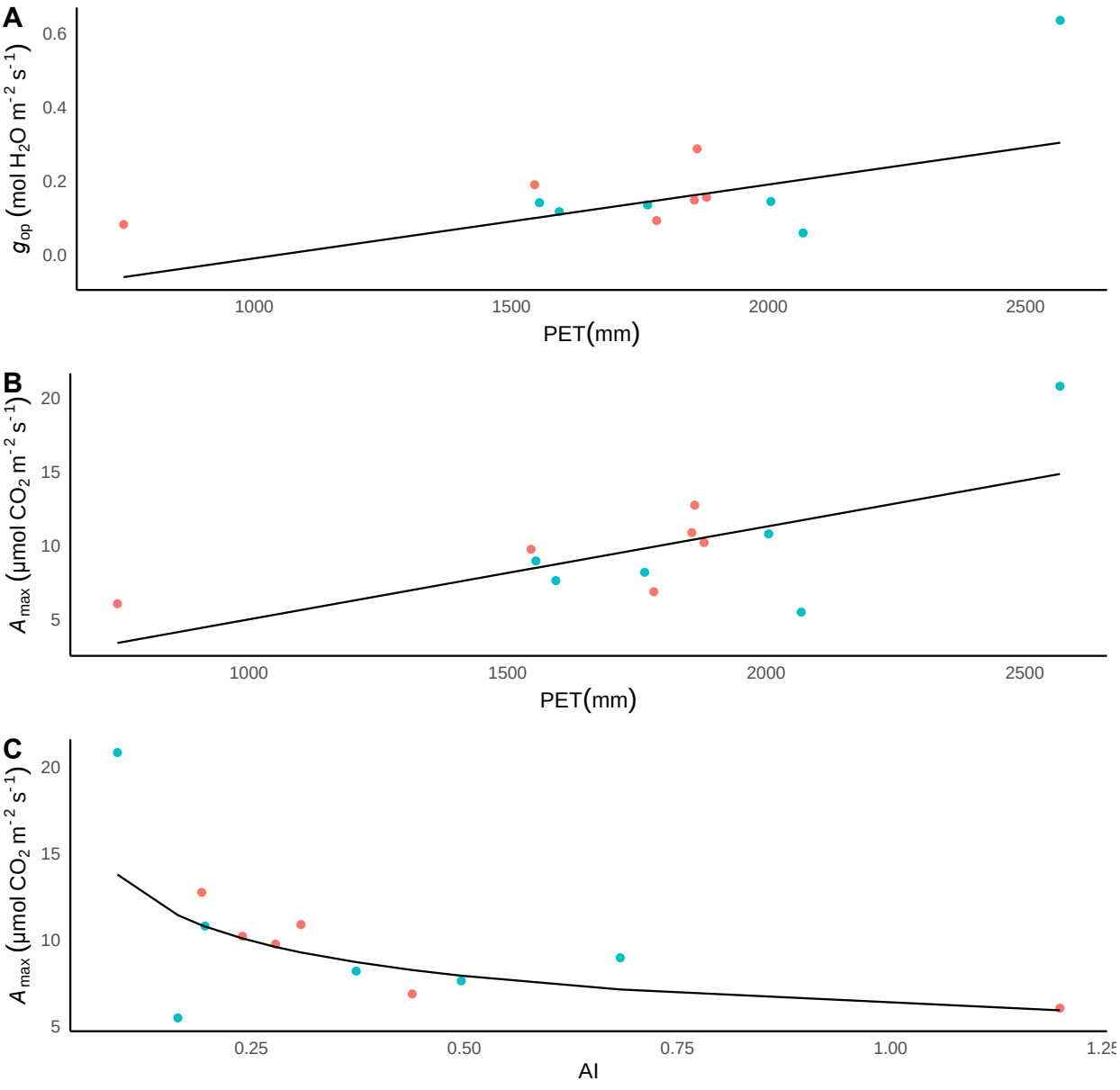

Figure 4.9: Relationships of gas exchange traits with leaf trichome and stomatal traits for 11 species within six Californian genera

Relationships of gas exchange traits with leaf trichome and stomatal traits for 11 species within six Californian genera, with a species with abundant trichomes (orange) and less abundant trichomes (blue). Panels A and B, plots of light saturated photosynthetic rate per leaf area (A_{max}) with total trichome density, both leaf faces (TD_{tot}) and total stomatal density, both leaf faces (SD_{tot}); Panels C and D, plots of operating mid-day stomatal conductance (g_{op}) with TD_{tot} and SD_{tot}. Plotted regression lines are significant at r = 0.63-0.94; P = 0.00002-0.023 (phylogenetic least-squares regression).

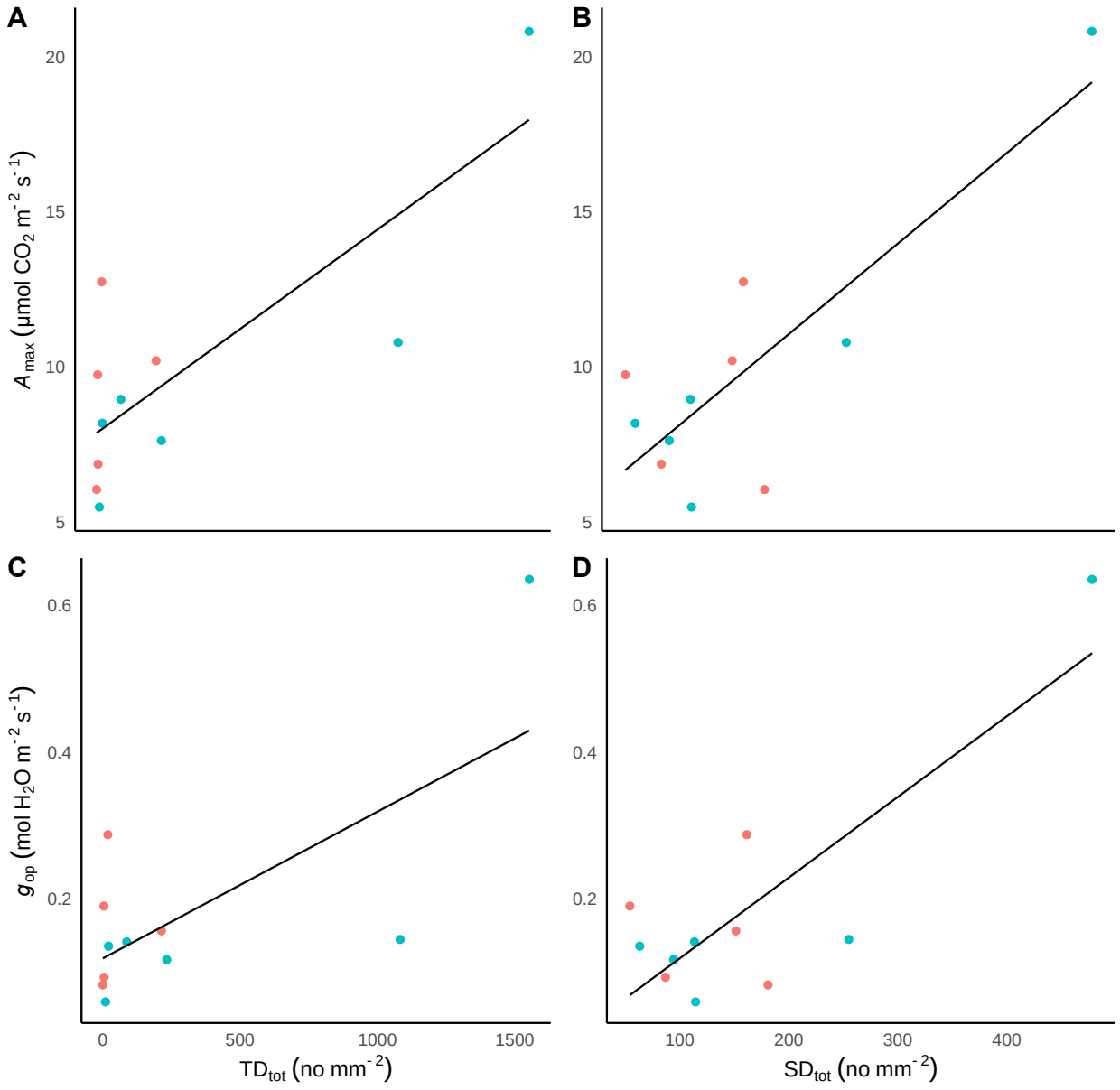

4.6 References

1 Jones, H. G. *Plants and Microclimate: A Quantitative Approach to Environmental Plant Physiology*. 3 edn, (Cambridge University Press, 2013).

2 Sack, L. & Buckley, T. N. Trait Multi-Functionality in Plant Stress Response. *Integrative and Comparative Biology* **60**, 98-112, doi:10.1093/icb/icz152 (2019).

3 Kenzo, T., Yoneda, R., Azani, M. A. & Majid, N. M. Changes in leaf water use after removal of leaf lower surface hairs on *Mallotus macrostachyus* (*Euphorbiaceae*) in a tropical secondary forest in Malaysia. *J. For. Res.* **13**, 137-142, doi:10.1007/s10310-008-0062-z (2008).

4 Ehleringer, J. R. & Björkman, O. Pubescence and leaf spectral characteristics in a desert shrub, Encelia farinosa. *Oecologia* **36**, 151-162, doi:10.1007/bf00349805 (1978).

5 Ehleringer, J. The influence of water stress and temperature on leaf pubescence development in *Encelia farinosa*. *Am. J. Bot.* **69**, 670-675, doi:doi:10.1002/j.1537-2197.1982.tb13306.x (1982).

6 Ripley, B. S., Pammenter, N. W. & Smith, V. R. Function of leaf hairs revisited: The hair layer on leaves *Arctotheca populifolia* reduces photoinhibition, but leads to higher leaf temperatures caused by lower transpiration rates. *Journal of Plant Physiology* **155**, 78-85, doi:https://doi.org/10.1016/S0176-1617(99)80143-6 (1999).

7 Wuenscher, J. E. Effect of leaf hairs of *Verbascum thapsus* on leaf energy exchange. *New Phytol.* **69**, 65-+, doi:10.1111/j.1469-8137.1970.tb04050.x (1970).

8 Parkhurst, D. F. Effects of *Verbascum thapsus* leaf hairs on heat and mass transfer reassessment. *New Phytol.* **76**, 453-457, doi:10.1111/j.1469-8137.1976.tb01481.x (1976).

9 Schreuder, M. D. J., Brewer, C. A. & Heine, C. Modelled influences of non-exchanging trichomes on leaf boundary layers and gas exchange. *Journal of Theoretical Biology* **210**, 23-32, doi:10.1006/jtbi.2001.2285 (2001).

10 Agrawal, A. A. *et al.* Phylogenetic ecology of leaf surface traits in the milkweeds (*Asclepias* spp.): chemistry, ecophysiology, and insect behavior. *New Phytol.* **183**, 848-867, doi:10.1111/j.1469-8137.2009.02897.x (2009).

11 Amada, G., Onoda, Y., Ichie, T. & Kitayama, K. Influence of leaf trichomes on boundary layer conductance and gas-exchange characteristics in *Metrosideros polymorpha* (*Myrtaceae*). *Biotropica* **49**, 482-492, doi:10.1111/btp.12433 (2017).

12 Weisstein, E. W. *"Conical Frustum."*, <https://mathworld.wolfram.com/ConicalFrustum.html> (2022).

13 *rgbif: Interface to the Global Biodiversity Information Facility API*. v. 3.3.0 (2020).

14 Hijmans, R. J., Cameron, S. E., Parra, J. L., Jones, P. G. & Jarvis, A. Very high resolution interpolated climate surfaces for global land areas. *Int. J. Climatol.* **25**, 1965-1978, doi:10.1002/joc.1276 (2005).

15 Zomer, R. J., Trabucco, A., Bossio, D. A. & Verchot, L. V. Climate change mitigation: A spatial analysis of global land suitability for clean development mechanism afforestation and reforestation. *Agriculture, Ecosystems & Environment* **126**, 67-80, doi:https://doi.org/10.1016/j.agee.2008.01.014 (2008).

16 Hengl, T. *et al.* SoilGrids250m: Global gridded soil information based on machine learning. *PLoS One* **12**, e0169748, doi:10.1371/journal.pone.0169748 (2017).

17 Hijmans, R. J. *et al.* (Version, 2013).

18 Hijmans, R. J., Phillips, S., Leathwick, J., Elith, J. & Hijmans, M. R. J. Package 'dismo'. *Circles* **9**, 1-68 (2017).

19 Perez, T. M. & Feeley, K. J. Weak phylogenetic and climatic signals in plant heat tolerance. *Journal of Biogeography* **48**, 91-100, doi:https://doi.org/10.1111/jbi.13984 (2021).

20 Harmon, L. J. *Phylogenetic comparative methods*. (Independent, 2019).

21 Freckleton, R. P., Harvey, P. H. & Pagel, M. Phylogenetic analysis and comparative data: a test and review of evidence. *Am Nat* **160**, 712-726, doi:10.1086/343873 (2002).

22 Orme, D. *et al.* The caper package: comparative analysis of phylogenetics and evolution in R. *R package version* **5**, 1-36 (2013).

23 Brodersen, C. R., Vogelmann, T. C., Williams, W. E. & Gorton, H. L. A new paradigm in leaf-level photosynthesis: direct and diffuse lights are not equal. *Plant Cell Environ.* **31**, 159-164, doi:10.1111/j.1365-3040.2007.01751.x (2008).

24 Grubb, P. J. A reassessment of the strategies of plants which cope with shortages of resources. *Perspect. Plant Ecol. Evol. Syst.* **1**, 3-31, doi:10.1078/1433-8319-00049 (1998).

5. Chapter 5: Conclusion

5.1 Discussion

Plant physiological response to the aboveground environment can be strongly influenced by leaf surface characteristics, including stomata and trichomes. The leaf-level responses to the environment are often determined by stomatal regulation, and I showed that this regulation is constrained by a safety efficiency trade-off. I also showed that leaves exhibit the ability to rehydrate via foliar water uptake, and that this uptake varies strongly across species with and without trichomes. Further, across diverse species, greater trichome abundance was associated with higher light-saturated gas exchange, and with drier and warmer conditions in species' native ranges.

In **Chapter 2**, I found support for multiple mechanistic drivers of the trade-off between maximum stomatal conductance and the water potential at 50% loss of maximum stomatal conductance (the g_{max}–Ψ_{gs50} trade-off). This trade-off can be explained by a greater sensitivity of stomatal closure in the face of drought arising in species with smaller, denser stomata. Another possible explanation was that a lesser sensitivity to stomatal closure during drought arises in species with lower leaf bulk osmotic potentials. This safety-efficiency trade-off could also be explained by with life history theory, by which species with lower leaf mass per area have lower g_{max} and lower Ψ_{gs50}. Lastly, the trade-off can be explained by theory that stomatal conductance evolves in dry conditions to maximize water use efficiency without risking hydraulic failure.

In **Chapter 3**, I demonstrated the ability for leaves of diverse Californian species to uptake water across the foliar surface, independently of their native climate. This ability, quantified as the hydraulic conductance to foliar surface water uptake (K_{surf}) declined with rehydration time. The magnitude and decline in K_{surf} with time pointed to pivotal roles of the cuticle and/or semi-permeable cell membranes in leaf rehydration. K_{surf} varied across six

intrageneric species pairs, being higher for species with greater trichome abundance in some genera, and but higher for species with lower trichome abundance in other genera.

In **Chapter 4**, I highlighted associations of trichome abundance and light-saturated gas exchange with drier and warmer conditions. These findings further support theory for behind the overall adaptation of leaf trichomes to arid climates, and the adaptation of species to dry conditions through avoidance mechanisms, i.e., mitigating shorter growing periods with high rates of gas exchange during periods of high moisture availability. This work points to new avenues of research to integrate the multiple potential functions of trichomes to determine their contribution to species' performance under different environmental conditions.

This work shows the major role and adaptive diversification of micro-scale leaf surface features in determining leaf function, that would scale up to influencing their ecology and distributions.